INTERMEDILYSIN-MEDIATED CELL ABLATION IN THE RAT AND ZEBRAFISH

A DISSERTATION

PRESENTED TO

THE FACULTY OF THE GRADUATE SCHOOL

AT THE UNIVERSITY OF MISSOURI

IN PARTIAL FULFILLMENT

OF THE REQUIREMENTS FOR THE DEGREE

DOCTOR OF PHILOSOPHY

BY

DR. MARINA MCCOY HANSON

DR. ELIZABETH C. BRYDA, DISSERTATION SUPERVISOR

DECEMBER 2016

The undersigned, appointed by the dean of the Graduate School, have examined the dissertation entitled

INTERMEDILYSIN-MEDIATED CELL ABLATION IN THE RAT AND ZEBRAFISH

presented by Marina M. Hanson,

a candidate for the degree of Doctor of Philosophy
and hereby certify that, in their opinion,
it is worthy of acceptance.

_____

Elizabeth C. Bryda, PhD

_____

Craig L. Franklin, DVM, PhD

_____

Yuksel Agca, DVM, PhD

_____

James Amos-Landgraf, PhD

_____

Kevin D. Wells, PhD

Dedication

This work is dedicated to all of my teachers.

In loving memory of my nonna, Francesca Nieczpiel. Thank you for believing in me and instilling in me that anything is possible if you work hard. Your legacy lives on.
Ti ameró per sempre

Acknowledgements

The work presented here could not have been accomplished without the assistance of many individuals.

First and foremost, I would like to thank Dr. Elizabeth Bryda for her mentorship and support. You have consistently guided me, inspired me, and encouraged me when I needed words of encouragement. Your contribution towards my success will never be forgotten. You are amazing!

Thank you to my other committee members for their experience and insight during my residency training and PhD research. I have enjoyed our scientific discussions and learned so much more than I ever could in a classroom.

Thank you to the comparative medicine faculty and fellow trainees, past and present. I have learned something from each of you and feel blessed to have had the pleasure of working with so many talented characters. Thank you to the graduate students, vet students, undergraduates, lab managers, technicians and animal care staff that assisted in this work.

Thank you to my family for recognizing my strengths early on in my life and nurturing them. It is because of my parents that I found my true passion in life. The supportive words from all my family members, especially my husband, Aaron, kept me going when the going got tough. They reminded me that I am capable of anything I can dream up and I cannot fully express in words just how vital it was to have you all with me on this journey.

Table of Contents

List of Tables

List of Figures

Chapter 1: Introduction

Cell Ablation

Cell ablation is an effective tool for the study of differentiation, cell migration, and tissue interaction. Selective cell ablation techniques in rodents have uncovered cell linage relationships [1, 2] and physiological mechanisms of disease [3, 4], as well as propelled transplantation research [5, 6]. In model species, such as zebrafish and *Xenopus*, which have great capacity to regenerate certain tissues or cell types, ablation facilitates the analysis of cell regeneration and regulation [7].

To accomplish constitutive ablation of cells, several methods have been established. Current ablation techniques used in the vertebrate include physical methods, such as microdissection, where progenitors of the investigated cell type are removed physically. Inducible cell ablation is commonly achieved by chemical methods such as cell-specific toxins. Alternatively, through the use of genetic methods, it is possible to render cells susceptible to prodrugs by transgenesis. In this method, a cell type–specific transgene codes for an enzyme such as thymidine kinase (Tk) or nitroreductase (NTR), which converts the prodrug into a cytotoxic product. Lastly, and the methodology investigated in this dissertation, are genetic ablation methods utilizing a transgene encoding a receptor, such as diphtheria toxin receptor or human CD59, which specifically recognizes a toxin, namely diphtheria toxin and intermedilysin (ILY), respectively. Such methods allow for distinct temporal and spatial control for inducible targeted cell ablation in vertebrates.

Physical Ablation

Physical ablation methods such as laser-assisted and microsurgery (microinjury) can be utilized if the tissue or cells of interest are easily accessible. Plasma-induced laser ablation can be accomplished by near-infrared and ultraviolet (UV) radiation. Plasma generation leads to formation of a cavitation bubble and resultant cell detachment and apoptosis [8-10]. Laser ablation has been used on individual cells in embryos of *Xenopus laevis* [11], zebrafish (*Danio rerio*) [12] and mice (*Mus musculus*) [13] [14]. Laser ablation has also been used to remove differentiated cells in zebrafish larva such as cardiomyocytes [15] and neurons [16, 17].

Laser mediated cell ablation is beneficial for assessment of tissue regeneration and local recovery following injury, which would not be possible with more widespread methods. However, the time required to anesthetize the animal, immobilize and perform ablation can be prohibitive. It is also difficult to focus the laser in the z-plane therefore cells proximal and distal to the targeted region will also be ablated [18].

Mechanical lesions to study regeneration post-injury have been utilized in the eye via photoablation with intense UV light or needle stab [19], though the same disadvantages are seen with such techniques as for laser ablation. Overall, physical methods of ablation are typically labor-intensive, time-consuming, and not as reproducible as genetic approaches. When a large number of samples are required, chemical or genetic methodologies have the clear advantage.

Chemical Ablation

Chemical-mediated ablation involves administration of drugs or compounds that have preferential cytotoxicity for specific cell types, inducing their death. The manner of cell death is specific to the drug utilized and can involve mechanisms such as disruption of ATP production, as in MPTP for neuronal death, or can induce death by mechanisms still not fully understood, as in 2-butoxyethenol (BE) administration for erythrocyte ablation [20]. The types of cells and tissues ablated by chemical means has been limited, most commonly targeting susceptible populations including erythrocytes, pancreatic cells and subclasses of neurons.

Phenylhydrazine (PHZ) and BE have been used in rats and mice to ablate erythrocytes, though repeated injection is required to induce clinically significant cell loss [21-23]. PHZ has been shown to have off-target effects, such as stimulation of lymphocytes and monocytes four days following injection [24, 25]. Response of BE in rats is delayed, variable and age-dependent with younger rats exhibiting more resistance to hemolysis [26]. Unfortunately, both PHZ and BE are hazardous substances which must be handled carefully to avoid human exposure [27, 28].

Pancreatic β cells are advantageously destroyed by streptozotocin (STZ) due to the glucose moiety present on the drug which increases its uptake by the glucose 2 transporter (GLUT2), which is more active in beta cells[29]. Uptake of this glucose analogue leads to DNA fragmentation death but the exact pathways have yet to be identified [29]. Interestingly, GLUT2 is also active in other insulin-producing cells such as renal tubular cells and hepatocytes, which explains the drug-induced side effects of nephropathy [30, 31] and hepatopathy [32, 33]. Additionally, β cell ablation via STZ is inconsistent due to

different sex and strain sensitivities, while failing to induce complete ablation even after days of toxic exposure [34-36].

Toxin-induced ablation of dopaminergic neurons act through inhibition of the mitochondrial electron transfer chain, leading to mitochondrial intoxication with enhanced production of ROS and reduced production of ATP [37, 38]. These toxins however do not exclusively act on dopamine neurons, exhibiting toxic effects in all cells [39]. MPTP is highly toxic to humans at low doses [40], while high doses have failed to induce ablation in some strains of rodents [41, 42]. Rotenone is less toxic to humans, however the model has low reproducibility with acute death observed unrelated to ablation of the target cell population [43]. Additionally, due to the low toxicity, rotenone must be administered daily for several weeks [44].

While chemical ablation has generated multiple widely-used models of disease, they often fail to induce complete ablation without toxic off-target toxic effects, and their activity is more easily influenced by sex and genetic background than other ablation methods. Therefore, there is a need for a genetic based model which can specifically ablate erythrocytes in a rapid manner without off target effects or human health concerns.

Genetic Ablation

Genetic ablation refers to the generation of transgenic animals lacking specific cell types as a result of targeted expression of a potentially lethal toxin to specific cell types with appropriate transcriptional regulatory elements, or promoters. Genetic ablation represents an extension of older methodologies including chemical or laser ablation of specific cell types. Ablation of specific cell types in transgenic animals relies on the fact

that virtually all differentiated cell types in the body can be characterized by the expression of highly specialized proteins whose synthesis is restricted to that cell type. Promoters, typically located around the coding region of the gene, are responsible for this restriction of protein expression, ensuring that genes are expressed in the appropriate cell types at the appropriate times during both embryological development and during cellular differentiation in the adult. The promoter can then be used to direct the expression of heterologous sequences, regardless of chromosome location, in transgenic animals. Thus, promoters allow for the targeted expression of genes that express toxic proteins or their receptor.

Genetic ablation is a powerful tool which allows the removal of specific cell types by targeting expression of toxin-producing enzymes or toxin-specific receptors. Although the well-established methods of physical surgery and laser-mediated ablation are controllable in time and space, they are labor-intensive, time-consuming, and not as reproducible as a genetic approach. Chemical approaches also fail to have the range of achievable ablation that genetic methods provide. Several genetic ablation systems have been commonly used in rodents and zebrafish which will be described here, concluding with the human CD59-ILY system which is the focus of this dissertation.

Thymidine kinase-ganciclovir

Dividing cells expressing the herpes simplex virus thymidine kinase (Tk) gene are susceptible to ablation when treated with anti-virals such as ganciclovir *in vitro* [45] and *in vivo* [46, 47]. The viral thymidine kinase monophosphorylates ganciclovir, producing a cytotoxic product which incorporates into the elongated DNA of replicating cells, terminating replication and resulting in apoptosis [48]. Due to its limitation of use to

replicating cells, this "suicide gene" technology has been largely utilized as targeted cancer therapy [49-53], where it is also noted to have "bystander" effects in non-expressing Tk cells [54, 55]. While advantageous for neoplastic cell ablation, Tk would be ineffective in cells not actively replicating, such as differentiated neurons, or in enucleated cells such as erythrocytes.

Nitroreductase-metronidazole

In contrast to Tk, the Nitroreductase (NTR)-metronidazole (Mtz) system is cell-cycle independent and, therefore, applicable to any target cell population [56]. Similar to Tk, *Escherichia coli* NTR reduces the nontoxic prodrug metronidazole (and historically prodrug CB1954) to a cytotoxin which is a potent interstrand DNA cross-linker. In dividing cells, this cross-linking halts DNA replication leading to cell death [57].

NTR has been the predominant cell ablation system used in zebrafish [58]. Zebrafish hepatocytes, pancreatic beta cells, and cardiomyocytes have been ablated utilizing NTR [59]. Ease of use has accelerated its practice as embryos can be incubated in water containing Mtz, allowing for high-throughput ablation studies [60]. However, optimal ablation of deeper tissues within the embryo may require longer incubation times [61]. Zebrafish embryos treated with Mtz for 24 hours were partially ablated, with 48 hours providing near complete ablation [59]. Unfortunately, zebrafish growth is so rapid that there is potential for regenerating cells to interfere with ablation. Additionally, not all cell types appear to be susceptible to NTR ablation which may be due to cell specific metabolism or uptake of the prodrug [61]. Furthermore, when used with the prodrug CB1954, NTR has been shown to have significant bystander effects when the cytotoxin diffuses from the target cell to nearby cells [62, 63] [64].

Bystander effects have been detected in transgenic mouse models which express NTR in renal podocytes, leading to injury and death of Bowman's capsule cells [65]. Destruction of T cells within the thymus and spleen has also been performed in transgenic mice expressing NTR, although a small reduction was also observed in wild type mice, indicating that doses required to induce ablation of target cells may also have non-specific toxicity [66].

One transgenic NTR rat has been generated to date, targeting ablation of central nervous system progenitor cells [67]. While ablation within the nervous system was achieved, treatment with CB1954 at mouse doses resulted in mortality in rats when given intraperitoneally [67]. DT-diaphorase, the enzyme which activates CB1954 to its cytoxic form, was found to have 10-fold higher affinity for CB1954 in in the rat compared to mouse and human [68].

Combined, these data have led researchers to find alternative conditional cell ablation murine models, such as diphtheria toxin receptor.

Diphtheria toxin

Diphtheria toxin (DT) is a potent toxin synthesized by the bacterium, *Corynebacterium diphtheria*, consisting of single precursor polypeptide, which is proteolytically-cleaved into two subunits, A and B. The binding of the larger B subunit to the cell surface diphtheria toxin receptor (DTR) initiates endocytosis where the smaller A subunit dissociates and passes through the membrane into the cytoplasm. Here, it encodes an ADP-ribosyl-transferase that catalyses the ADP ribosylation of elongation factor-2, resulting in the inhibition of protein synthesis and subsequent cell death[69]. It has been estimated that one molecule per cell is sufficient to kill a cell [70]. The extreme toxicity of

DT therefore provides a powerful way of killing cells. This sequence of cell death has been employed in cell ablation in two ways: by generating transgenes which drive expression of either the A subunit only (DTA models) or the human diphtheria toxin receptor (DTR models) (Figure 1.1).

In DTA models, cells are ablated when the promoter driving expression is active, typically resulting in a loss of that cell lineage. Resultant cell death and subsequent release of the A subunit from dying cells will not kill neighboring cells due to the absence of the B subunit required for endocytosis [70]. Lineage-restricted expression of DTA has been used in mice to understand skeletal myogenesis [71, 72], hematopoetic progenitor cells [73],and maternal vasculature remodeling in the placenta [74]. Tamoxifen- induced, Cre-mediated recombination of DTA for conditionally regulated cell ablation has been used in mouse embryonic forebrain [75] and hippocampus [76]. No transgenic rats utilizing DTA have been generated to date.

DTA-mediated ablation has been successful in the zebrafish lens [77] and exocrine pancreas [78, 79], but only in transient transgenic embryos. Stable genetic cell ablation using DTA has thus far been unsuccessful in zebrafish. Because of its high toxicity, minimal leakiness of the promoter used results in unintended cell death and inability to maintain viable founders [78]. Leakiness has also been observed in floxed mice homozygous for DTA (sequence flanked by two *loxP* sites), developing degenerative abnormalities in multiple tissues, which was somewhat attenuated by transgene redesign [80].

Additionally, mice which initially expressed DTA in B cells gradually lost expression throughout life as continuous proliferation and differentiation of B progenitor

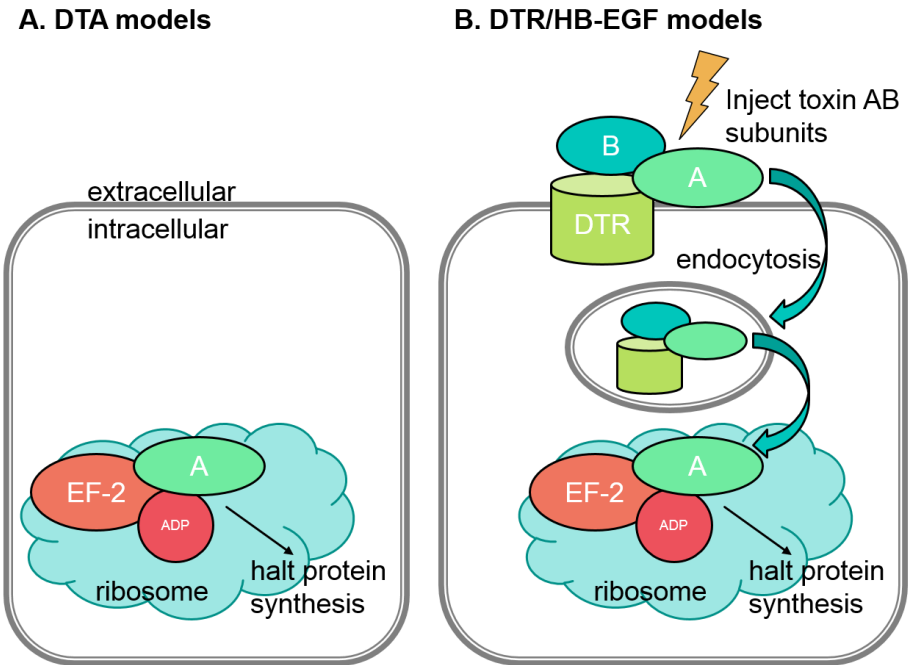

Figure 1.1. Diphtheria toxin-mediated cell ablation. A. In DTA-mediated ablation models, cells produce diphtheria toxin subunit A which catalyzes ADP ribosylation (red) of elongation factor 2 (EF-2) halting protein synthesis. **B.** In DTR mediated models, systemic injection of diphtheria toxin A and B chains binds to diphtheria toxin receptor (DTR) inducing endocytosis. The A subunit then dissociates and exits the endosome where it halts protein synthesis.

cells selected for a subset of circulating B cells that do not functionally express DTA [81]. Therefore the design of genetic ablation methods in cells which can reconstitute themselves must be considered carefully.

An alternative approach to inducible ablation uses transgenic expression of DTR, also called simian or human heparin-binding EGF-like growth factor (HB-EGF) [82]. Expression of DTR on the cell surface allows binding of the B subunit of DT following systemic administration of the toxin and subsequent receptor-mediated endocytosis, dissociation of the A subunit and cell death using the same pathway as for DTA models [83]. Simian and human EGFs used in genetic ablation bind DT with approximately 10^5-fold higher affinity than rodent heterologues [84]. Therefore, expression of the DTR/HB-

EGF transgene renders naturally DT-resistant rodent cells highly susceptible to DT intoxication and cell death [85]. DT in mice has been administered intraperitoneally [86], intravenously [87], and subcutaneously [88], readily crosses the blood brain barrier [88], and antibody response to the toxin is not neutralizing [89]. DTR has been used in mice to ablate many tissues including sertoli cells [90], alpha and beta cells within the pancreas [91, 92], growth hormone-expressing cells in mouse pituitary [93], as well as B and T lymphocytes using an inducible DTR [89].

However, expression of DTR on dendritic cells had unwanted off-target effects, such as impaired lymph node migration of dendritic cells and lymph node hypocellularity, indicating the biological function of EGFs are not fully understood and could modulate the cellular microenvironment unexpectedly [94]. Additionally, mortality of mice following repeated DT injections supports the growing theory that DT can ablate rodent cells not expressing DTR, even though affinity is much lower [94].

Using the phage-derived Cre/*loxP* recombinase system, DT-mediated ablation of specific target cells can be achieved by breeding the respective Cre transgenic mice with mice harboring an inducible DTR transgene [89]. While use of this inducible DTR mouse has led to wide application of cell-specific ablation by using the 'zoo' of available Cre-expressing mouse strains [95], this methodology can only ablate cells actively synthesizing protein. Therefore, enucleated cells such as erythrocytes, thrombocytes, keratinocytes and differentiated lens fiber cells are unable to be ablated [96].

Intermedilysin-mediated ablation

The studies summarized above demonstrate that genetic ablation can be used to generate mutant animals that lack specific cells *in vivo*. These transgenic mice can be used to create animal models of certain human diseases and to ask questions about cell lineage relationships. While the aforementioned ablation methods have clear advantages, their limitations highlight a need for additional ablation methodologies. Therefore, the work described here utilizes a novel approach through cell lysis mediated by the specific binding of intermedilysin (ILY) to its receptor, human CD59 (hCD59).

Human CD59

CD59, a small protein of approximately 77 amino acids and weighing 20 kDa, is ubiquitously expressed in all human tissues and circulating cells [97]. CD59 is among the most important complement-regulatory proteins, protecting mammalian cells against complement-mediated pore formation and lysis [98]. The complex, multiprotein complement cascade is an essential branch of the innate immune system which targets pathogens for lysis via the membrane attack complex (MAC). Activation of the classical pathway or alternative pathway leads to assembly of the C5b678 complex followed by binding of multiple C9 subunits which become the MAC [99]. CD59 acts at the final stages of MAC formation by binding to the C5b678 complex and the first C9 molecule, preventing further C9 polymerization and pore formation [100, 101].

CD59 is associated with the cell membrane via a glycolipid structure which is covalently attached to the C-terminus, known as a glycosyl-phosphatidylinositol (GPI) anchor. With its GPI anchor, CD59 can attach to the outer leaflet of the cell membrane [102]. GPI-anchored proteins, such as CD59, have essential biological functions as GPI-

anchor deficiency is embryonic lethal [103]. Loss of CD59 results in rare paroxysmal nocturnal hemoglobinuria. The absence of CD59 makes erythrocytes more susceptible to destruction leading to complement-induced anemia and hemoglobinuria [103, 104].

CD59 also has multiple glycosylation sites, allowing for many glycoforms [105]. The glycans are proposed to restrict the rotational freedom of the protein on its GPI anchor, thereby stabilizing the active site for the C5b678 complex and C9 [106, 107]. The glycans may also play a role in preventing packing of multiple CD59 molecules of the cell surface [108].

Intermedilysin

Cholesterol-dependent cytolysins (CDCs) are pore-forming bacterial toxins produced by a diverse group of pathogenic Gram-positive bacteria [109]. CDCs are important virulence factors for the bacteria producing them. Toxins of the CDC superfamily form pores in lipid bilayers through the oligomerization of their membrane attack complex/perforin fold domain, although the structure and size of the pore differs slightly between toxins. Most CDCs bind to cholesterol-rich membrane domains via a cholesterol-recognition motif and neighboring undecapeptide. Instead of a transmembrane alpha helix, such binding triggers oligomerization, forming a "pre-pore" prior to insertion, revealing membrane domains and transitioning to the pore state [110].

Cholesterol was thought to be the sole CDC receptor until the discovery of intermedilysin (ILY), as most CDCs use only cholesterol (Figure 1.2 A). Intermedilysin (ILY) is secreted by the bacteria *Streptococcus intermedius* and has been isolated from brain abscesses, liver abscesses and less commonly skin, appendix and dental abscesses

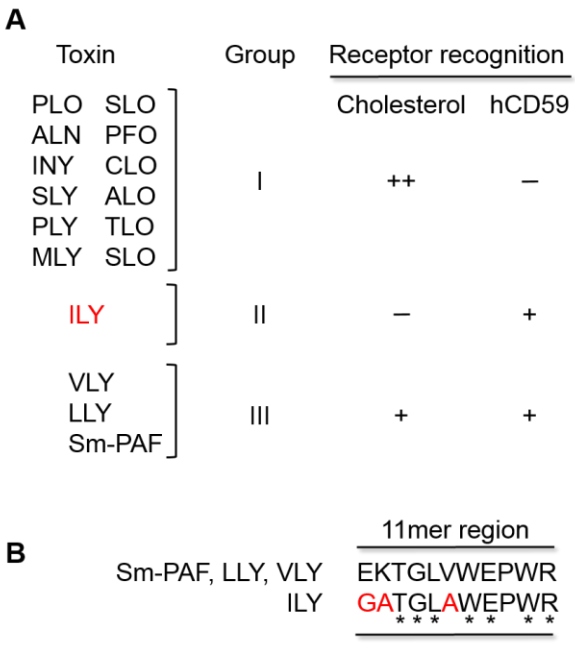

Figure 1.2. ILY and related cytolysins A. CDCs and their respective receptor recognition. **B.** Amino acid sequences of group II and III 11mer region, signature motif for hCD59-binding. ILY differs at the 3 amino acids in red. Amino acids marked with (*) are conserved among all CDCs.

[111, 112]. While ILY is grouped with CDCs, it does not require membrane cholesterol to bind and is active only on human cells [109, 113]. Giddings et al. later demonstrated that ILY uses human CD59 as its membrane receptor [114], but pore formation by ILY still required cholesterol [115]. Three other CDCs, vaginolysin (VLY), lectinolysin (LLY) and *Streptococcus mitits*-derived human platelet aggregation factor (Sm-PAF) have also evolved to recruit hCD59, though these toxins also bind to membrane cholesterol and have a weaker interaction with hCD59 compared to ILY [116]. All of the human CD59-binding CDCs contain the signature motif (undecapeptide or 11mer region) for hCD59 recognition. ILY is distinct from Sm-hPAF, LLY and VLY in this region by 3 amino acids conferring its specificity to hCD59 alone (Figure 1.2 B) [109].

No other proteins are necessary for the binding of ILY to hCD59 [114]. ILY binds to a subset of the residues required for the interaction between hCD59 and the MAC although the interface is reduced compared to the MAC to allow for disengagement from hCD59 [117]. It is this peptide region spanning residues 42-58 [118, 119] that promotes oligomerization of ILY monomers on the cell surface and the structural rearrangements required for pore formation. In contrast, the interaction of cholesterol with the cholesterol recognition motif and undecapeptide is required for the maintenance of the ILY prepore at the membrane as hCD59 is released. ILY disengages from hCD59 during the prepore-to-pore transition [120] [117].

ILY, like most CDCs, is composed of four structural domains (D1-D4) and weighs approximately 50 kDa [109, 113, 121]. Domain 1 at the top of the molecule acts as the foundation for the other domains. Domain 2 is long and thin and acts as the bridge between domains 1 and 4. Domain 3 packs against domain 2 and becomes the β-hairpins prepore, and later, the transmembrane β-barrel pore [122]. Domain 4 at the bottom of the toxin was found to be the protein region responsible for the human specificity of ILY [109] and for cholesterol binding in all CDCs. Domains 1-3 do not contribute to the human specificity of ILY [115], while domain 4 contains membrane binding interface consisting of three loops (L1-L3). At the tip of domain 4, a simple Threonine-Leucine pair in L1 recognizes and binds cholesterol.

After domain 4 of ILY binds to residues 42-58 of hCD59, the ILY cholesterol recognition motif and undecapeptide is oriented to the lipid bilayer, where loops L1–L3 undergo cholesterol-dependent membrane insertion and propagate monomer-monomer interactions [123, 124]. Here, ILY disengages from hCD59 while remaining bound to

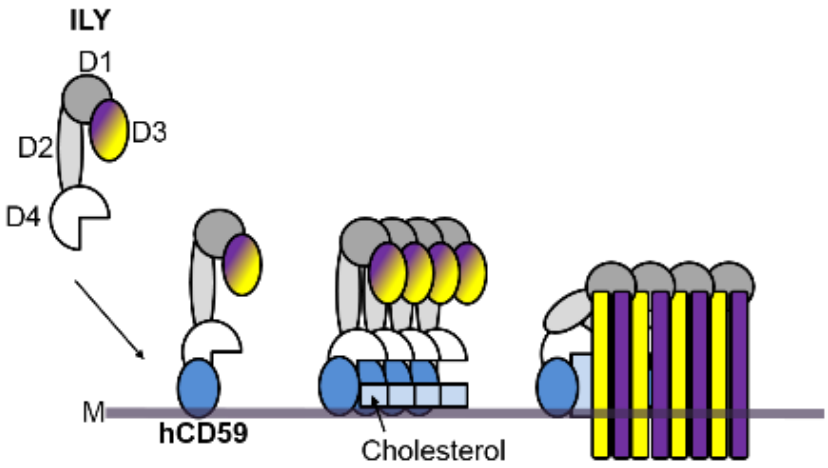

Figure 1.3. ILY binding and pore formation. ILY binds to hCD59 (blue) and interacts with cholesterol to form the prepore. The prepore then converts to the active pore, penetrating the cell membrane. (M).

cholesterol as it undergoes oligomerization. Oligomerization of the prepore changes the interface between domains 2 and 4, causing a rotational shift, supporting domain 2. Domain 2 then bends, weakening its interaction with domain 3. When domain 2 folds overs and completely dissociated from domain 3, the active pore has been generated [125] (Figure 1.3). Removal of membrane cholesterol prevents L1–L3 membrane insertion and appears to trap ILY in an oligomeric prepore state. The final pore contains approximately 45 ILY molecules [126], with a pore size of 300 Å [122] consistent with other CDC pores (Figure 1.4) [125].

Due to its large pore size, ILY generally leads to osmotic lysis of the cell [127], although alternative cell death pathways have been discovered. Specifically, in erythrocytes, ILY induces programmed necrosis or necroptosis [128, 129]. This necroptosis also occurs with other pore-forming toxins, such as streptolysin O and streptolysin S (Streptococcus pyogenes) [130, 131] and RtxA (Kingella kinga) [132] though the pathways are distinct.

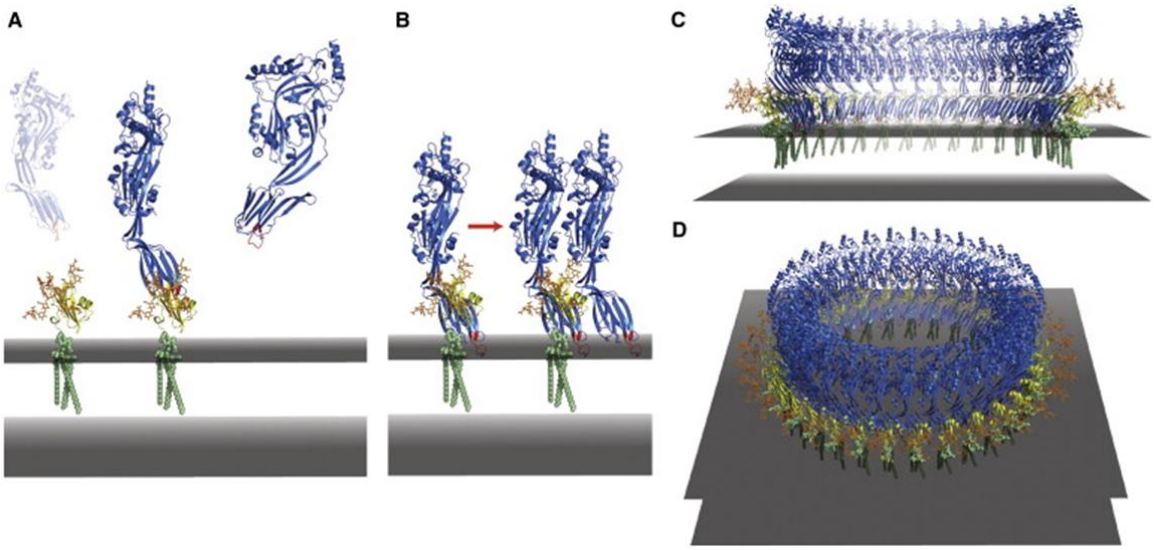

Figure 1.4. Model for ILY pore formation (From Johnson et al. 2013). **A.** Soluble ILY (blue ribbons) targets human cell membranes by binding GPI-anchored CD59 (yellow ribbons). Modeling of CD59 glycosylation reveals that binding is not obstructed by sugars (orange sticks) and that the ILY undecapeptide loop (red) is positioned proximal to the plane of the membrane (gray slab). CD59 GPI anchor is shown in light green. **B.** CD59 coordinates ILY monomers on the membrane through two distinct interfaces, nucleating an early prepore state. **C.** Cross-section through the prepore oligomer. **D.** Full oligomeric ring. Used with permission from Cell Reports.

ILY-mediated ablation in the mouse

To test if conditional and tightly regulated cell ablation could be achieved with dosing of ILY in genetically engineered mice that express human CD59 on specific cell types, two mouse strains were created: one expressing hCD59 on erythrocytes and one with expression on endothelial cells [133]. From these mouse models, many positive features of ILY-mediated ablation emerged. ILY was shown to bind only to erythrocytes expressing human CD59, as wild-type mice were resistant to hemolysis. Furthermore, erythrocytes from cow, chicken, rabbit, rat, mouse, dog, cat, horse, and sheep were all found to be resistant to ILY-mediated lysis [113]. This confirms that ILY is specific for hCD59, suggesting that this system can be used to generate cell ablation models in a variety of

species. Erythrocytes were lysed rapidly within 10 minutes of ILY administration and lysis was dose-dependent with the ability to induce a lethal hemolytic event [133] [134].

The purpose of this work was to extend the application of ILY-mediated ablation to novel species, namely rat and zebrafish, thus demonstrating its utility as an innovative method for rapid conditional targeted ablation in a variety of cell types.

Chapter 2: Materials and Methods

Protocols for generation of transgenic animals and ILY studies were approved by the University of Missouri Institutional Animal Care and Use Committee.

Transgene Design and Generation

*SD-Tg(CD59-HBA1)Bryd (*hCD59^{RBC}*)*

The CD59-HBA1 plasmid was obtained from our collaborator, Dr. Xuebin Qin (Temple University School of Medicine). The approximately 10 kb transgene contains human CD59 cDNA (NM_000611.5) under transcriptional control of the alpha globin promoter with alpha globin gene regulatory elements (locus control region) [135].

SD-Tg(CD59-Ins1)Bryd (RIP-hCD59)

The PGKneobpA plasmid was obtained from Addgene (#13442; Cambridge, MA). The plasmid was digested with *Hind*III and *Xba*I in NEB 2.1 buffer (New England BioLabs, Ipswich, MA) overnight at 37°C to linearize. The 3212 bp fragment was isolated following gel electrophoresis with the Nucleospin Extract II Kit (Macherey-Nagel, Bethlehem, PA). CloneAmp HiFi PCR Premix (Clontech, Mountain View, CA) was used to produce a 622 bp amplicon of the rat insulin 1 promoter (NC_0055100.4, *Rattus norvegicus*) [136] utilizing wild type Sprague-Dawley genomic DNA as the template and the primers RIP-*Eco*RI and RIP-*Hind*III (Appendix). The amplicon included a homology region to the PGKneopbpA backbone at the 5' end and to the hCD59 fragment at the 3' end. The hCD59 fragment was also produced through CloneAmp PCR using a plasmid containing the hCD59 cDNA [133] with the primers hCD59-*Eco*RI and hCD59-*Xba*I (Appendix). The

hCD59 fragment contained homology to the insulin promoter fragment at the 5' end and to the PGKneobpA backbone at the 3' end. The following PCR thermocycler parameters were used for both fragments: 98°C for 10 seconds (s), 50°C for 30s, 72°C for 15s, for 35 cycles. In-fusion HD Cloning system (Clontech, Mountain View, CA) was then used to insert the insulin promoter and hCD59 fragments into the PGKneobpA backbone. Five µl of the In-fusion reaction was used to transform 50 µl of Stellar competent cells (Clontech) following the manufacturer's protocol. Cells were plated on LB agar with ampicillin (final concentration: 100 µg/ml) for positive selection of desired clones. Twenty-four colonies were selected and cultured in LB broth with ampicillin for 15 hours with shaking at 250 rpm at 37^{o}C. Following boiling lysis plasmid preparation [137], 10 µl plasmid DNA was digested with 1 µl *Hind*III, 1 µl *Sac*II, 2 µl NEB3 buffer and 7 µl water for each clone. Three and a half µl gel loading dye (purple, 6x; New England BioLabs, Ipswich, MA) was added to 20 µl of digest and run on a 1% TAE agarose gel at 95 V for 45 minutes with 3 µl GeneRuler 1kb DNA ladder (ThermoFisher Scientific, Waltham, MA). Two clones positive on diagnostic digest were prepared for DNA sequencing using the QIAprep Miniprep kit (Qiagen,Valencia,CA) following the manufacturer's protocol, and were submitted to the DNA Core, University of Missouri (Columbia, MO) for nucleotide sequence analysis using the T7 primer. Clone 22 was confirmed to have the correct insertion. Plasmid DNA was digested with *Hind*III and *Sac*II to isolate the 1308 bp transgene for pronuclear injection.

SD-Tg(CAG-LSL-ZsGreen1-hCD59)Bryd (ihCD59)

Plasmid pCAG-*loxP*STOP*loxP*-ZsGreen1 was obtained from Addgene (#51269). The plasmid was digested with *Sac*I to linearize. CloneAmp HiFi PCR Premix was used to

produce a fragment of P2A and hCD59 with homology arms to the *Sac*I-digested ends of the plasmid with addition of a mutation in ZsGreen to eliminate the stop codon which is necessary for co-expression of both ZsGreen and hCD59 using the P2A peptide. The following PCR thermocycler parameters were used: 98°C for 10 seconds (s), 55°C for 15s, 72°C for 5s, for 35 cycles. The 500 bp amplicon and linearized plasmid were purified following agarose gel electrophoresis using the NucleoSpin Extract II Kit (Macherey-Nagel). In-fusion HD Cloning system (Clontech) was used to insert the P2A-hCD59 element into the ZsGreen plasmid. 2.5 µl of the In-fusion reaction was used to transform 50 µl of Stellar competent cells (Clontech) following manufacturer's protocol. Cells were plated on LB agar with carbenicillin (final concentration: 100 µg/ml) for positive selection of desired clones. Twenty-four colonies were selected and cultured in LB broth with carbenicilin for 15 hours with shaking at 250 rpm at 37°C. Following boiling lysis plasmid preparation [137], 10 µl plasmid DNA was digested with 1 µl *Pst*I, 2 µl NEB3 buffer and 7 µl water for each clone. 3.5 µl gel loading dye (purple, 6x; New England BioLabs) was added to 20 µl of digest and run on a 1% TAE agarose gel at 70 V for 80 minutes with 3 µl GeneRuler 1 kb DNA ladder (ThermoFisher). Four clones positive on diagnostic digest were prepared for DNA sequencing using the QIAprep Miniprep kit (Qiagen) following the manufacturer's protocol, and were submitted to the DNA Core, University of Missouri (Columbia, MO) for nucleotide sequence analysis using the M13 primer (Appendix). Clone 4 was confirmed to have the correct insertion, including the single nucleotide change in the stop codon of ZsGreen and was used for DNA for microinjection. Plasmid DNA was digested with *Spe*I to isolate the 4121 bp transgene for pronuclear injection.

pCS2-hCD59 and mutant hCD59

The pCS2P+ plasmid was obtained from Addgene (#17095). The plasmid was digested with *EcoR*I in NEB cutsmart buffer (New England BioLabs) for 45 minutes at 37°C to linearize. The 4095 bp backbone was isolated following gel electrophoresis with the Nucleospin Extract II Kit (Macherey-Nagel). CloneAmp HiFi PCR Premix (Clontech) was used to produce an 1154 bp amplicon of ZsGreen, P2A peptide and hCD59 utilizing the ihCD59 plasmid (Figure 5.2) as the template and the primers pCS2-iCD59 F and pCS2-iCD59 R (Appendix). The amplicon included a homology region to the pCS2 backbone at the 5' and 3' ends. The following PCR thermocycler parameters were used for both fragments: 98°C for 10 seconds (s), 55°C for 15s, 72°C for 30 s, for 35 cycles. In-fusion HD Cloning system (Clontech) was then used to insert the ZsGreen-P2A-hCD59 fragment into the pCS2 backbone. Five µl of the In-fusion reaction was used to transform 50 µl of Stellar competent cells (Clontech) following the manufacturer's protocol. Cells were plated on LB agar with carbenicillin (final concentration: 100 µg/ml) for positive selection of desired clones. Twenty-four colonies were selected and cultured in LB broth with ampicillin for 15 hours with shaking at 250 rpm at 37ºC. Following boiling lysis plasmid preparation [137], 10 µl plasmid DNA was digested with 1 µl *Pst*I, 1 µl *Ndel*I, 2 µl NEB 3.1 buffer and 6 µl water for each clone. Three and a half µl gel loading dye (purple, 6x; New England BioLabs) was added to 20 µl of digest and run on a 1% TAE agarose gel at 95 V for 45 minutes with 3 µl GeneRuler 1 kb DNA ladder (ThermoFisher). Four clones positive on diagnostic digest were prepared for DNA sequencing using the QIAprep Miniprep kit (Qiagen) following the manufacturer's protocol, and were submitted to the DNA Core, University of Missouri (Columbia, MO) for nucleotide sequence analysis using

the M13 primer. Four clones were confirmed to have the correct insertion; clone 11 was used for mRNA synthesis. Plasmid DNA was digested with *Hind*III-HF and *Not*I-*HF* in cutsmart buffer for 3 hours at 37°C to isolate the 1177 bp transgene. The mMESSAGE mMACHINE® SP6 transcription kit (ThermoFisher) was used to synthesize capped mRNA for microinjection following manufacturer's protocol. Briefly, a transcription reaction was assembled using 2 µl enzyme mix, 1 µg linearized plasmid, 2 µl 10x reaction buffer, 10 µl 2x NTP/CAP, 5 µl nuclease-free water. The reaction was incubated at 37°C for 2 hours then purified using the MEGAclear™ Kit (ThermoFisher).

Mutant (Mut) hCD59 mRNA was generated by modifying the pCS2-hCD59 plasmid to delete the ILY-binding domain of hCD59, 81 bp in length. Utilizing the method described by Perez-Pinera et al. [138], a 25 µl total reaction containing 12.5 µl CloneAmp HiFi PCR Premix, 3 µl 2.5 µM ILY-del F primer, 3 µl 2.5 µM ILY-del R primer, 3.3 µl (100 ng) template pCS2-hCD59 and 3.2 µl water was assembled. The following PCR thermocycler parameters were used: 98°C for 10 seconds (s), 55°C for 15s, 72°C for 30s, for 30 cycles. The QIAquick PCR purification kit (Qiagen) was used prior to ligation and *Dpn*I digestion following manufacturer's protocol. To remove template plasmid, 1 µg of the PCR product was digested with *Dpn*I in cutsmart buffer at 37°C for 1 hour. QIAquick purification was repeated. Ligation of the PCR product was performed using a 20 µl total reaction containing 2 µl 10x T4 DNA ligase buffer (Promega, Madison, WI), 1 µl (143 ng) PCR product, 16 µl water, and 1 µl T4 DNA ligase (Promega). The reaction was incubated at 16°C overnight then inactivated for 10 min at 65°C. To confirm deletion, PCR was performed in a 20 µl reaction containing 4 µl GoTaq Flexi Buffer (Promega), 1.2 µl MgCl2, 3.2 µl 1.25 µM DNTPs, 0.3 µl mutCD59 F primer, 0.3 µl mutCD59 R primer, 0.2 µl GoTaq

(Promega), 9.8 µl water. The following PCR thermocycler parameters were used: 1 cycle at 95°C for 2 min, 35 cycles of 95°C for 30s, 63°C for 30s, 72°C for 30s, and 1 cycle at 72°C for 7 min. Mut hCD59 mRNA was then generated as for pCS2-hCD59 using mMESSAGE mMACHINE SP6 transcription kit (ThermoFisher).

Preparation of insert and microinjection

The inserts were prepared for microinjection through gel purification using the NuceloSpin Extract II Kit following the manufacturer's protocol. Wash and elution buffers were pre-filtered through a 0.02 micron filter (Whatman Anotop 10 plus, Sigma-Aldrich, St. Louis, MO) before use. DNA was injected into the pronucleus of Hsd:SD (Envigo, Indianapolis, IA) 0.5 day embryos at a concentration of 4 ng/µl. Surviving embryos were transferred to SAS SD (Charles River Laboratories, Fredrick, MD) pseudopregnant recipients as described in rat embryo collection and transfer.

Rat Embryo Collection and Transfer

For embryo collection, sexually immature (approximately 5 weeks old, 80 g body weight) female SD:Hsd (Envigo) rats were injected IP with 0.2 ml (20 IU) P.G. 600 (cat # 16820; Valley Vet, Marysville, KS) diluted with sterile saline on day 1 at 0900. SD was used due to the ease of use of this outbred stock in transgenic animal generation, its high fecundity, and its utility as a pharmacological and toxicity model. On day 3, rat embryo donors received a second injection IP of 0.2 ml (40 IU) human chorionic gonadotropin (hCG) (EMD Millipore, Billerica, MA) at 1100 and were mated with proven SD:Hsd stud males. Female 2- to 4-month old SAS SD (Charles River) embryo recipients were synchronized

using 0.2 ml IP (40 µg) leutinizing hormone releasing hormone (LHRH) (Sigma, Saint Louis, MO) at 0900 and were mated with vasectomized male rats 4 days later.

The next morning after mating, donor rats were euthanized and oviducts were removed to a plate containing a 50 µl drop of hyaluronidase (1mg/ml) for each oviduct to release the zygotes and remove attached cumulus cells. Embryos were then transferred to HEPES with BSA (4 mg/ml) for microinjection. Recipients were anesthetized using 5.5 mg ketamine and 1mg xylazine per 100 g body weight IM. Injected embryos were transferred to recipients surgically through a midline dorsal skin incision followed by bilateral exposure of the oviducts. If needed, 10% epinephrine was applied to the ovarian bursa for hemostasis. Using a 125 µl stripper tip pipette, embryos were transferred to the oviduct via infundibular approach. The skin incision was closed with a metal wound clip which was removed 7 days post-surgery.

Genotyping

DNA from tail snip biopsies collected from 2 week old rats was extracted using the Extract-N-Amp Tissue PCR Kit (Sigma-Aldrich). Each 0.5 cm tail snip was incubated with 50 µl of extraction solution with 12.5 µl tissue preparation solution for 10 minutes at room temperature, followed by 5 minutes at 95ºC using a heat block. Then 50 µl neutralization solution B was added to each sample before removing 200 µl for the genotyping assay. Genotyping assays were optimized to detect 0.1 copies of the transgene using plasmid DNA in 20 ng SD WT DNA. The expected amplicon size and primers used to identify transgene-positive animals were as follows: 400 bp, hCD59 F and hCD59 R for SD-Tg(CD59-HBA1)Bryd; 772 bp, RIP-hCD59 F and RIP-hCD59 R for SD-Tg(CD59-

Ins1)Bryd; 935 bp, iCD59 F and iCD59 R for SD-Tg(CAG-LSL-ZsGreen1-hCD59)Bryd (Appendix).

PCR was performed in 20 µl reactions containing: 30-40 ng genomic DNA, 10 µl Extract-N-Amp PCR reaction mix and 0.3 µl each of 25 µM primers. Reactions were performed in 200 µl thin walled PCR tubes and thermocycler parameters were 1 cycle at 95°C for 4 min 30s, 34 cycles of 94°C for 30s, 57.9°C for 30s, 72°C for 30s, and 1 cycle at 72°C for 10 min. Products were analyzed using the QIAxcel Advanced capillary electrophoresis system with the QIAxcel DNA Screening Kit, QX Alignment Marker 15 bp/3 kb, XQ DNA Size Marker 100 bp-2.5 kb. The AM320 Injection Method with injection of 10s at 5 kV and separation of 320s at 6 kV was used.

For digital droplet PCR (ddPCR), genomic DNA was extracted from liver or tail using the Qiagen DNeasy blood and tissue kit. All primers and probes were ordered from Integrated DNA Technologies (Coralville, IA). Each PCR reaction consisted of a 26 µl solution containing 13 µl ddPCR supermix for probes (Bio-Rad), 480 mM primers for ZsGreen and rat gamma-glutamyltransferase 1(*Ggt1;*NC_005119.4)(Appendix), 192 mM probe (Appendix), 3 µl template DNA (10 ng/µl) and 1.25U *Mse*I restriction enzyme. Droplets (~14,000/reaction) were generated on the Bio-Rad QX-200 following the manufacturer's instructions. Samples were transferred on a 96-well plate and thermal cycled to the endpoint (C1000 Touch Thermal Cycler; Bio-Rad) using a standard protocol; initial denaturation at 95°C for 10 min, followed by 40 cycles of melting at 94°C for 30s and annealing/elongation at 60°C for 1 minute, before droplet stabilization by 10 min incubation at 98°C. After cycling, the 96-well plate was immediately transferred on a QX200 Droplet Reader (Bio-Rad) where flow cytometric analysis determined the fraction

of PCR-positive droplets vs. the number of PCR-negative droplets in the original sample. Data was analyzed using Poisson statistics to determine the target DNA template concentration in the original sample.

Flow Cytometry

Whole blood was collected from human, the *hCD59*^{RBC} founder rat, and a transgene-negative littermate into heparinized microhematocrit tubes. Blood was then transferred to 1.5 ml microfuge tubes with 1 ml DPBS. Samples were centrifuged at 5000 x g for 5 min to pellet erythrocytes. The supernatant was removed and the erythrocyte pellet was washed twice with 1 ml DPBS followed by centrifugation until the supernatant was clear. Erythrocytes were then incubated with 1:200 mouse anti-human CD59 antibody (MAB1759; Millipore, Bellerica, MA). Cells were washed with DPBS then incubated with 1:200 Alexa Fluor 750-conjugated donkey anti-mouse IgG antibody (ab175738; Abcam, Cambridge, MA). Controls were incubated with either primary or secondary antibody only. Samples were analyzed with a Beckman Coulter CyAn ADP Flow Cytometer (Indianapolis, IN).

Cell culture

Cell culture experiments were performed using CRL-2057 RIN-m cells (ATTC, Manassas, VA). Cells were cultured in 25 cm^2 or 75 cm^2 sterile flasks (ThermoFisher) containing RPMI-1640 medium (ATCC 30-2001), fetal bovine serum (final concentration of 10%; ATCC 30-2020) and penicillin-streptomycin solution (final concentration 50 IU/mL penicillin and 50 μg/mL streptomycin; ATCC 30-2300). Cells were passaged 2-3 days before nucleofection and after reaching 70-85% confluency. DNA electroporation was

performed using the Nucleofection 4D System (Lonza Ltd, Basel, Switzerland) set to program DE130 and following the general protocol for adherent cells available from the manufacturer. Briefly, cells were harvested and suspended with tripLE (ThermoFisher) and counted. Cells were centrifuged at 90 x g at room temperature for 10 minutes then resuspended in room temperature nucleofection solution SF (Lonza) to a final concentration of 3 $x10^6$ cells per 100 µl. For each nucleofection, 100 µl of cell suspension was mixed with 5 µg of ihCD59 plasmid (2 µg of maxGFP control plasmid from Lonza). Controls included an untreated well (cells with solution and DNA but no nucleofection program) and no DNA control (cells with solution and program but no DNA). Samples were then transferred to cuvettes and were quickly transferred to a 6-well culture plate containing RPMI media after the nucleofection program. After 24 hours, TAT-Cre recombinase (EMD Millipore) was added to induce ZsGreen/hCD59 expression at a final concentration of 4 µM. Expression of GFP/ZsGreen was monitored via fluorescent microscopy at 30 minutes, 1 hour, 2 hours, and 3 hours post addition of TAT-Cre. Uninduced cells had DPBS added instead of TAT-Cre. TAT-Cre was removed after 3 hours and media renewed. ILY was added 48 hours after nucleofection at a final concentration of 10 ng/µl in DPBS. Control wells had DPBS with no ILY added. Cells were incubated with ILY at 37°C for 20 minutes with shaking at 75 rpm then imaged using a Nikon eclipse TS100 inverted scope (Melville, NY) and Nikon intensilight C-HGFI fiber illuminator.

Administration of ILY

His-tagged recombinant ILY was produced as described previously [114] and provided by our collaborator, Dr. Xuebin Qin (Temple University School of Medicine). ILY was expressed in *E. coli*, and purified with a His-column as described in Hu et al [133].

Endotoxin was completely removed by Endotoxin Removing Gel (Cat#20339, Pierce, Rockford, IL). To assess the activity of each lot of ILY before *in vivo* administration, ILY activity was tested via the *in vitro* hemolytic assay described below and in Hu et al [133].

All experimental rats were weaned at 3 weeks old and were housed 2-3 rats per cage on ventilated racks (Thoren, Hazelton, PA) with Paperchip bedding (Sheperd, Watertown, TN) and Nestlets (Ancare, Bellmore, NY) as enrichment. They were fed LabDiet 5008 (St. Louis, MO) ad libitum and provided acidifed water (pH 2.3-3.0). All animals were housed in the same room under the following room conditions: 70-74°F, 40-70% humidity, and 14:10 light:dark cycle.

In vitro hemolysis assay

Three *hCD59*^{RBC} Tg+ (2 males, 1 female) and three Tg- littermates (2 females, 1 male) at approximately 8 weeks old were used for the *in vitro* hemolysis assay. Rat blood was collected by venipuncture from lateral saphenous vein into heparinized microhematocrit tubes. Blood was washed with DPBS and centrifuged at 3000 x g for 5 min at room temperature to isolate erythrocytes. Erythrocytes were incubated with serially-diluted ILY at 37°C for 30 min. The OD_{415nm} of the supernatants was measured using a Bio-Rad plate reader (Hercules, CA) to detect free hemoglobin.

The *in vitro* hemolysis assay was also performed as described above with the incubation of Tg+ erythrocytes at 37°C or 28°C for 45 minutes.

SD-Tg(CD59-HBA1)Bryd

One founder was generated and crossed to Hsd:SD to establish rat stock SD-Tg(CD59-HBA1)Bryd. This rat stock (RRRC#754) is available through the Rat Resource and

Research Center (www.rrrc.us). For convenience, we refer to the rat line as *hCD59*^{RBC}. All rats used in this study were either hemizygous for the transgene (Tg+) or transgene-negative littermates (Tg-). Rats 6-8 weeks old, weighing 120-200 grams, were randomly assigned to dose groups and ILY was administered in equivalent volumes via intravenous tail (11 Tg+ females, 12 Tg+ males, 2 Tg- females, 2 Tg- males) or intraperitoneal injection (4 Tg- females, 3 Tg+ females). Blood was collected from lateral saphenous vein into heparinized microhematocrit tubes. Tubes were centrifuged at 9000 x g for 5 minutes and percent packed cell volume was quantified using a Critocaps Micro-Hematocrit Tube Reader (Thomas Scientific, Swedesboro, NJ). Plasma was diluted 1:4 with DPBS and analyzed using Bio-Rad plate reader at OD_{415nm}. Rats were euthanized via CO_2 inhalation and tissues were immediately collected and placed in 10% formalin fixative for 24 hrs. Tissues were then paraffin-embedded, sectioned, stained with hematoxylin and eosin or Carstairs' method for fibrin and platelets [139].

SD-Tg(CD59-Ins1)Bryd

Rats hemizygous for the transgene were used for all *in vivo* experiments with ILY. Blood glucose was tested in each rat by collecting a drop of blood from the lateral saphenous vein and reading with OneTouch UltraMini Meter (OneTouch, Shelton, CT).

SD-Tg(CAG-LSL-ZsGreen1-hCD59)Bryd

Rats hemizygous for the ihCD59 transgene were crossed to LE-Tg(TH-Cre)3.1Deis [140] (RRRC #659) available from the Rat Resource and Research Center. Rats hemizygous for both transgenes are referred to as TG. Control rats were negative for either or both transgenes. ILY was administered at a dose of 500 ng/g BW IP at 3 weeks of age. Rats

were then tested in the cylinder test at 12 weeks of age. For the cylinder test, rats were placed in an acrylic cylinder and behavior was recorded for 5 minutes. ANY-maze behavior tracking software (Stoelting Co., Wood Dale, IL) was used to record the rats and score number of rears (fore paws leaving the ground), time spent grooming and number of hind limb steps. The test was repeated for a total of 3 trials per rat with a minimum 10 minute rest between trials.

Intracerebroventricular (ICV) injection of ILY

ILY was also administered to TG and control rats 10-12 weeks old via intracerebroventricular (ICV) injection. For ICV injections, rats were anesthetized with using 5.5 mg ketamine and 1mg xylazine per 100 g body weight IP. The rats were then mounted into a stereotaxic frame (Stoelting Co.) and the dorsal skull was clipped and scrubbed with povidone iodine and ethanol. A scalpel was used to make a 1 cm incision on midline, exposing the sutures of the skull. The stereotaxic coordinates (from bregma) of A/P -0.4 , D/V -3.5, and M/L +1.4 were used to make a 1mm hole in the skull using a rotary saw with a 1 mm burr tip (Dremel, Racine, WI). A 10 µl Hamilton syringe was used to deliver either 10 µl or 1 µl of ILY to the right lateral ventricle. The needle was lowered and raised at a rate of 0.2 mm per second and the needle was left in place for two minutes before and after injection. As the needle was removed a cotton-tipped applicator was used to apply pressure to the injection site. The skin incision was closed using 4-0 multifilament braided suture matieral in a continuous horizontal mattress pattern. Rats were monitored twice daily post-injection for clinical signs.

Behavior testing

Open traveled) was measured over 10 field motor activity (locomotion, total distance minutes in ICV-injected TG and control rats. The apparatus used was a standard 4-rat open field activity box (100 cm x 100 cm). Rats were recorded overhead with dimmed light conditions. Each rat was tested on days -1, 1, 3, 7, 15 with day 0 being day of surgery and ICV injection. For tapered ledged beam test, rats were first trained for 3 days to traverse the beam over 4 trials per day. The beam apparatus measured 165 cm long and tapered from 6 cm to 1.5 cm in width. A 0.5 cm ledge extended from the sides of the beam to prevent a fall due to missteps. Rats traversed the beam at an approximately 10 degree incline toward a rat cage with their cage mates present. On testing days, rats received four trials and number of left and right hind foot slips was recorded, noting where slips occurred on the beam (zone 1, 2, or 3). The water maze test was a black circular pool (218 cm in diameter) conceptually divided into four equal quadrants for the purpose of data analysis. The water temperature was approximately 20°C. Two cm below the surface of the water was a clear circular platform (10 cm diameter) hidden from the rats' view by tinting the pool water with white acrylic paint. The swimming path of the rat was recorded in the test session using a video camera mounted above the center of the pool and analyzed using AnyMaze behavior software. The water maze was enclosed by white curtains with several external visual cues (yellow star, red circle, and blue square). On each day, rats received two consecutive trials on days 9 through 14 post-surgery. A different starting location was used each trial, which consisted of swimming followed by sitting on the platform for 30 seconds. Any rat that did not find the platform within 90s was given a score of 90 and was guided to the platform by the experimenter. Memory retention was evaluated 24 hours after

the last training trial in a 30s probe task in the absence of the escape platform. The time spent in the target quadrant was recorded. On days when multiple tests were performed, locomotor was performed first, followed by tapered beam and water maze with a minimum 1 hour rest between tests. Rats were weighed after each day of behavior testing.

Brain collection and imaging

Sixteen days after ILY injection, rats were euthanized via CO_2 inhalation followed by exsanguination via cardiac puncture. The jugular vein was severed and perfusion with 60 ml saline following by 60 ml 4% paraformaldehyde was performed via the left ventricle of the heart. Brains were removed and post-fixed in 4% paraformaldehyde for 24 hours. Brains were then moved to 30% sucrose and stored at 4°C. The substantia nigra and ventral tegmental area were sectioned using a cryostat set to -20°C and 40 µm section thickness. Free-floating sections were placed into 24-well culture plates containing PBS. Sections were placed onto slides and mounted with ProLong Diamond Antifade Mountant with DAPI (ThermoFisher). Slides were stored at 4°C protected from light. Sections were imaged using a wide-field microscope. ZsGreen-positive neurons were counted using ImageJ software (https://imagej.nih.gov/ij/).

For immunohistochemistry (IHC) staining, 40 µm free-floating sections were incubated with mouse anti-hCD59 PE-conjugated antibody 1:400 (eBioscience, San Diego, CA) overnight at 4°C and protected from light. Sections were washed 3 times for 5 mins each in DPBS. Sections were then mounted on glass microscope slides and mounted using ProLong Diamond anti-fade as above.

Zebrafish

For salt tolerance testing, embryos were exposed to a range of NaCl salt concentrations in E3 media (Appendix) at 10 hours post fertilization (hpf) overnight (14 hours).

For temperature tolerance testing, wild type zebrafish embryos (n=100) were collected and aged to 28 hpf in egg water (Appendix). Fifty embryos (control) were incubated at 28.5°C and 50 embryos were incubated at 37°C in a dry incubator for 60 minutes. Fish were then monitored daily until 72 hpf.

For ILY immersion, embryos at 24 hpf were dechorionated by incubating for 5 mins at 28°C in pronase (Sigma-Aldrich) diluted to 2mg/mL with egg water. Embryos were then rinsed 5 times in egg water and transferred to a 96-well plate, one embryo per well. ILY was then added to each well for a final concentration of 2 pM to 400 pM followed by incubation at 37°C for I hour. Mortality was assessed by touching each embryo with forceps and detecting movement.

Zebrafish embryos were microinjected at the one-cell stage with 1200 pg ihCD59 mRNA, mutant iCD59 mRNA, or GFP mRNA. Uninjected embryos from the same clutch were used as controls. Following injection, embryos were moved to a 24-well tissue culture dish, 10 embryos per well, containing 1 mL E3 supplemented with 90 mM NaCl. ILY or saline control was added to embryos aged at 10, 24 and 36 hpf. Embryos were incubated at 37°C for up to 1 hour. Mortality was assessed at 20 minutes, 1 hour, and 1 day following ILY immersion.

For intraperitoneal (IP) injection, adult fish were anesthetized with clove oil (Appendix) and placed in dorsal recumbency on a moistened sponge restrainer. A 28g Hamilton syringe was used to deliver either 6 µl (500 ng/g body weight) of ILY, heat-inactivated ILY, or

saline into the peritoneal cavity or given a sham needle poke. Fish were recovered in system water and monitored twice daily for morbidity and mortality.

Chapter 3: A novel rat model of intravascular hemolysis

Chapter 3 was published in Physiological Genomics and been included in this dissertation with permission from the American Physiological Society.

Hanson MM, Liu F, Dai S, Kearns A, Qin X, Bryda EC. *Rapid conditional targeted ablation model for hemolytic anemia in the rat.* Physiological genomics. 2016; 48 (8):626-32.

Introduction

A variety of methodologies have been used to selectively ablate tissues and specific cell types in animal models including microdissection, laser-based techniques, the use of chemicals and antibodies and genetic approaches [141]. An example of one such effective strategy for cell ablation is the use of human CD59 (hCD59) and intermedilysin (ILY) [133, 134]. Human CD59 is a cell membrane receptor which inhibits formation of the membrane attack complex during complement activation [114]. Intermedilysin (ILY), a toxin produced by the human pathogen, *Streptococcus intermedius*, binds specifically to hCD59 inducing pore-formation and cell lysis [113]. Previous work has shown that by engineering mice which express hCD59 on a cell type of choice, lysis can be induced rapidly through administration of ILY [133, 142]. The hCD59-ILY system has many advantages: 1) cell ablation occurs rapidly and specifically; 2) cell lysis is dose-dependent; 3) humans have antibody to ILY, making it a relatively inert toxin with little lab safety concerns [133]. The effectiveness of the hCD59-ILY cell ablation system was first demonstrated in a conditional mouse anemia model and has since been used to generate

additional mouse models that allow specific ablation of immune, epithelial or neural cells [133, 142].

To extend this work to another animal model species, we chose to test the effectiveness of the hCD59-ILY system by creating a rat anemia model. The rat remains the ideal model for the study of cardiovascular physiology and pathology, hypertension, and related diseases due to its size and associated wealth of historical data. Additionally, rats are the pre-dominant species used by the pharmaceutical industry, making them more appropriate for drug and therapy trials [143-145]. Transgenic technologies have recently advanced for efficient production of genetically engineered rats removing previous barriers to generating desired models in the rat [26, 27]. Despite such advances, there are currently no conditional genetic rat models of anemia.

Appropriate animal models are necessary to understanding the pathophysiological effects of anemia and for development of therapies. To this end, several rodent models have emerged to study intravascular hemolysis, anemia and life-threatening sequelae. Phenylhydrazine (PHZ) has been used in rats and mice to induce hemolysis, though it requires repeated injection for induction [21, 22]. PHZ has also been shown to act as a mitogen, stimulating lymphocytes and monocytes four days following injection [24, 25]. While PHZ-treated mouse erythrocytes can be used to model cell deformability, aggregability was inhibited in contrast to the marked aggregability seen with thalassemia patients [146]. 2-butoxyethanol (BE) administration in rats induces hemolysis and thrombosis similar to patients with hemolytic anemias, though similar to PHZ, requires repeated administration to achieve anemia [23, 147-150]. Response of BE in rats is delayed, variable and age-dependent with younger rats exhibiting more resistance to

hemolysis [26]. Unfortunately, both PHZ and BE are hazardous substances which must be handled carefully to avoid human exposure [27, 28]. Therefore, there is a need for a genetic based model which can specifically ablate erythrocytes in a rapid manner without off target effects or human health concerns.

Our studies described here demonstrate that the hCD59-ILY ablation system is effective across species by describing the generation of the first conditional genetically engineered rat model of intravascular hemolysis.

Results

Generation of SD-Tg(CD59-HBA1)Bryd rats

In order to generate a rat strain that expressed human CD59 specifically on erythrocytes, a total of 544 Sprague-Dawley (SD) zygotes were injected with the transgene, resulting in 72 live pups with one female founder animal (Table 3.1). The hCD59 transgene contained the expected sequence and included a signaling peptide (Figure 3.1). Founder rats were identified using the genotyping assay described in the methods section and was confirmed to have sensitivity to 0.1 copies of the transgene (Figure 3.2). The colony was maintained by mating hemizygous transgene positive animals to wild-type Hsd:SD animals, either in pairs or trios, to maintain as an outbred stock. Both male and female rats are fertile and litter size averages 12 pups per litter with expected Mendelian inheritance. No abnormalities in transgene positive animals were noted up to 1 year of age by means of gross necropsy. No sex difference was observed in baseline hematocrit or response to ILY (data not shown), therefore both sexes were used for all experiments. Rats are available through the Rat Resource and Research Center (stock RRRC#754; www.rrrc.us).

Signaling peptide
ATG GGA ATC CAA GGA GGG TCT GTC CTG TTC GGG CTG CTG CTC GTC CTG

GCT GTC TTC TGC CAT TCA GGT CAT AGC Mature peptide CTG CAG TGC TAC AAC TGT CCT

AAC CCA ACT GCT GAC TGC AAA ACA GCC GTC AAT TGT TCA TCT GAT TTT

GAT GCG TGT CTC ATT ACC AAA GCT GGG TTA CAA GTG TAT AAC AAG TGT

TGG AAG TTT GAG CAT TGC AAT TTC AAC GAC GTC ACA ACC CGC TTG AGG

GAA AAT GAG CTA ACG TAC TAC TGC TGC AAG AAG GAC CTG TGT AAC TTT

AAC GAA CAG CTT GAA AAT GGT GGG ACA TCC TTA TCA GAG AAA ACA GTT

CTT CTG CTG GTG ACT CCA TTT CTG GCA GCA GCC TGG AGC CTT CAT CCC TAA

Figure 3.1. cDNA sequence of human CD59 with signaling peptide (green) and mature peptide (gold).

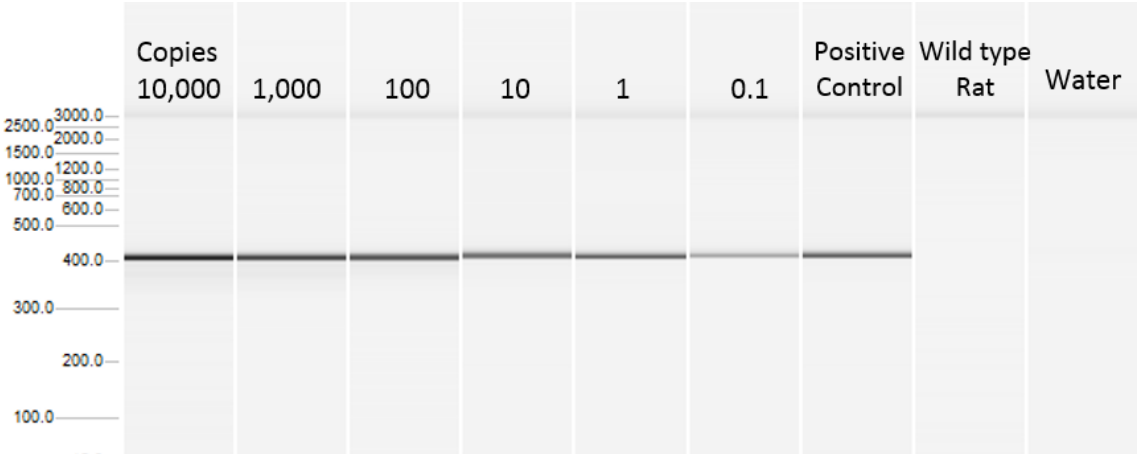

Figure 3.2. Optimization of PCR genotyping assay for hCD59RBC. WT SD genomic tail DNA was spiked with decreasing amounts of plasmid. Positive control: 40 ng DNA from mouse *hCD59*^{RBC} model [133].

Table 3.1. Efficiency of transgenesis for SD-Tg(CD59-HBA1)Bryd	
Number of embryos injected	544
Total number of post-injection live born rats (%)	72
Number of transgene-positive rats (%)	1/72 (1.39)

Expression of hCD59 on erythrocytes

Flow cytometry was used to confirm expression of human CD59 on transgene-positive rats (Figure 3.3A-C). HumanCD59-specfic antibodies coupled to FITC were incubated with human erythrocytes (positive control), Tg- rat erythrocytes (negative control) and Tg+ rat erythrocytes. Tg+ rats had an increase in fluorescence (95%) compared with 0% in Tg- rats (Figure 3.3B-C). Expression of hCD59 on Tg+ erythrocytes was similar to the human positive control sample (Figure 3.3A).

ILY-mediated hemolysis

Erythrocytes isolated from Tg+ rats were sensitive to ILY-mediated lysis in a dose-dependent manner. *In vitro* incubation with ILY induced significant lysis at and above 31.5 pM ($p<0.005$) compared to Tg- rat erythrocytes (Figure 3.4A). Even at the highest tested concentration of 1000 pM, there was no lysis observed in Tg- erythrocytes, indicating that ILY does not bind to rat CD59, consistent with previously published results [133]. Similarly, Tg- rats injected with 100 ng/g body weight (BW) intravenously maintained a normal packed cell volume (PCV) with a pre-dose mean PCV of 51.25% ± 1.1 SEM and 5 days post-dose PCV of 47.25% ± 0.9 SEM (Figure 3.4B).

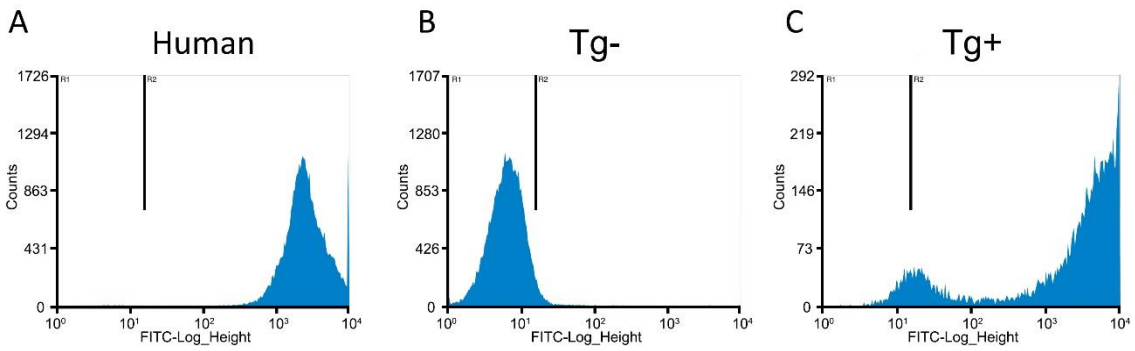

Figure 3.3. SD-Tg(CD59-HBA1)Bryd rats express human CD59. FACS analysis of erythrocytes isolated from (A) human (positive control), (B) Tg- rat (negative control), and (C) Tg+ rat. Erythrocytes in R2 are positive for hCD59.

In contrast, Tg+ rats injected with the same dose of ILY experienced rapid hemolysis and death in 2 out of 3 rats within minutes of injection. PCV's for the 2 dying rats measured 0% as there were no intact red cells observed in the samples.

The remaining rat had a minimal PCV of 13% which then began to recover over the next 5 days post-injection with a PCV of 37% (Figure 3.4B). When ILY was injected intravenously at doses below 50 ng/g BW to Tg+ rats, no significant decrease in hematocrit was observed compared to saline-injected controls (Figure 3.4C). However, at higher intravenous doses (range 52-200 ng/g BW), rats became anemic within 10 minutes, as evidenced by a mean reduction in hematocrit of 43% ± 2.6 SEM compared to 8.667% ± 3.4 SEM in the saline controls (Figure 3.4C). At doses above 100 ng/g BW IV, rats were ataxic, tachypneic, and laterally recumbent within minutes after injection. Hemoglobinemia (Figure 3.4D) and hemoglobinuria (data not shown) was present as soon as 10 minutes post injection (MPI) in Tg+ rats but not Tg- rats. Plasma OD readings at 415 nm showed a significant increase ($p=0.016$) in plasma hemoglobin (hemoglobinemia) in Tg+ rats after ILY treatment compared to unaffected Tg- rats (Figure 3.4E).

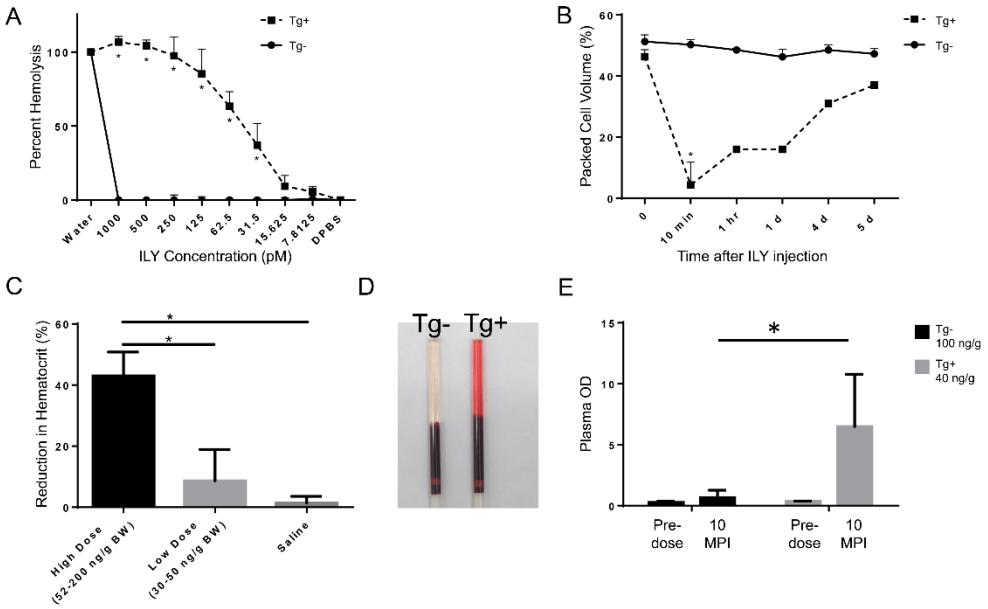

Figure 3.4. ILY induces rapid and dose-dependent intravascular hemolysis. (A) *In vitro* assay of Tg- (n=3) and Tg+ (n=3) erythrocytes incubated with ILY performed in triplicate. * *P*<.01 *t* test. MPI=minutes post-injection, DPI=days post-injection. (B) Packed cell volume over time of Tg- (n=4) and Tg+ (n=3) rats dosed with 100 ng/g BW ILY intravenously **P*< .001 *t* test. (C) Dose-dependent reduction in hematocrit 10 minutes post ILY intravenous injection or saline control in Tg+ rats (high dose n=9; low dose n=9; saline n=5). **P*<.0001 One-way ANOVA. (D) Hemoglobinemia of Tg+ rat dosed 10 MPI with 40 ng/g BW ILY compared to Tg- dosed with 100 ng/g BW ILY (E) Measurement of plasma OD415 before ILY treatment and 10 minutes after

Anemia and thrombosis

To test the effects of ILY via a non-vascular route of administration, we dosed Tg- rats with 500 ng/g BW ILY via intraperitoneal injection. All Tg- rats survived with no clinical signs observed. Hematocrits remained within the normal range with a pre-dose mean PCV of 43.5% (± 1.3 SEM) and 5 DPI mean PCV of 48.5% (± 1.5 SEM)(Figure 3.5A). We also treated Tg+ rats with ILY at the same dose (500 ng/g BW) via intraperitoneal injection (Figure 3.5A). The Tg+ rats had relatively normal hematocrits at 10 minutes post injection (mean 42.667% ± 0.9), however, 24 hours later, one rat was found dead and the remaining two were found moribund and were euthanized.

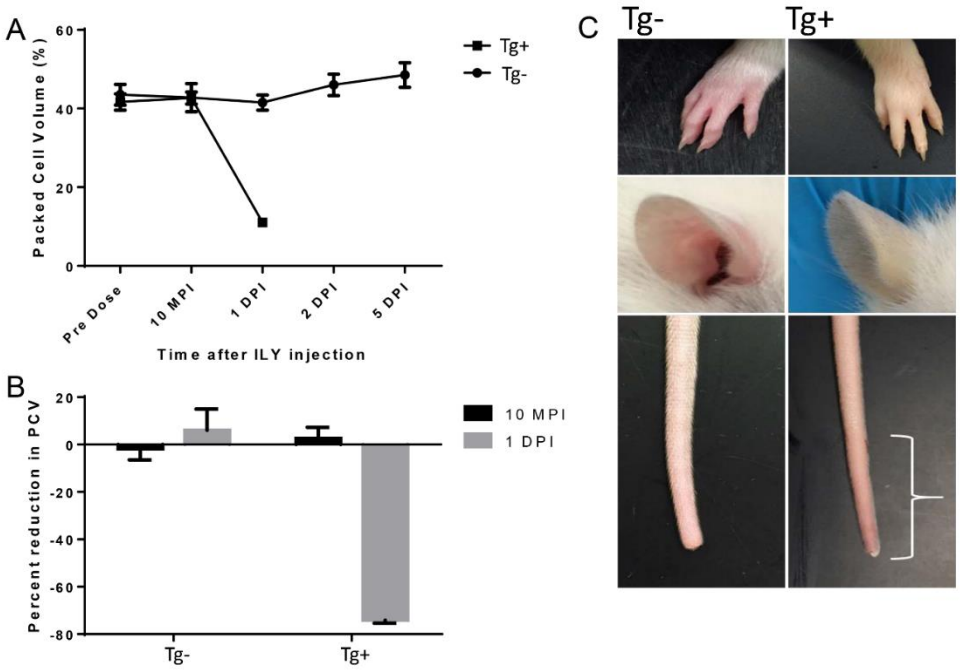

Figure 3.5. Effect of high intraperitoneal doses of ILY on phenotype. (A) Packed cell volume of Tg- (n=4) and Tg+ rats (n=3) given intraperitoneal ILY at 500 ng/g BW. (B) Change in hematocrit over time in rats dosed IP with ILY at 500 ng/g BW. (C) Gross images of control and Tg+ rats 1 day post ILY treatment. Note paleness of paw and ear pinna in Tg+ compared to Tg-. The tail tip of the Tg+ rat had mild reddening (white bracket).

Hematocrit at time of euthanasia was 11% (mean reduction in PCV of 74.085% ± 0.9) (Figure 3.5B). Grossly, the pinna and feet were markedly pale compared to Tg- cage mates. The distal third of the tail was mildly reddened as a result of early ischemia (Figure 3.5C).

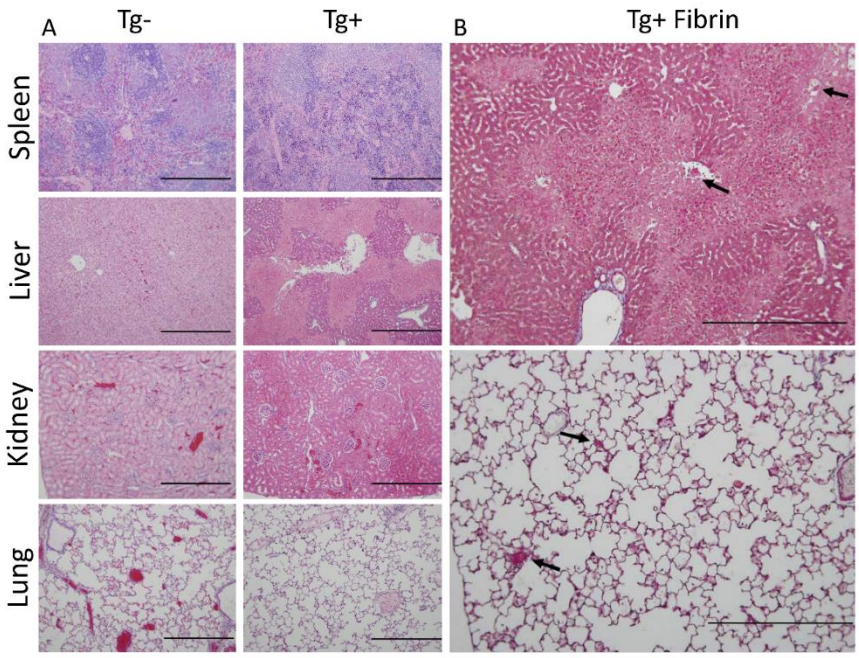

Figure 3.6. Histopathological changes in Tg+ rats 24 hours after ILY administration. (A)Hematoxylin and esosin-stained sections from spleen, liver, kidney and lung of Tg- and Tg+ rats dosed with 500 ng/g BW ILY IP. (B) Liver (upper image) and lung (lower image) from Tg+ ILY-treated rat stained with Carstairs' method to detect fibrin and platelets. Black arrows denote microthrombi. Scale bar=50 µm. Images were taken using a Zeiss Axiophot microscope (Germany), 10x/0,30 Zeiss dry objective (100x total magnification) with Olympus DP-70 camera and acquisition software (Melville, NY).

We further examined the pathophysiologic characteristics of ILY-treated Tg+ rats in tissue sections. After 24 hours, the livers, spleens, kidneys and lungs from Tg+ and control rats were removed and processed for histological analyses. Thrombi and anemia were evident in the Tg+ kidneys and lungs with proteinaceous debris and heme deposits (Figure 3.6A). The Tg+ spleens exhibited red pulp depletion and hematopoiesis (Figure 3.6A). In contrast, ILY-treated Tg- rats had no significant lesions (Figure 3.6A; left images). Upon staining for fibrin (Carstair's method), there was evidence of severe acute multifocal hepatic necrosis with multiple thrombi present within hepatic and pulmonary vessels (Figure 3.6B) in Tg+ rats.

Discussion

Our findings demonstrate the utility of the hCD59-ILY system in development of a rapid conditional targeted ablation model in the rat. Transgenic rats positively expressed hCD59 on erythrocytes. Erythrocytes isolated from Tg+ rats lysed in a dose-dependent manner while control erythrocytes were unaffected, highlighting the specificity of ILY to human CD59, even at high doses. When ILY was administered to Tg+ rats intravenously, lysis occurred rapidly within 10 minutes of dosing. By inducing intravascular hemolysis rapidly, compensatory mechanisms are prevented from confounding pathologic sequelae. The degree of anemia can be controlled by the dose of ILY given allowing researchers to induce mild to severe anemic phenotypes depending on research goals (Figure 3.4C). The *hCD59*^{RBC} rat phenotype mimics human clinical manifestations of intravascular hemolysis, including anemia, hemoglobinemia, hemoglobinuria and histopathological lesions of proteinaceous debris, heme deposits, microthrombi, and sudden death. Tg- rats administered ILY had no gross or microscopic lesions.

Of note, one rat did survive the 100 ng/g BW dose, exhibiting a minimum hematocrit of 13% and recovering to 37% 5 DPI. Due to technical difficulties this rat received the ILY injection over a longer period of time compared to other injected animals. This slower administration is consistent with a previous study in the hCD59+ mouse whereby mice injected slowly survived a dose which was lethal when ILY was administered as a bolus [134]. Therefore, researchers utilizing this model should be cognizant of duration and rate of ILY administration.

The intraperitoneal dose route was five times higher than the lethal intravenous though it did not immediately induce death. This could be due to the first pass effect of

intraperitoneal injections compared to direct delivery of ILY to the targeted erythrocytes. This delayed ablation of erythrocytes observed at the 24 hour time point, however, still resulted in mortality and a severe anemia with histopathological changes. Depending on the goals of the researcher, intraperitoneal injection may be preferred over intravenous tail injection, even though the intraperitoneal route of administration may require more ILY to mediate the desired outcome.

The hCD59-ILY system is easy to use and has many advantages to researchers studying intravascular hemolysis and anemia. Rats can be dosed intravenously or intraperitoneally to achieve lysis. As only small amounts of toxin are used and humans have anti-ILY antibodies [133], ILY is a safer alternative to other drug-induced models of hemolysis (2-Butoxyethanol, Diphtheria toxin). Additionally, ILY interaction is highly specific to human CD59. We have not observed off-target effects due to binding to rat CD59 or other non-specific targeting and thus this lack of detectable off-target effects confers an advantage compared to other drug-mediated lysis methods. For example, erythrocytes from rats treated with 2-Butoxyethanol (BE) had enhanced adherence to extracellular matrix, as well as BE-related changes in erythrocyte morphology [151]. Such effects complicate interpretation of results. In contrast, ILY binds to hCD59, forming pores in the cell membrane leading to lysis [152, 153]. This method of cell ablation occurs so rapidly, there is no effect on morphology or flow properties. Sex differences are also observed in rats treated with BE due to differences in drug metabolism [154, 155]. We have shown that male and female Tg+ rats have no difference in response to ILY, thus allowing both sexes to be used for experimentation. We were able to induce hemolysis using a single

dose of ILY. Other rodent hemolysis models typically require multiple injections or gavage, increasing animal stress and expense [22, 150].

Several mutant rodent models have been generated to model human inherited blood disorders and resulting hemolysis. Targeted deletion of mouse CD59 induces spontaneous intravascular hemolysis. However mice only develop minor anemia with slight increases in plasma hemoglobin [156]. The *sph/sph* mutant mouse model produces abnormal erythrocytes with increased fragility, leading to severe hemolytic anemia with expected thrombosis and infarction [157]. Similar to the CD59 knock out mouse, the *sph/sph* mouse model is not inducible and cannot be used to perform a dose dependent study for the hemolysis-associated sequelae, and therefore may not be appropriate for some studies.

The generation of the mouse hCD59 anemia model was the first demonstration of the hCD59-ILY system to achieve rapid conditional cell ablation [133]. We aimed to extend the usefulness of this novel ablation system to another species and because rats have long been the preferred model for vascular and hematology studies [143] we utilized the same transgene to create a rat anemia model. Comparing the mouse and rat models, rat erythrocytes were more sensitive to ILY *in vitro*, requiring lower concentrations of ILY to achieve 50% lysis (1000 pM for mouse, 125 pM for rat) [133]. However, *in vivo*, the rat model appears to require a higher dose to achieve a similar degree of anemia observed in the mouse. 30 ng/g BW of ILY in the mouse achieved an approximate 30% reduction in hematocrit [133], whereas doses of up to 50 ng/g BW in the rat resulted in a 10% reduction (Figure 3.3C). Interestingly, both models had lethality observed at doses over 100 ng/g BW (Figure 3.4B, 3.5A) [134]. This new rat model not only exhibits a similar phenotype to the hCD59 mouse but provides additional advantages. For example, in applications where

researchers need more blood volume for analysis, or need to perform serial blood collection, the rat model has the distinct advantage. Importantly, the larger size of the rat facilitates easier imaging and data collection of cardiovascular parameters, such as performance of heart catheterization and echocardiography studies. Specifically, the *hCD59*^{RBC} rat could be bred with the many cardiovascular disease models already developed in the inbred rat strains for further understanding how the hemolytic anemia contributes to these cardiovascular diseases. For example, hemolytic uremic syndrome (HUS) results in damage to erythrocytes and endothelial cells with the cardinal lesion of thrombotic microanigiopathy (TMA) [158]. Symptoms of patients with HUS and TMA can include hypertension [159], myocardial infarction [160] and stroke [161]. By crossing the *hCD59*^{RBC} rat with the commonly used SHR or Lyon Hypertensive (LH) inbred strains, the relationship between hypertension, hemolytic anemia and endothelial damage can be explored and compared to the history of data collected in these rat models. Furthermore, the rat is the preferred and more popular model for myocardial infarction and stroke as opposed to the mouse; therefore, it would be most appropriate to utilize our model when studying these symptoms of HUS in the face of hemolytic anemia.

A limitation to this model is the potential variability in ILY activity. As ILY is a bacterial product, the activity and ability to induce lysis can fluctuate. Therefore, we recommend testing each lot with the *in vitro* hemolysis assay described in the methods to determine activity prior to performing *in vivo* experiments. ILY should also be stored on ice until used to preserve lytic activity, as prolonged incubation at room temperature has been shown to decrease activity [113]. Another potential source of phenotypic variability may be due to the genetic background of the model. As the outbred SD background is the

most common rat stock used in drug toxicology and pharmacokinetics studies [162], this genetic background was considered the most appropriate for creating the model. The susceptibility of transgene positive animals to ILY-induced hemolysis was uniform but it is possible that the slight variations in response to ILY seen among individual animals could have been due to background genetic differences. Because of this potential, as with any model on an outbred background, it is important to study sufficient numbers of individuals to account for variability. A benefit of the outbred nature of the model could be in providing an opportunity to explore genetic factors altering individual susceptibility to erythrolysis.

In summary, we generated a novel rat model to study hemolytic anemia and have validated the use of the hCD59-ILY ablation system in a novel species, the rat.. Upon administration of ILY, disease occurs rapidly and specifically, similar to the already established mouse hCD59 anemia model. The *hCD59*^{RBC} rat demonstrates the effectiveness and advantages of the hCD59-ILY system and provides the scientific community with the first inducible genetic ablation model of erythrocytes in the rat.

Chapter 4: A novel rat beta cell ablation model

Introduction

The prevalence of Type 1 diabetes (T1D) is increasing with 10% of all diabetes mellitus cases being type 1 (insulin-dependent) [163-165]. Selective destruction of insulin-producing pancreatic β cells follows inflammation within the islets of Langerhans, however the etiology in both humans and animals has not been well characterized [166-169]. Currently investigators have a wide variety of models for diabetes research. Spontaneous models, such as the NOD (non-obese diabetic) mouse and BB (Bio Breeding) rat, develop diabetic signs similar to humans including hyperglycemia, glycosuria, and insulin-dependence [170-172]. While pancreatic insulitis is observed in these models, the inherent problem exists that disease onset is inconsistent and incidence is only 80% in female NOD mice, 20% in male NOD mice, and as low as 60% in the BB rat [163, 173, 174]. Additionally, treatments shown to be successful in the NOD strain prove ineffective in diabetic humans [175, 176]. Toxin-induced models via administration of alloxan and streptozotocin (STZ) have been widely used as rodents will develop T1D as β cells are destroyed. However, beta cell ablation is inconsistent due to different sex and strain sensitivities [34-36]. Moreover, such drug-induced models have side effects such as nephropathy [30, 31] and hepatopathy [32, 33].

Therefore, transgenic models of T1D have emerged to further T1D research through selective ablation of β cells without off-target effects. Such models prove worthy of transplantation studies, where complete ablation of beta cells could help discover new therapies. The *INS*-TRECK-Tg mouse model utilizes diphtheria toxin-mediated cell ablation to induce clinical signs of T1D by two days post toxin injection [177]. While this

model offers more complete β cell ablation than STZ, 100% ablation was not achieved and degree of ablation was not dose-dependent. Additionally, the pancreatic islets of transgene-positive mice lacked normal morphology [92]. While the transgenic mouse has advantages over spontaneous and STZ models, there is still a need for a rat model, especially where the rat's larger size is advantageous for microsurgery, vascular organ transplantation and when greater sampling volumes are required.

Therefore, we aimed to simultaneously test the application of ILY-mediated ablation in solid organs as well as characterize a novel rat model of T1D through generation of a transgenic rat, referred to hereafter as RIP-hCD59, which expresses human CD59 specifically on pancreatic β cells rendering them susceptible to lysis following ILY administration. While a founder animal was generated and bred, transgene-positive offspring failed to develop hyperglycemia following both IV and IP administration of ILY, and an unexpected anemia was observed following ILY administration IV.

Results

Utilizing primers from Chai et al. [136] for the rat insulin 1 (*Ins1*) promoter, a 622 bp amplicon was produced and used to construct the transgene plasmid (Figure 4.1). In-Fusion cloning successfully produced 18/24 clones that carried the desired inserted DNA sequence as verified by restriction endonuclease digest (Figure 4.2). Four clones with the appropriate restriction endonuclease digest pattern were sequenced and all had the expected nucleotide sequence. One was selected for propagation of the plasmid and subsequent gel purification. A 1.3 kb DNA fragment was isolated and prepared for microinjection (Figure 4.3). From the 355 0.5 day-old embryos in which the DNA was introduced by pronuclear injection, 67 live pups were recovered.

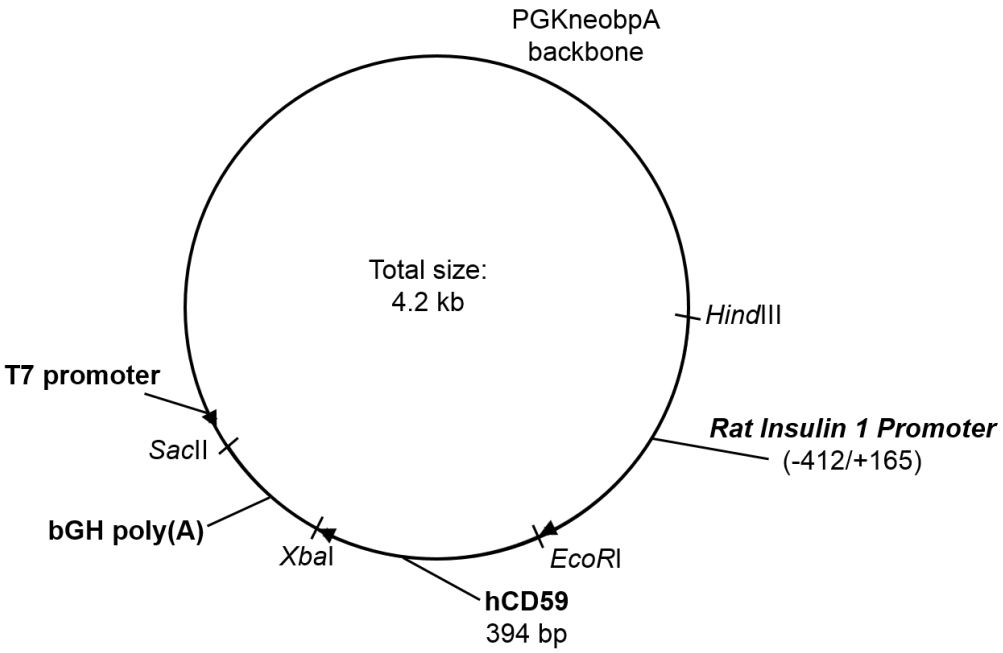

Figure 4.1. RIP-hCD59 plasmid used to generate the transgenic rat. Schematic representation of the pPGKneo-RIP-hCD59 plasmid used to prepare DNA for zygote injection.

Overall efficiency of random transgenesis was 0.36% (1/274) (Table 4.1). DNA extracted from tail biopsies from live born pups were screened using PCR primers specific for the RIP-hCD59 transgene and one positive founder was identified (Figure 4.4). The transgenic stock was maintained by breeding the male founder rat to Hsd:SD females (Envigo). Offspring of the founder inherited the transgene indicating germline transmission (data not shown).

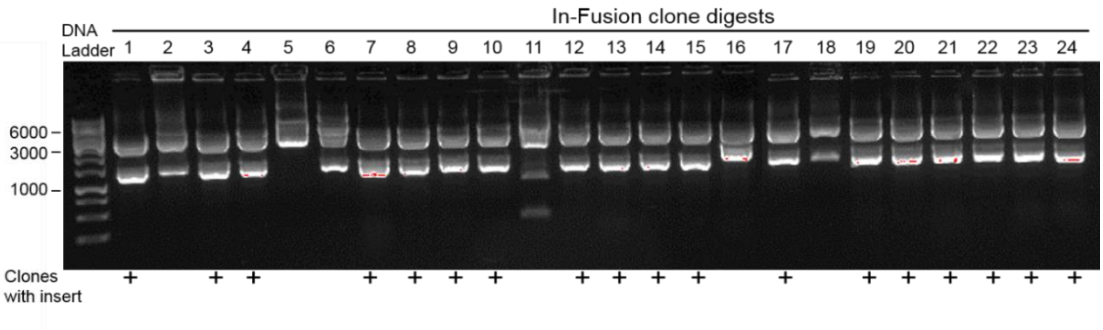

Figure 4.2. Resultant clones from In-Fusion cloning. Restriction digest with *Hind*III and *Sac*II to identify positive clones. 18/24 clones tested were positive (+) for the insert. GeneRuler 1 kb DNA ladder. Expected band sizes of 2900 bp and 1300 bp.

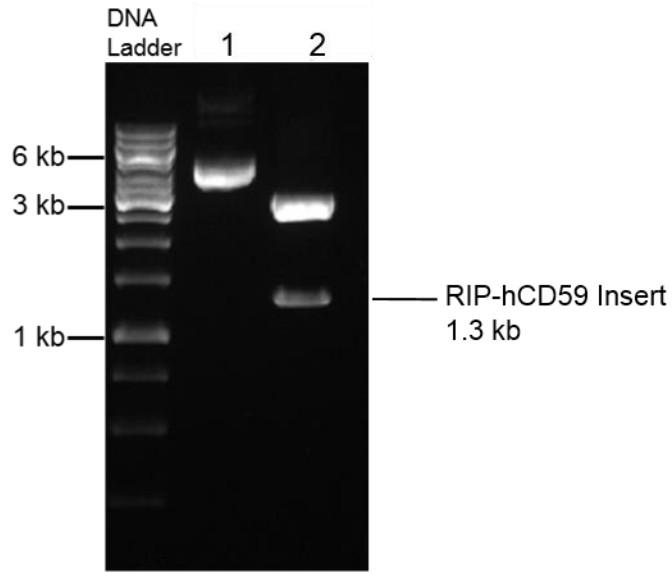

Figure 4.3. Isolation of insert for microinjection. DNA ladder: 1kb GeneRuler. Lane 1: Uncut plasmid. Lane 2: Digest. Plasmid was digested with *Hind*III and *Sac*II to liberate the 1.3kb insert and purify for microinjection.

Table 4.1. Efficiency of transgenesis for RIP-hCD59	
Number of embryos injected	355
Number of embryos transferred	274
Percent survival	77.2
Total number of post-injection live born rats (%)	67/274 (24.5)
Number of transgene-positive rats (%)	1/67 (1.5)

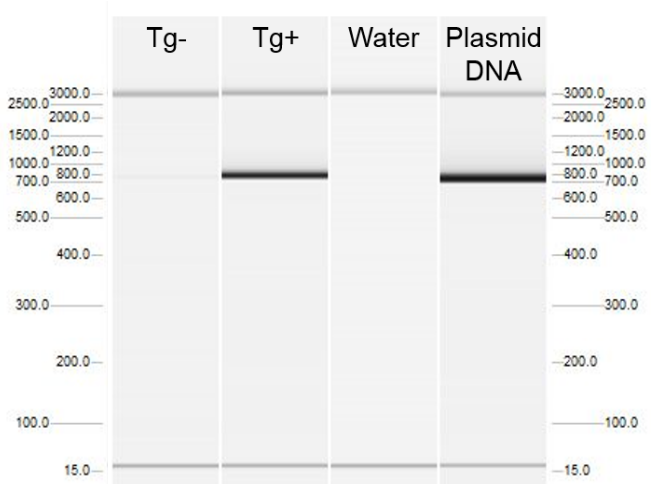

Figure 4.4. Genotyping of pups recovered after pronuclear microinjection. One RIP-hCD59 transgenic founder rat (Tg+) was identified via PCR amplification of genomic DNA with hCD59 primers (Table 1). A representative transgene-negative rat is shown for comparison (Tg-). RIP-hCD59 plasmid DNA was used as the positive control. Water (no template) was used as a negative control.

Two transgene positive (Tg+) rats (one male and one female) were dosed with ILY at a dose of 45 ng/g body weight (BW) IV. Immediately after injection of ILY (1-2 minutes) the rats became ataxic, recumbent, and had increased respiratory rate. By 8 minutes after injection, the rats were quiet, alert and responsive. Three hours post injection, the rats had

marked hematuria. Packed cell volume 24 hours post injection was 21 and 23 percent of normal which is indicative of anemia. Unfasted hyperglycemia was defined to be over 250 mg/dL. Rats remained normoglycemic over the 5 days (range 97-239 mg/dL) and no other clinical abnormalities were observed (Figure 4.5).

Six Tg+ rats (2 males, 4 females) were dosed with ILY at 100ng/g BW IP. Rats were clinically normal after injection and no clinical signs were observed at any time prior to euthanasia 14 days after ILY injection. Blood glucose was monitored and all rats remained normoglycemic throughout the study (range 106-143 mg/dL) (Figure 4.6 A). Packed cell volume for all rats 24 hours post ILY injection was normal with no reduction observed (Figure 4.6 B).

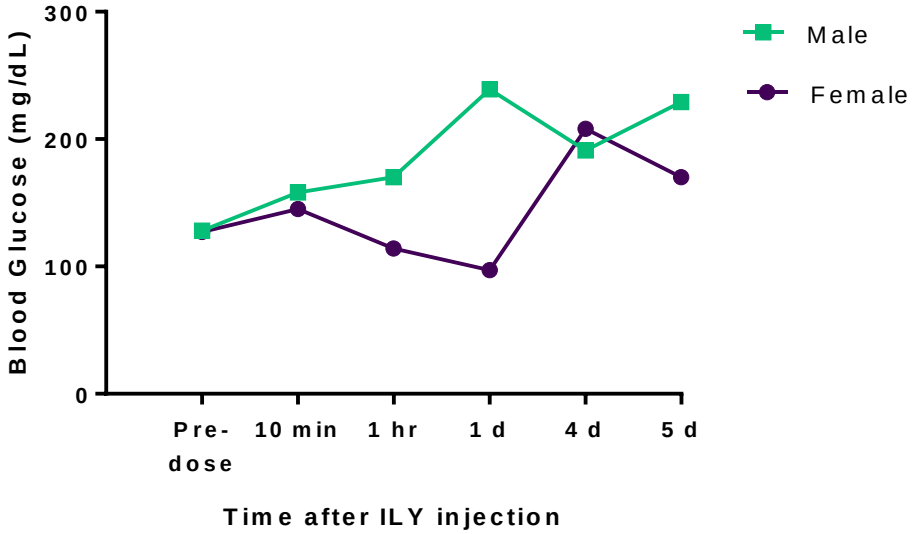

Figure 4.5. Effect of ILY administration on blood glucose. One male and one female transgene-positive rats were dosed with ILY 45 mg/g body weight IV. Blood glucose was monitored until 5 days (d) post injection.

A

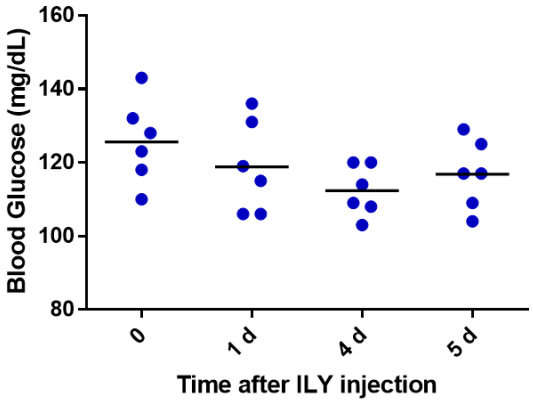

B

Packed Cell Volume (%)

Rat ID	Sex	Pre Dose	1 Day Post ILY
197 RL	F	47	48
382 RL	F	47	49
386 RL	F	45	45
387 RL	F	46	45
350 RL	M	50	50
348 RL	M	48	55
Mean		47.2 ±0.70	49 ±1.52

Figure 4.6. Intraperitoneal dosing of RIP-hCD59 rats with ILY. (A) Six transgene-positive rats were dosed with 100 ng.g body weight ILY IP. Blood glucose was monitored for 5 days post-injection. (B) PCV was monitored before and after injection of ILY (mean ±SEM).

Discussion

Our goal was to demonstrate that ILY-mediated ablation could be used in solid organs through the generation of a rat model which expresses hCD59 on β cells in the pancreas. Rapid depletion of these insulin-producing cells would result in Type 1 Diabetes, providing investigators with a novel rat model superior to existing models. However, IV (45 ng/g BW) and IP (100 ng/g BW) injection of ILY into Tg+ positive rats failed to induced hyperglycemia as expected following ILY administration. In IV injected rats, an unexpected outcome of anemia was also observed. As the RRRC also maintains the stock SD-Tg(CD59-HBA1)Bryd which expresses hCD59 on erythrocytes, genetic contamination from this stock was a concern. Strain-specific PCR assays confirmed there was no genetic contamination as all rats were positive for the RIP-hCD59 transgene and negative for the CD59-HBA1 transgene. Additionally, previous experiments have demonstrated that ILY does not induce anemia in transgene-negative rats at doses as high as 100 ng/g BW IV and 500 ng/g BW IP. Therefore, it is unlikely that this is a non-specific binding of ILY and is instead a result of extra-pancreatic expression of the transgene conferring expression of hCD59 on erythrocytes. Due to the ectopic expression of this transgenic model and successful development of the inducible rat model, it was decided to halt further characterization of the RIP-hCD59 rat.

Efficiency of Transgenesis

Generation of the RIP-hCD59 transgene was efficient utilizing In-Fusion cloning technology. This PCR-based cloning system uses amplicon homology to the vector backbone with a 15 bp overlap. Inserting multiple fragments, the promoter and hCD59

cDNA, was accomplished simultaneously with 18/24 clones exhibiting the correct bands following diagnostic restriction digest. The transgene showed little toxicity at the injection concentration of 4 ng/ul with 77.2% survival. This survival is consistent with results seen by others who have microinjected DNA constructs into the pronuclei of rat zygotes (58-72%) [178]. Similarly, efficiency of transgenesis was as expected for SD rat pronuclear injection at 1.5% [178, 179]. For the number of embryos transferred, more live pups were expected as Popova et al [178] reported an average of 30.6% offspring from transferred rat embryos. Unfortunately, our rodent housing facility had multiple cases of neonatal mortality prior to genotyping, which is performed at approximately two weeks of age. Any tissue recovered from dead pups was collected for genotyping, although none of the dead pups were positive for the transgene. These samples were excluded from Table 4.1 as total number of dead pups was difficult to determine. In total, one germline-competent founder was produced. Success is often limited when only one founder is recovered since position effects and copy number influence the level and specificity of transgene expression, thereby decreasing the likelihood of achieving the desired transgenic model with ideal expression [180]. Position effects can be overcome by using a targeted gene insertion strategy to a safe-harbor location within the rat genome, such as the *Rosa26* locus [181].

Sperm from RIP-hCD59 founder offspring was cryopreserved if future investigation is warranted.

ILY-mediated ablation

ILY was administered via two routes of administration to induce ablation of pancreatic β cells. Forty-five ng/g BW IV was selected as the starting dose as it was the dose observed to induce moderate to marked anemia in both the rat and mouse models expressing hCD59 on erythrocytes [133, 182]. Unexpectedly, ILY immediately induced clinical signs consistent with intravascular hemolysis including hematuria. Following observation of clinical signs, a packed cell volume (PCV) was performed, revealing that the rats were anemic (21 and 23%) post ILY injection. Since PCV was not performed prior to dosing it is unknown if rats were anemic prior to ILY treatment, although rats appeared healthy (not pale, bright, alert, responsive). While blood glucose did increase following ILY injection, it did not achieve levels consistent with other diabetic models as non-fasted blood glucose levels >300 mg/dL are typically observed in STZ-induced rats one week post injection [183]. Hyperglycemia >400 mg/dL was observed 3 days after diphtheria toxin (DT) administration in a diphtheria toxin receptor-mediated β cell mouse model [92]. Since DT ablation occurs more slowly than ILY-mediated ablation, it is expected that hyperglycemia would have occurred in RIP-hCD59 rats within a similar time or sooner. Fasted blood glucose levels for nondiabetic Sprague-Dawley rats are less than 200 mg/dL[184]. One rat reached a peak blood glucose of 239 mg/dL on day 1 only, slightly above the normal upper limit for SD rats. Since rats were not fasted for the study, postprandial blood glucose elevation could not be ruled out. Had ablation of beta cells occurred, diabetic levels would certainly have been reached within the 5 days of testing as the half-life of plasma insulin is approximately 4-5 minutes in the rat, therefore rats would

have been expected to develop hyperglycemia without supplemental insulin injection [185].

Additionally, cautious interpretation of blood glucose measured using a handheld glucometer is warranted, especially in the presence of anemia. Glucometers, such as the OneTouch used in these experiments, measures whole blood glucose, which is less accurate in rodents when measuring levels in the 200-300 mg/dL range versus plasma glucose due to the higher normal hematocrit in rodents versus humans [186, 187]. Variations in hematocrit affect accuracy of glucometers as hematocrit alters blood viscosity and thus permeability into the test strip [188]. Low hematocrit falsely elevates blood glucose as less red blood cells leaves more of the test strip covered by glucose-plasma [186, 189].

As hemolysis was observed with the IV route of administration, an alternate route of intraperitoneal injection was tested. The rats were given a higher dose of 100 ng/g BW to counteract any first-pass drug effect from this route of administration. Additionally, 100 ng/g BW IV has been shown to be a lethal dose in the rat anemia model [182]. Our hypothesis was that this dose would be sufficient to induce β cell ablation while avoiding the severe intravascular hemolysis observed via IV administration. Hematocrits were within normal ranges before and after ILY injection, however blood glucose levels also remained stable with no hyperglycemia observed (Figure 4.6).

Due to ectopic expression and lack of diabetic phenotype, further experiments with ILY were not performed. It is possible that higher doses could induce beta cell ablation via the IP route considering that doses of 500 ng/g BW were required to induce anemia in the RBC model [182]. In humans, beta cell loss has reached 70-80% at time of diagnosis [169]. To produce overt diabetes in the NOD mouse, 90% of β cells must be destroyed [190]. Our

interpretation of the results is that we failed to ablate enough cells to induce a diabetic phenotype, and we cannot rule out the possibility that no ablation occurred. Pancreas histopathology from injected rats along with immunohistochemical staining for insulin or hCD59 would help determine if any ablation was achieved.

Promoters for β cell-specific expression

The RIP-hCD59 transgenic rat highlights the importance of transgene promoter selection with respect to tissue-specific expression. Our results indicate that hCD59 was expressed in extra-pancreatic cells, namely erythrocytes, as demonstrated by the intravascular hemolysis and resultant hemoglobinuria observed following IV administration of ILY.

The insulin gene is highly conserved among species. While humans and pigs have only one insulin gene, rats and mice have two, *ins1* and *ins2*. *Ins2* is an orthologue to insulin in other mammals while *ins1* is a partially-transcribed retrogene containing the regulatory elements and first intron from *ins2* [191]. Promoters of both genes have been used to achieve β cell expression, though phenotype varies greatly (Table 4.2).

Table 4.2. Transgenic models of diabetes

Transgenic Line	Promoter	Species	Ectopic expression	Reference
57BL/6-ins2(BAC)-TRECK-Tg	Rat *ins2*	Mouse	unknown	Matusoka et al [92]
RIP-luc	Rat *ins2*	Mouse	none observed	Smith et al [39]
Rip-Cre	Rat *ins2*	Mouse	hypothalamus	Song et al [40]
RIP-CreER	Rat *ins2*	Mouse	none observed	Dor et al [41]
RIP-DTR	Rat *ins2*	Mouse	none observed	Thorel et al [42]
RIP-PTHrP	Rat *ins2*	Mouse	stomach, intestines, liver, brain, skin	Vasavada et al [192]
MIP-luc	Mouse *ins1*	Mouse	none observed	Park et al [43]
RIP-FRK	Rat *ins1*	Mouse	none observed	Anneren et al [44]
RIP1-E-cadherin	Rat *ins1*	Mouse	none observed	Dahl et al [193]
SD-Tg(RIP7-RLuc-YFP)211	Rat *ins2*	Rat	none observed	Ghislain et al [45]

Table 4.2 summarizes these murine transgenic models and also lists in which models ectopic expression was observed, though it is unclear if tissues aside from pancreas were evaluated for expression in some models.

While the rat insulin 2 promoter has been used to generate several mouse models of β cell transgene expression, it also has been documented to have extra-pancreatic expression in hypothalamus [194], stomach, intestines, liver, brain, skin [192]. Additionally, RIP-CreER mice [195] had functionally abnormal β cells which exhibited an increase in apoptosis when Cre was expressed, indicating that Cre may be toxic to cells when highly expressed [196]. Therefore, caution should be used before generating any

novel models for Cre expression in β cells. The MIP-GFP mouse, utilizing mouse insulin 1 promoter, has expression restricted to β cells in mice 6 weeks of age, though older animals were not examined [197]. As ILY will bind to hCD59 inducing lysis, cell specificity is crucial in generating ablation models where off-target cell death can lead to unwanted clinical signs, such as anemia.

As extra-pancreatic expression was not observed in the model utilizing the rat insulin 1 promoter, this promoter was selected for β cell-specific expression of hCD59 in the RIP-hCD59 rat. The promoter region described as RIP3.1 was utilized, as Chai et al. demonstrated high levels of expression of *Ds*Red following transgene delivery in rats [136]. RIP3.1 includes the first exon and intron of the *ins1* gene which generated robust β cell-specific transgene expression compared to previous studies which excluded the transcriptional start site [198, 199]. However, in our model, we failed to see such specificity. As location of the transgene was random, the position within the genome could affect modulating transcription factors, such as Pdx-1 and NeuroD1 which are normally repressed in non-β cells. These factors have been shown to activate the insulin gene in non-β cells [200, 201] and could explain why our model exhibited ectopic expression in erythrocytes, although expression of such factors have yet to be identified in hematopoietic cells.

This promoter infidelity could be avoided by use of the porcine insulin promoter, which differs in sequence at the A3 and E1 elements potentially reducing non-β cell activation by their corresponding transcription factors in the rat. Additionally, the GAGA box is absent in the pig, which is bound by pur-1, which activates the promoter in non-β cells (Figure 4.7) [202, 203].

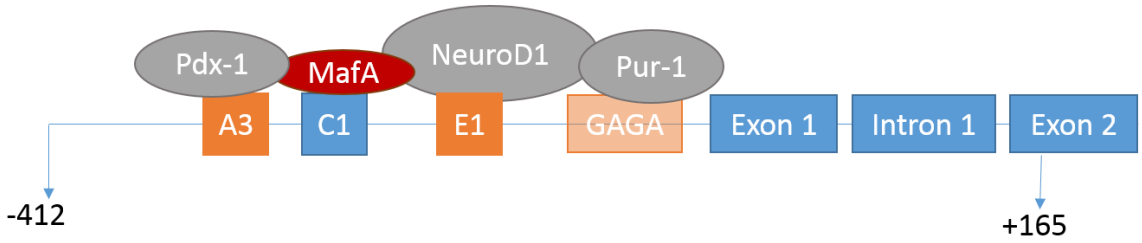

Figure 4.7. Rat insulin 1 promoter. RIP3.1 promoter used to generate RIP-hCD59 rat contained the sequence from -412 to +165. Regulatory elements in orange differ between rat and pig, with GAGA absent in pigs. Transcription factors in grey are expressed in non-β cells, while MafA (red) is expressed in β cells only.

Furthermore, a transgenic mouse model utilizing the porcine insulin promoter detected no transgene transcripts in extra-pancreatic tissue [204]. Of the β cell-specific promoters used and described to date, the porcine insulin promoter holds the most promise for producing a transgenic animal with selective expression in pancreatic β cells.

As there is still a need for an inducible transgenic rat model of type 1 diabetes, a suitable alternative for the generation of a β cell ILY-mediated ablation model would be to generate a new transgenic rat utilizing the porcine insulin promoter (PIP). The new PIP-hCD59 transgene could further be improved over the RIP-hCD59 transgene by targeted insertion into the safe-harbor *Rosa26* locus and adding a fluorescent protein marker to hCD59 via a P2A peptide for easier detection of desired hCD59 expression in β cells, as screening for ectopic expression in other tissues.

Chapter 5: A Cre-mediated rat ablation model

Introduction

As cell ablation continues to be a powerful technique to study the function of cells within the body, validity of the hCD59-ILY system in solid organs became a relevant goal. The novel rat model expressing hCD59 on erythrocytes (Chapter 3) highlighted many advantages that will prove applicable to other cell types such as: 1) rapid lysis of cells within ten minutes of ILY administration, 2) dose-dependent lysis, 3) and lack of toxic effects in wild type animals, even at high concentrations. While generation of the hCD59 rat anemia model is exciting, the scientific community would benefit from an inducible system for ablation in a wide range of cell types.

To corroborate the aforementioned advantages of the hCD59-ILY system in solid organs, the ihCD59 transgene was generated which utilizes the Cre-*loxP* system to express hCD59 and the fluorescent protein, ZsGreen, when Cre recombinase is present. ZsGreen is a fluorescent protein derived from *Zoanthus* reef coral and has been shown to have 3-fold higher mean fluorescence than *Aequorea victoria* green fluorescent protein in cell culture [205]. ZsGreen has been expressed in rat megakaryocytes [206] and multiple mouse tissue types without negative effects [207]. ZsGreen serves as a reporter for hCD59 via a porcine teschovirus-1 (P2A) peptide. The 2A peptide mediates a ribosomal skip between the C-terminal glycine and proline, resulting in separate ZsGreen and hCD59 polypeptides in a 1:1 ratio [208, 209]. The transgene expression is driven by the cytomegalovirus (CMV) early enhancer/chicken beta actin (CAG) promoter [210] for ubiquitous expression. However, ZsGreen/hCD59 are only expressed when Cre recombinase is present due to a

polyadenlyated stop cassette flanked by *loxP* sites upstream of the fluorescent protein [211]. In the presence of Cre, the DNA between the *loxP* sites is excised and transcription of downstream elements can proceed. Therefore, tissue specificity of ZsGreen/hCD59 can be regulated in transgenic rats which express Cre recombinase under transcriptional control of a tissue-specific promoter.

With this transgene, ablation models for many different cell types can be generated utilizing available Cre rats. Currently, the rat lacks the diverse "Cre zoo" that is available in the mouse, as there are limited transgenic rats which have tissue specific expression of Cre recombinase [212]. However, with recent technical advances in generation of transgenic rats, such as the availability of genome editing methods such as CRISPR/Cas9, more Cre rats can be swiftly produced [213].

To validate our inducible hCD59 (ihCD59) rat strain, we bred them to strain LE-Tg(TH-Cre)3.1Deis [140] (RRRC #659; hereafter referred to as TH-Cre). This rat strain allows expression of Cre recombinase in tyrosine hydroxylase (TH)-expressing dopaminergic neurons of the substantia nigra (SN) and ventral tegmental region (VTA) within the brain. In animals carrying both the ihCD59 transgene and the TH-Cre transgene, it was expected that TH-positive neurons in the brain would express ZsGreen and hCD59 and therefore be susceptible to ILY-mediated ablation.

Many diseases and disorders are related to the loss of TH-neurons and dopamine, including alcoholism, drug addiction, and Parkinson's disease. TH-neuron dysfunction and degeneration is a classic feature of Parkinson's disease, which affects every 115 per 100,000 people [214-216]. Neuronal loss of greater than 60% within the SN results in the classic symptoms observed in Parkinson's disease, such as motor deficits and cognitive

impairments in visuospatial learning and memory [217]. Currently, there is no cure for Parkinson's disease and novel treatments that have been successful in rodents fail to translate to human medicine [218]. A reason for this lack of treatment options is the lack of appropriate animal models which would allow researchers to further study the local and systemic effects of neuron loss. By generating a rat which selectively and rapidly loses TH-neurons, we can begin to understand the role such loss plays in disease progression without confounding factors found in other models.

To recapitulate such diseases, an array of ablation techniques have been used in rodents to mimic disease and study neurodegeneration. Neuronal ablation can be accomplished through physical means by surgical removal or destruction of the brain region of interest although such ablation is non-specific and damage to other cell types is often unavoidable [219]. Toxin-based ablation, using 6-hydroxydopamine (6-OHDA) injected directly into the brain is another method which ablates neurons with preference for dopaminergic subtypes [220]. 6-ODHA, similar to surgical ablation, involves precise delivery [221]. Alternatively, MPTP (1-methyl-4-phenyl-1,2,3,6-tetrahydropyridine) - mediated ablation, can be injected intraperitoneally or intranasally but requires repeated daily administration [222, 223]. As a potent neurotoxin, MPTP is extremely harmful to humans and care must be taken when performing such procedures [224]. Collectively, all these methods require more time, expertise and skill from the researcher while providing crude and often non-specific ablation. Additional off-target effects of these drugs remains unknown. Thus there is a need for a more refined technique of neuron ablation as the rat remains the ideal model species for neuroscience [219, 225].

Genetic-based techniques, such as optogenetic control of dopaminergic neurons in parkinsonian rats, have been used to establish the relationship between neuronal circuitry and behavioral phenotypes [226]. However, such technology does not result in neuron loss, and therefore, does not fully represent the hallmark neurodegeneration in Parkinson's disease. While some proteins like KillerRed and miniSOG have been used in zebrafish and *C. elegans* for light-induced ablation [227, 228], such techniques have yet to be applied to the rat. Furthermore, optogenetic models require technical expertise to precisely insert the fiber optics to the brain region of interest [229].

Demonstrating dopaminergic neurons can be ablated following administration of ILY would not only provide a valuable model of Parkinson's disease but would also validate the hCD59-ILY system for use in solid organs, which has yet to be confirmed in the rat. As more Cre rats are generated and become available, this inducible model will have endless possibilities to allow investigators to ablate any tissue, providing a multitude of models for many scientific endeavors.

Results

Generation of ihCD59 transgene

In-Fusion cloning successfully produced 15/24 clones that carried the desired inserted DNA sequence as verified by restriction endonuclease digest (Figure 5.1). Four clones with the appropriate restriction endonuclease digest pattern were sequenced and all had the expected nucleotide sequence. One was selected for propagation of the plasmid, subsequent gel purification and in vitro testing.

In vitro *testing of inducible hCD59*

To test function of the transgene *in vitro,* rat insulinoma cells (RIN-m), were transfected with the ihCD59 plasmid (Figure 5.2A) as well a maxGFP control. After transfection, only cells with the maxGFP plasmid expressed GFP via fluorescent microscopy. To induce the ihCD59 transgene, TAT-Cre recombinase was added at 4 uM for 3 hours (Figure 5.2B). At removal, approximately 10% of ihCD59-transfected cells were positive for ZsGreen. At 12 and 24 hours post TAT-Cre, approximately 80% of the cells were positive (Figure 5.3 top row). MaxGFP transfected cells incubated with TAT-Cre were unaffected and maintained GFP expression. At 24 hours post induction, ILY or saline was added to both iCD59 and maxGFP transfected cells as well as uninduced iCD59 transfected cells (no TAT-Cre added). Cells were checked for lysis 20 minutes after incubation with ILY. There were no intact cells present in the induced ihCD59 cells in the wells treated with ILY and ZsGreen could only be detected in one cell fragment (Figure 5.3 bottom row). MaxGFP cells treated with ILY were unaffected and maintained GFP expression. Uninduced ihCD59 cells treated with ILY were also unaffected and remained negative for ZsGreen expression. Saline treated cells had no lysis observed in any groups following the incubation.

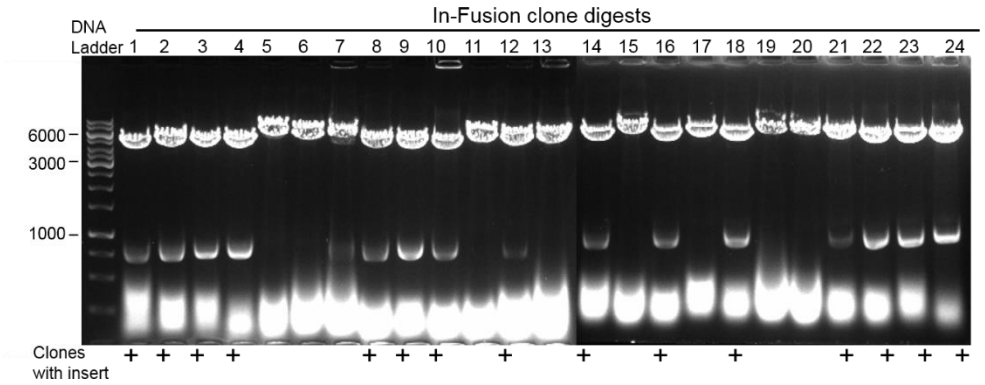

Figure 5.1. In-Fusion cloning results. Selected clones following restriction enzyme digest with *Pst*I following boiling lysis plasmid preparation. 15/24 clones had the expected band sizes of 6000 and 900 bp (+). DNA ladder: 1 kb GeneRuler.

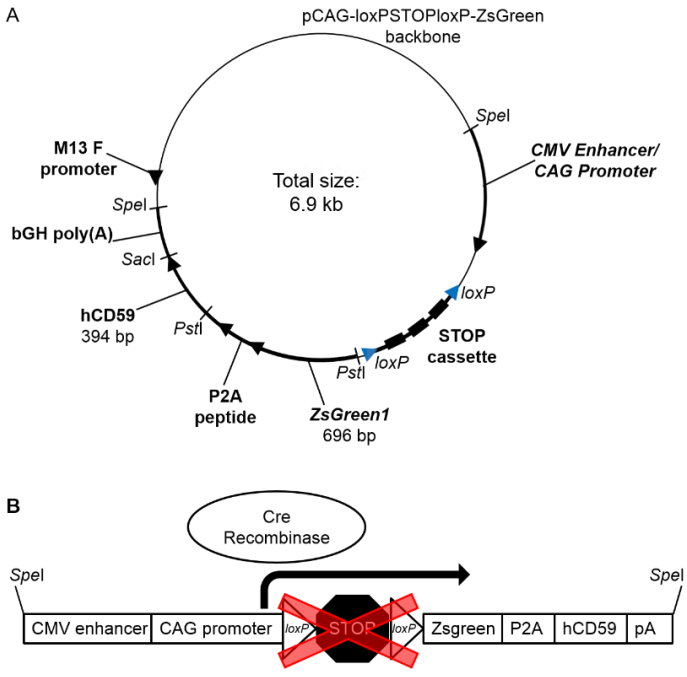

Figure 5.2. ihCD59 plasmid and recombination. A. The P2A peptide and hCD59 were cloned into the pCAG vector backbone using In-Fusion cloning. **B**. When Cre recombinase is present, the stop cassette is excised leading to expression of ZsGreen and hCD59.

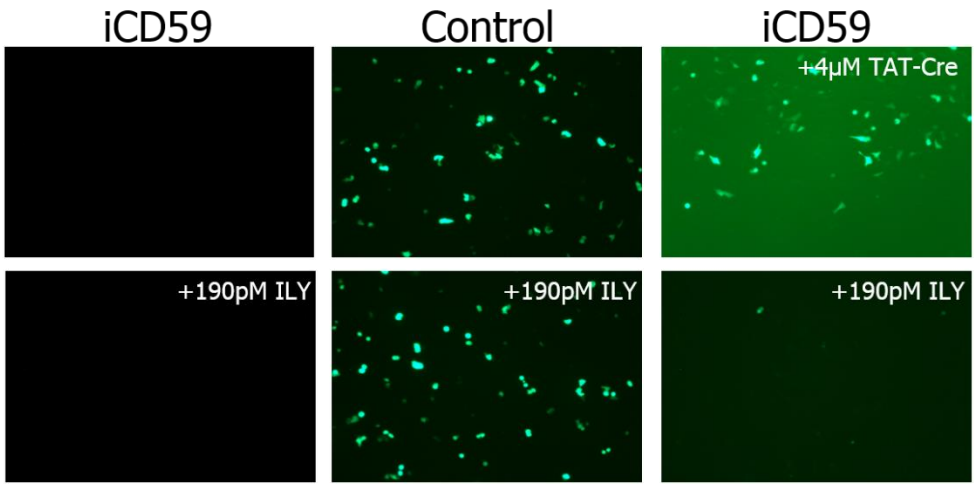

Figure 5.3. *In vitro* expression of ihCD59 and ILY-mediated lysis. RIN-m cells were transfected with ihCD59 (left and right panels) or control (maxGFP, center) plasmids. TAT-Cre was added to induce ihCD59 (right) and cells were imaged 24 hours later (top panels). After the addition of ILY, induced ihCD59 cells had lysed (bottom right), while control and induced ihCD59 cells were unaffected (bottom center and left).

Generation ihCD59 transgenic rats

A 4 kb DNA fragment was isolated and prepared for microinjection. From the 227 0.5 day-old embryos injected with linearized ihCD59 DNA, 70 live pups were recovered. Overall efficiency of random transgenesis was 1.32% (3/227) (Table 5.1). DNA extracted from tail biopsies from live born pups were screened using PCR primers specific for the ihCD59 transgene and 3 founders were identified: ear tag numbers 533RI (male), 541RI (male), 548RI (female). Each founder was maintained as a separate stock by breeding to wild-type Hsd:SD (Envigo) and stocks were correspondingly designated ihCD59.533, ihCD59.541 and ihCD59.548. Offspring of the founders inherited the transgene indicating germline transmission (data not shown)., Digital droplet PCR (ddPCR) was performed to

estimate transgene copy numbers of 1 copy and 3 copies for offspring from founders 533RI and 541RI, respectively (Figure 5.4).

In vivo expression of ZsGreen and hCD59

To test tissue-specific Cre recombination, each line was crossed to TH-Cre hemizygous rats. Brains from double hemizygous 2 week old pups were removed and cut into 5 mm thick transverse sections and imaged using a fluorescent dissecting microscope. Ventral brain regions exhibited ZsGreen expression in all ihCD59 stocks (Figure 5.5). Transgene-negative pups had no ZsGreen expression. When immunohistochemical (IHC) staining was performed for ZsGreen and hCD59 in double hemizygous rats (ihCD59.533 only to date), neurons in the SN and VTA were positive for ZsGreen and hCD59 (Figure 5.6).

Table 5.1. Efficiency of transgenesis for ihCD59

Number of embryos injected	306
Number of embryos transferred	227
Percent survival	74.2
Total number of post-injection live born rats (%)	70/227 (30.8)
Number of transgene-positive rats (%)	3/70 (4.3)

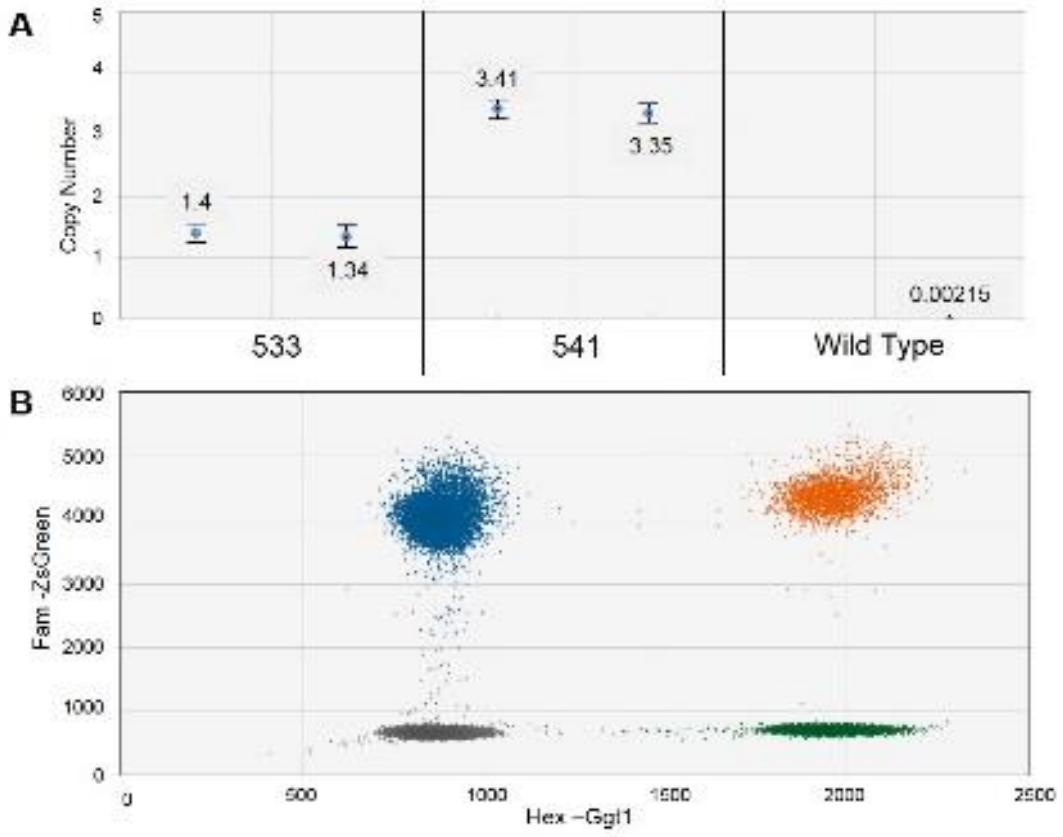

Figure 5.4. Digital droplet PCR. A. Copy number v s of ZsGreen, respectively, with SD wild type control rats. **B.** 2-D plot of droplet fluorescence of *ZsGreen* (blue), *Ggt1* (green) and double positive (orange) droplets. ariation for ZsGreen in ihCD59 stocks 533 and 541 illustrating 1 and 3 copy number

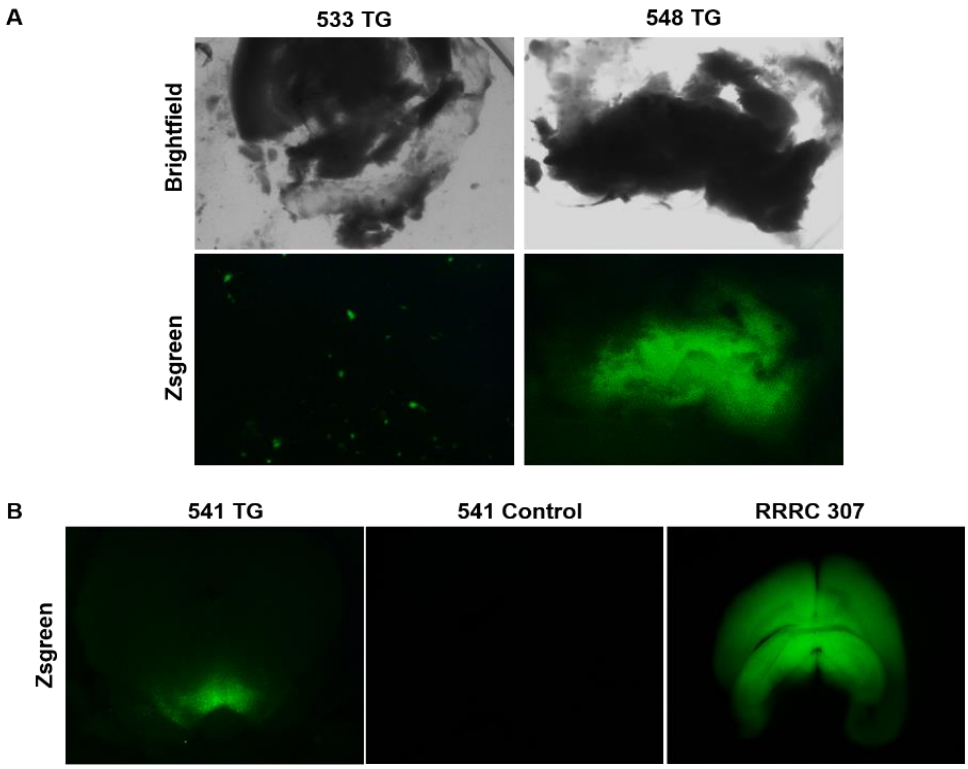

Figure 5.5. Brain fluorescent imaging. Rats were euthanized and fresh brain sections of the SN/VTA were placed in DPBS and imaged with a Leica dissecting scope. A. Brightfield and ZsGreen for stocks 533 and 548. B. ZsGreen images for stock 541 double hemizygous rat (TG; left), wild type control littermate (center) and positive control (F344-Tg(UBC-EGFP)F455Rrrc; RRRC#307; right).

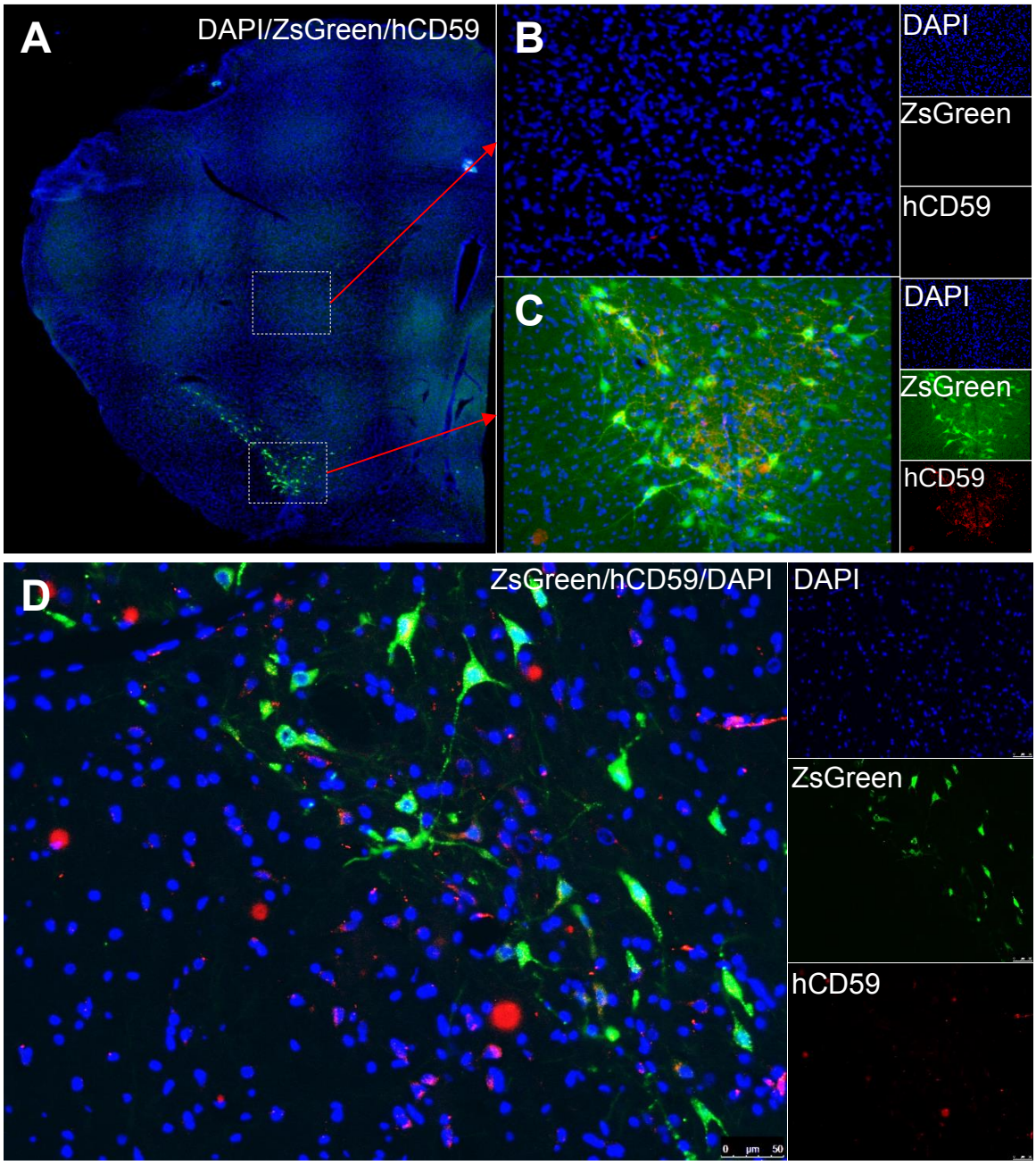

Figure 5.6. Immunohistochemistry of ihCD59 rats. A-C. Stock 533. A 40 µm cryosection (A) of the SN was stained for hCD59 (red). While no expression was seen in other brain regions (B), the neurons of the SN were positive for ZsGreen and hCD59 (C, merged). **D. Stock 541.** Co-localization of ZsGreen and hCd59 in neurons of the SN. Blue is DAPI nuclear staining. Green is endogenous ZsGreen fluorescent protein. Credit: Shen Dai, Temple University.

Cylinder task following intraperitoneal administration of ILY

Rats generated by crossing ihCD59.541 with TH-Cre that were either double hemizygous (TG) or had only one of the transgenes or transgene negative (control) were injected IP with 500 ng/g BW ILY. All rats were normal after injection and no clinical signs were observed. Cylinder test showed no difference in mean total number of rears, including both wall-dependent (forepaws touching wall) and wall-free (no forepaw contact with walls of cylinder) (Figure 5.7A). Similarly, there was no difference in the mean time spent grooming during the study (Figure 5.7B). Lastly, both TG and control animals took a similar number of hindlimb steps during the cylinder test (Figure 5.7C). When behavior testing was complete, brains were collected for cryosectioning and imaging. No gross lesions were observed at necropsy in the brain or other major organs dissected (heart, lungs, liver, kidney, GI tract, spleen, stomach, reproductive organs, and bladder).

Intracerebroventricular administration of ILY

TG and control animals from lines ihCD59.533, .541 and .548 were dosed with ILY via intracerebroventricular (ICV) injection. Four rats (line 541, 2 TG, 2 control, all female) were dosed with 10 µl ILY. The two TG rats died post-operatively during skin closure. One control rat was found dead approximately 20 hours after injection following an uneventful recovery from surgery. The other control rat had a long recovery from surgery but survived to study completion.

Figure 5.7. Cylinder test apparatus. Rats were recorded for 5 minutes within the cylinder with the assistance of a mirror. Rat is exhibiting wall-free rearing behavior.

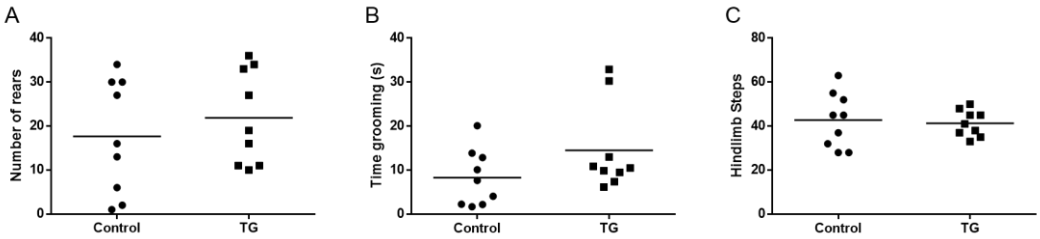

Figure 5.8. Cylinder test results for ihCD59.541. Rats were injected with ILY 500 ng/g BW IP. Cylinder behavior test was performed to observe changes in rearing (A), grooming (B), and hind limb steps (C). Three rats were tested per group for 3 trials. TG: double hemizygous for ihCD59 and TH-Cre. Control: Lacking one or both transgenes.

Due to the unexpected mortality with 10 µl ILY, all subsequent rats were injected with 1 µl ILY ICV. Of the 38 rats injected with 1 µl ILY ICV, all recovered from surgery and anesthesia and were quiet, alert and responsive 6 hours post-operatively. However, two TG (533, male) were found dead the next morning after surgery. At necropsy, one rat had hematuria.

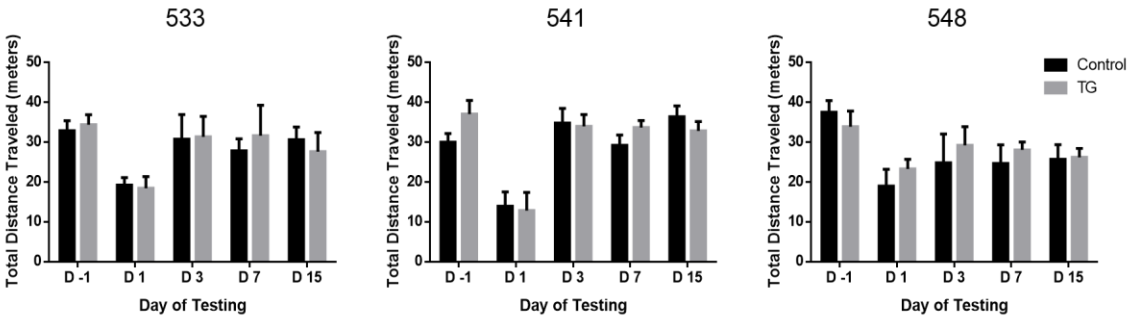

Figure 5.9. Open field test for ICV injected rats. Distance traveled was recorded for each rat in each group for 10 minutes. Data expressed as mean ±SEM. 533 TG, n=5; control, n=7; 541 TG, n=6; control, n=7; 548 TG, n=7, control n=7.

Behavior testing

For all stocks, total distance traveled in the open field test was similar between TG and control animals. The day after surgery (D1) all rats traveled less, though average distance traveled for each group returned to near pre-injection distance (Figure 5.8). Similarly, TG and control rats had a similar number of foot slips on the tapered beam test prior to surgery. Foot slips were the greatest the day after surgery but most rats returned to near pre-surgery baseline (Figure 5.9). Over the 6 days of training in the Morris water maze, all rats were able to locate the hidden platform and complete the task more rapidly at each subsequent test day (Figure 5.10; top row). On the day of testing, when the hidden platform was removed, TG and control rats performed similarly in time spent in the target quadrant which had previously contained the platform (Figure 5.10; bottom row).

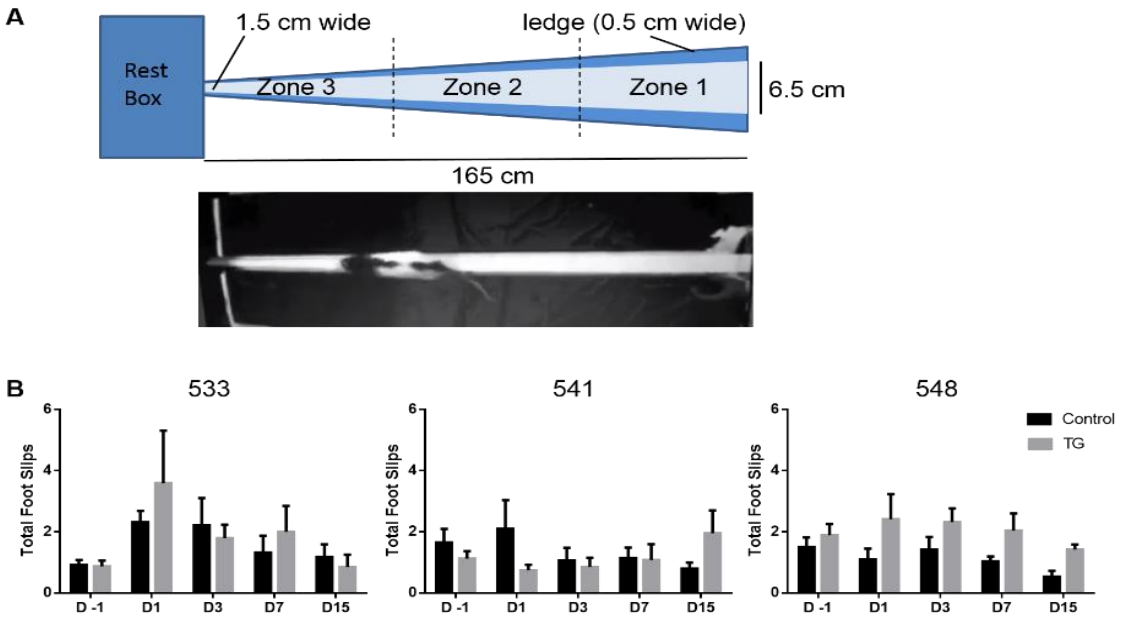

Figure 5.10. Tapered beam test for ICV injected rats. A. Tapered beam was 165 cm in length, decreasing in width nearer the rest box. Rats traversed the beam starting at zone 1. The beam was covered with a white rubber mat and a black cloth was placed beneath the beam to aid in software tracking. **B.** Number of total hind foot slips was recorded over the duration of the study with D-1 as the day before surgery, proceeding to 15 days after surgery (D15). Data expressed as mean ±SEM. 533 TG, n=5; control, n=7; 541 TG, n=6; control, n=7; 548 TG, n=7, control n=7.

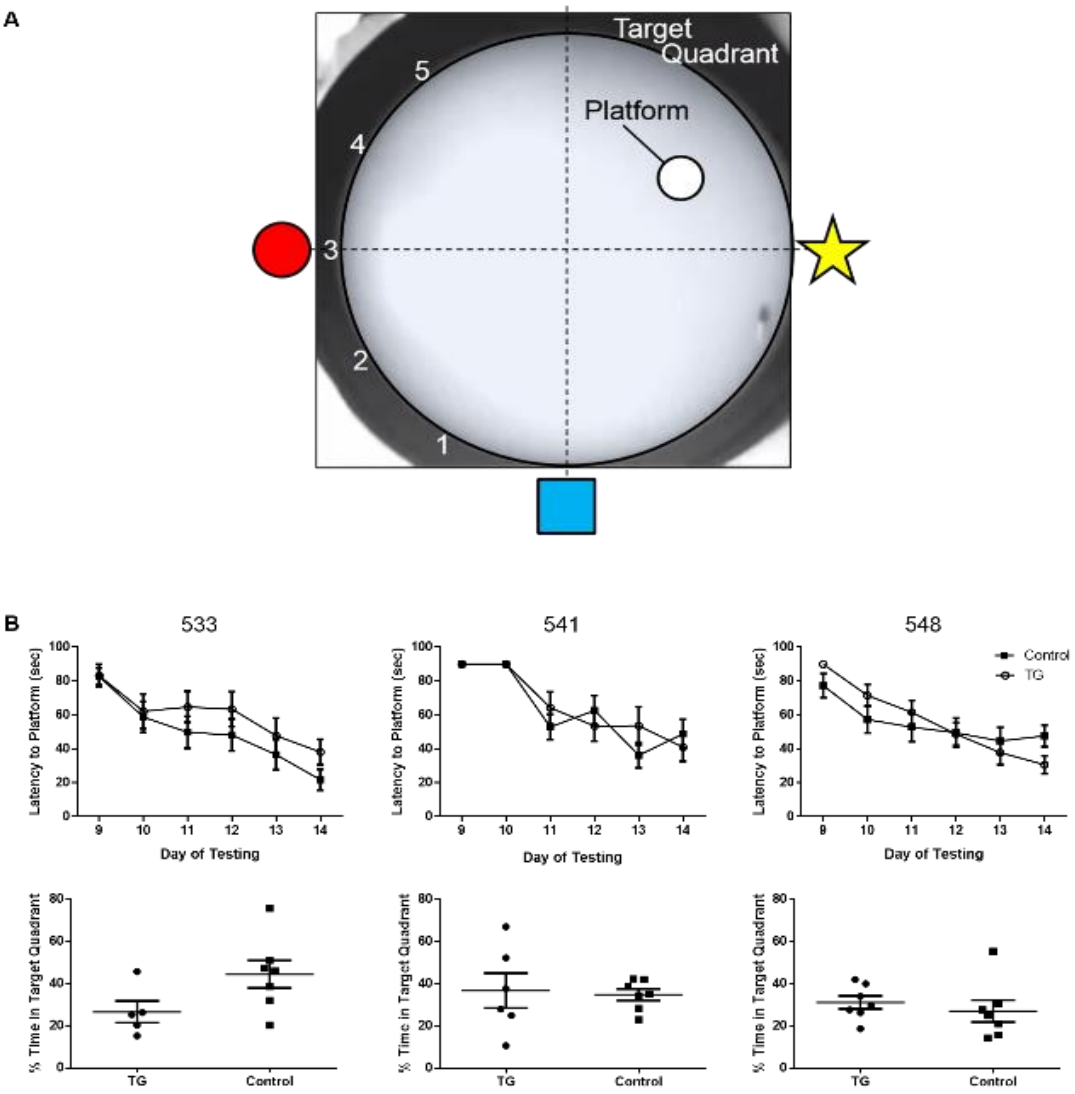

Figure 5.11. Morris water maze for ICV injected rats. A. Yellow star, red circle and blue square represent location of those visual cues in the maze. Numbers indicate start locations. White circle is hidden platform within the target quadrant. Rat swimming in maze is visible in lower right quadrant. **B.** Rats were trained in Morris water maze (MWM). Time taken to reach the platform (latency; top row) during training days was recorded. Time spent in the target quadrant during probe trials was recorded (bottom row). Data expressed as mean ±SEM. 533 TG, n=5; control, n=7; 541 TG, n=6; control, n=7; 548 TG, n=7, control n=7.

Post-mortem quantification of ZsGreen-positive neurons

At necropsy, brains were collected and a cryostat was used to create 40 µm sections of the SN and VTA. Slides of these sections were imaged for expression of ZsGreen. Sections from TG and control rats of line 533 were negative for ZsGreen (Figure 5.11). Sections from stock 541 TG rats were positive for ZsGreen in the SN and VTA, while control rats were negative (Figure 5.12). For TG rats receiving ILY via ICV injection, number of ZsGreen-positive neurons varied with rats 1, 2, 4, and 5 showing an approximately 50% reduction while rats 3 and 6 had an average number of neurons similar to the uninjected control (Figure 5.13). All TG rats (7-9) receiving 500 ng/g BW IP had a reduction in ZsGreen-positive neurons compared to uninjected control (Figure 5.13). Cell counts were not performed on control rats or any rats of stock 533 as there were no ZsGreen-positive neurons. Brain tissue from rats found dead could not be used to be used to produce quality sections for imaging and counting.

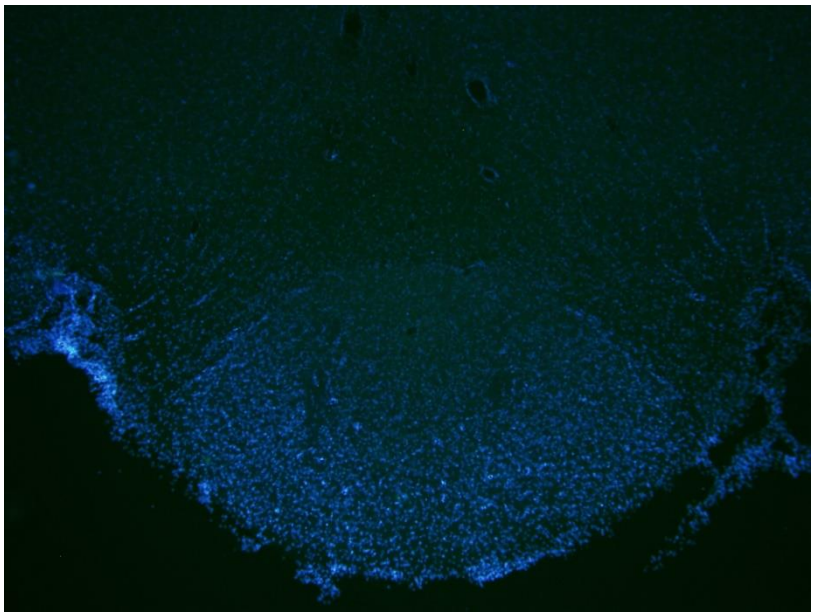

Figure 5.12. Absence of ZsGreen-positive neurons in iCD59.533. Merged ZsGreen/DAPI confocal fluorescent image of VTA of representative TG rat stock 533.

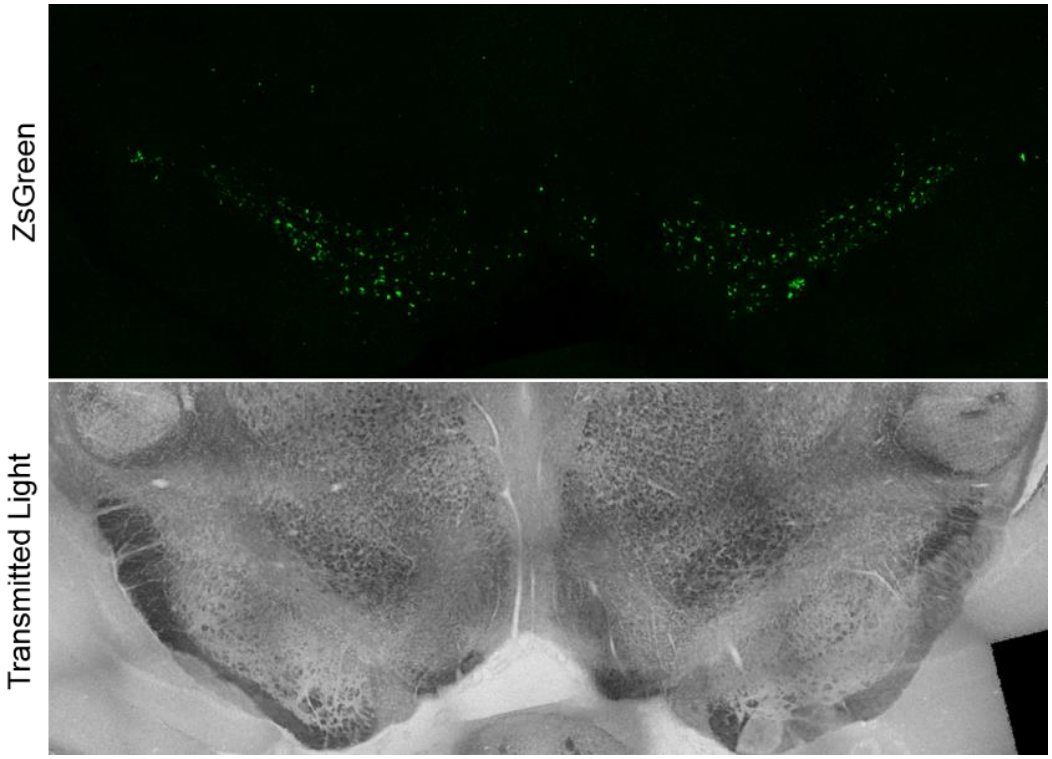

Figure 5.13. Expression of ZsGreen in neurons of ihCD59.541. Confocal 40 μm Z-stack fluorescent image (top) and transmitted light (bottom) of SN/VTA demonstrating ZsGreen positive neurons.

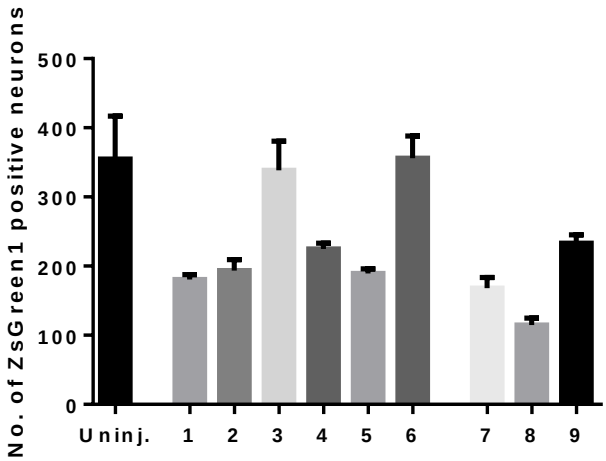

Figure 5.14. Ablation of ZsGreen positive neurons in ILY-treated TG rats. Merged ZsGreen/DAPI fluorescent images of brain sections of the SN/VTA were counted (3 per rat) using ImageJ. Data expressed as mean ±SEM. Uninj, uninjected; 1-6, ICV-injected; 7-9, IP-injected.

Discussion

Our goal was to generate a novel conditional cell ablation rat model utilizing Cre-lox technology and the hCD59-ILY system, thus demonstrating the versatility of ILY-mediated lysis in whole organs. To construct the ihCD59 transgene, a 350 bp fragment containing a P2A self-cleaving peptide sequence followed by hCD59 was cloned into pCAG-*loxP*STOP*loxP*-ZsGreen vector immediately downstream of ZsGreen. Simultaneously, the stop codon of ZsGreen was mutated for bicistronic expression. Testing of this construct *in vitro* in a rat insulinoma cell line demonstrated expression of ZsGreen. Moreover, ZsGreen-positive cells were susceptible to lysis by ILY after a brief incubation. The 4kb transgene was then successfully microinjected into 0.5 day SD embryos. Three founders were generated and were crossed to LE-Tg(TH-Cre)3.1Deis [140] for expression of ZsGreen and hCD59 in tyrosine hydroxylase (TH) positive dopaminergic neurons. In dopaminergic neurons, Cre recombinase was produced, excising the stop cassette located

between the *loxP* sites, leading to expression of ZsGreen visualized by gross and confocal imaging. Furthermore, in at least one founder stock (533), anti-CD59 antibody co-localized with ZsGreen in the substantia nigra as expected. Lastly, both IP and ICV administration of ILY resulted in a reduction of ZsGreen positive neurons in some of the rats, although clinical signs of neuronal loss were lacking.

Transgene generation

The ihCD59 transgene was successfully constructed using in-fusion cloning. The PCR-based method utilizing a high-fidelity *Taq* polymerase enabled the simultaneous mutation of ZsGreen's stop codon as well insertion of the P2A sequence and hCD59. The stop codon mutation was essential as 2A peptides act through a "ribosomal skip" mechanism which results in a breakage between the glycine and proline peptides at the C-terminus of the P2A peptide. Thus ZsGreen is generated first, followed by hCD59, which gains a proline residue at its N-terminus. While ZsGreen remains in the cytosol, hCD59 translocates to the cell membrane due to the presence of its signaling peptide [208]. 2A peptides have now been widely used in a variety of species, having the advantage over IRES where the protein downstream of the IRES has less expression [230-232].

In vitro expression

Testing of the ihCD59 construct *in vitro* using a rat insulinoma cell line demonstrated that there was no expression of ZsGreen until TAT-Cre recombinase was added to the media. Once added, cells began expressing ZsGreen and we hypothesized that hCD59 would be co-expressed. However, immunocytochemistry and western blot analysis using anti-hCD59 antibodies failed to identify hCD59 in transfected cells, although positive control HEK-293 cells (ATCC), which are known to express human CD59 [233],

were negative as well. Even though we were unable to detect hCD59 via antibody methods, the receptor was functionally active as ZsGreen-positive cells were lysed after incubation with ILY. Cells transfected with ihCD59 that were uninduced (no TAT-Cre) were still intact after incubation with ILY (Figure 5.3). Similarly, maxGFP transfected cells (no hCD59) were intact and still green post-ILY treatment. Together these results support that ZsGreen and hCD59 are being co-expressed and hCD59 is a functional receptor for ILY.

In vivo expression

To confirm *in vivo* expression, rats double hemizygous for the ihCD59 and TH-Cre transgenes (TG) were euthanized to collect fresh brain sections at the level of the SN/VTA. All three founder stocks (533, 541, and 548) had appropriate ZsGreen expression (Figure5.5). To confirm co-expression of hCD59 *in vivo*, additional rats from stock 533 and 541 were sectioned at the level of the substantia nigra using a cryostat and sections were labeled with mouse anti-human CD59 antibody, conjugated to PE. DAPI was used for nuclear staining. Upon imaging, neurons within the substantia nigra were positive for ZsGreen and hCD59 (Figure 5.6). Brain regions lacking TH-positive dopaminergic neurons were negative for ZsGreen and hCD59 (Figure 5.6). As the 548 stock bred poorly and had limited experimental animals, IHC was not performed and maintenance of the stock was discontinued following the behavior studies.

ILY ablation and behavioral phenotype

To confirm that ILY can ablate hCD59-expressing cells within whole organs and to establish a novel model of Parkinson's disease (PD), rats were dosed with ILY either IP or ICV to induce neuronal cell death and then subjected to a battery of behavioral tests used to assess Parkinson-like clinical signs. An initial small cohort of stock 541 animals was

injected with 500 ng/g BW ILY IP as this was a sufficient and simple administration regime to induce ablation in the *hCD59*^{RBC} rat (Chapter 3). Previous work by Hu et al. demonstrated that ILY was present in brain macrophages post injection in the mouse [134]. As blood brain barrier permeability is similar between rats and mice [234], we hypothesized that ILY would cross the blood brain barrier in the rat, inducing neuronal lysis. While rats exhibited a reduction in the number of ZsGreen neurons (Figure 5.14), they failed to exhibit any signs of PD and were clinically normal until euthanasia. When evaluated via the cylinder test, both TG and control rats injected with ILY performed similarly with no significant difference in rearing, grooming or hind limb footsteps (Figure 5.8). While some PD models using rotenone exhibit dyskinesia, presenting as instability with a reduction of rearing, grooming and stepping in the cylinder test [235, 236], other models fail to have PD signs unless greater than 50% of the neurons are ablated using paraquat or 6-OHDA [237]. This may explain why although there was a reduction in neurons in our model, perhaps the reduction was not great enough to result in an observed phenotype.

As IP injection of ILY failed to produce signs of PD, ablation was attempted by dosing ILY directly into the brain with an ICV surgical injection. Similar to the outcome seen with IP injected rats, we failed to observe a behavioral phenotype consistent with PD in ICV injected rats. As all groups performed similarly in open field and tapered beam tests (Figures 5.9 and 5.10), any ataxia or proprioceptive defects observed were likely a result of the surgical procedure itself. Because of the limited number of rats available for these studies, we did not include all possible controls in these experiments. Addition of sham-injected and uninjected groups would confirm if surgery or the anesthetic protocol is

responsible for the behavioral changes observed. The tapered beam test has been used to detect motor deficits in PD rat models; however, the test is most robust when severe lesions are present with rats continuing to perform well with up to 74% neurons ablated [238]. Therefore, other behavior tests to assess motor deficits for PD should have been included. The ladder rung test [239, 240] and skilled paw-reaching task [241, 242] are additional behavior tests that may better correlate degree of ablation with PD clinical signs when used with the tapered beam and open field tests. The ladder rung test requires rats to traverse an irregular pattern of rungs and foot faults (either total misses of a rung or slips) are recorded. Foot placement accuracy assesses both stepping and grasping, which can unmask subtle impairments. In the paw-reaching task, rats must reach through a hole to obtain a food reward with their fore paws. A 10-point evaluation of reaching and grasping determines if motor impairment exists.

In addition to the motor deficits observed with PD, patients also experience cognitive deficits [243]. Such deficits are comparably observed in rodent models of PD and may be present before motor deficits manifest [244, 245]. In all groups tested, no difference was observed between TG and control rats in the water maze task, although latency to platform did decrease, indicating that rats effectively learned the maze using the distal cues provided (Figure 5.11). To further validate these findings addition of other memory behavioral tests, such as the exploratory Y-maze, could have been used [246]. For all behavior tests performed in ICV-injected rats, multiple rat handlers were involved, which could also account for the lack of phenotype observed between TG and control rats. Rats respond differently to different handlers [247], and may therefore have more anxiety

with a new handler when completing a task, leading to a faster run on the tapered beam and thus more foot slips.

Post-mortem evaluation of ICV-injected rats indicated a reduction of ZsGreen-positive neurons in some rats compared to an uninjected control. Rats at received 10 µl ILY were unable to be evaluated as the brain tissue was too friable for cryosectioning. Paraffin-embedding with nissl staining or tyrosine hydroxylase IHC may help determine the level of ablation achieved at this dose. For rats injected with 1 µl ILY, counts varied and complete ablation was not achieved. It is possible that there was a technical error in ILY administration which led to the variability in ablation. Rising dose studies as well as an implanted cannula rather than single injection could be used establish dose-dependent ablation with ICV-injected ILY. Alternatively, ILY could be injected directly into the substantia nigra, as has been done with ILY-mediated ablation in the mouse [142].

Interestingly, experimental rats of stock 533 had no ZsGreen expression (Figure 5.12). Our working hypothesis is that the ihCD59 transgene for this line was silenced. Examining and comparing pedigrees for stocks 533 and 541, offspring of the 533 founder (generation 1) expressed ZsGreen (Figure 5.5A) but we observed no ZsGreen expression in the second generation of offspring (Figure 5.15B). Currently, stock 541 animals at generation 3 are still expressing ZsGreen. (Figure 5.15A). Future experiments will be performed with stock 541 and as part of quality control, the strain will be continually monitored for ZsGreen expression at each generation.

The random integration approach used to generate transgenic rats results in multiple lines of rats, each with a unique site of integration and copy number, and therefore, different levels of expression. The presence of foreign DNA, especially in high copy number tandem

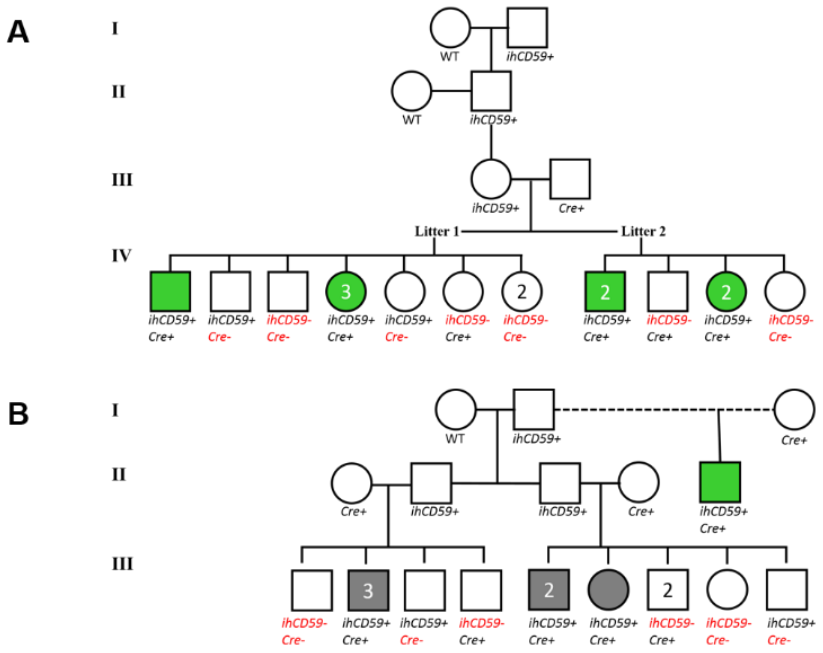

Figure 5.15. Pedigrees from iCD59.541 (A) and iCD59.533 (B) indicating breeding of founder rats (generation I) to WT and TH-Cre (*Cre+*) rats to produce rats used for ICV injection of ILY. Green: positive for ZsGreen/hCD59; gray: no expression.

repeats, is known to induce epigenetic changes, namely histone modification marked by methylation at CpG islands, with the end result being the silencing of any transcriptional elements [248-250]. However, stock 533 had only 1 copy of the transgene inserted as estimated by ddPCR, compared with 3 copies per genome in stock 541 (Figure 5.4). Therefore it is most likely that the silencing of stock 533 is due to suppressive regulatory elements at the insertion region. Addition of flanking insulators as well as targeted insertion to the Rosa26 locus could be employed in future transgenic rats to diminish endogenous effects on the transgene thus improving expression [251, 252].

In conclusion, the ihCD59 transgene was successfully used to ablate cells both *in vitro* and *in vivo*, demonstrating application of the hCD59-ILY system in solid organs. Future generation of tissue specific Cre rats would provide the research community with a wide variety of ablation models to study.

Chapter 6: ILY-mediated ablation in zebrafish

The following work was a collaborative effort with Dr. Anand Chandrasekhar and Suman Gurung (Department of Biological Sciences, University of Missouri, Columbia, MO).

Introduction

One of the classic approaches to study the *in vivo* functions of selected cell populations is cell ablation. Cell ablation can be achieved through a variety of techniques, including physical excision to chemical disruption, though these techniques are often crude and lack selectivity [253, 254]. A genetic strategy could therefore offer the greatest specificity by directing expression of a receptor on the cell type of interest which is specific for a toxin. However current receptor-toxin systems have failed to be rapid, specific, dose-dependent, and applicable to a wide variety of cell types [78, 79]. Moreover, none of these methods have proven to be effective for use in multiple species, such as mice, rats, and zebrafish [255]. In zebrafish specifically, there is a need for a cell ablation system which induces lysis rapidly as embryos develop quickly into free-swimming fish by 72 hours post fertilization (hpf).

Zebrafish can be used in research as an alternative to mammalian species and are quickly emerging as a popular research model as numbers used nears that of rodents [256]. Due to their small size and simple husbandry, zebrafish are easier to house and maintain than rodents, lowering research costs. In contrast to fruit flies and worms, zebrafish are vertebrates, sharing a high degree of homology with mammals and humans [257]. Zebrafish embryos develop externally and are transparent providing unparalleled opportunities for researchers to scrutinize the fine details of embryonic vertebrate

development [258]. Additionally, zebrafish are prolific breeders and methods for transgenesis are highly efficient, making them ideal for genetic studies and genetically manipulation [259, 260].

Ablation studies in zebrafish have been used to explore developmental functions of specific cells during embryogenesis, cell regeneration and lineage tracing [261, 262]. Generation of a genetic ablation model in a species with high fecundity and proficient transgenesis would refine and replace other less efficient physical or chemical ablation models. Ablation can be accomplished through physical, chemical, or genetic methods. Physical and chemical methods often limit cell type susceptible to lysis and do not ensure complete removal of the target tissue nor prevent accidental ablation of unintended cell populations [263]. Thus genetic techniques have moved to the forefront of cell ablation through the production of transgenic animals that express toxin-specific receptors. The diphtheria toxin receptor (DTR) system has been used in rodents and zebrafish successfully for some cell types [79, 89, 264-266]. However, due to the mechanism of ablation, this system can only be used in cells actively synthesizing protein.

In zebrafish and *Drosophila*, the newest ablation method utilizes the *E. coli* nitroreductase receptor (NTR) which converts metronidazole (MTZ) to a toxic drug in cells expressing the receptor [267, 268]. While use of a tissue specific promoter should confer specificity with this technique, it has been demonstrated to have by-stander effects when dying cells release the toxic drug to nearby cells [269]. In addition, fish must be treated with MTZ at near-toxic concentrations for 24 hours to induce cell death and a delayed continuous cell loss is observed after MTZ removal [270]. A delay in cell ablation is a significant confounder as cells swiftly divide and regenerate in developing zebrafish.

A rapid method, such as ILY-mediated ablation, would eliminate this variable and allow for more controlled studies of regeneration.

However, challenges emerge when applying an ablation system optimized for mammals to a fish species which has different physiological parameters. Mammalian body temperature is 37°C, while zebrafish are maintained in water at approximately 28.5°C. Phosphate buffered saline (PBS) is isotonic to mammalian blood at a concentration of 150 mM NaCl while E3 medium used for zebrafish embryos is 5 mM NaCl [271]. Early data published by Nagamune et al. (1996) determined the optimal activity parameters for ILY *in vitro* [113]. Activity of ILY begins to decrease at temperatures below 20° and is completely lost at salt concentrations less than 50 mM NaCl [113]. Considering these data, our goal was to assess the feasibility of ILY-mediated ablation in zebrafish with the long-term goal of generating a novel rapid method of cell ablation in zebrafish thus demonstrating the multi-species advantage of the hCD59-ILY system.

Results

Optimization of ILY for embryo immersion

ILY activity was compared at 28°C and 37°C using the *in vitro* hemolysis assay. Incubation at 28°C did not significantly affect the activity of ILY (Figure 6.1). To determine if embryos can tolerate the high NaCl concentrations necessary for ILY, embryos were incubated in high salt solutions. Concentrations greater than 95 mM NaCl resulted in zebrafish mortality with survival of 36/50 at 105 mM (Figure 6.2).

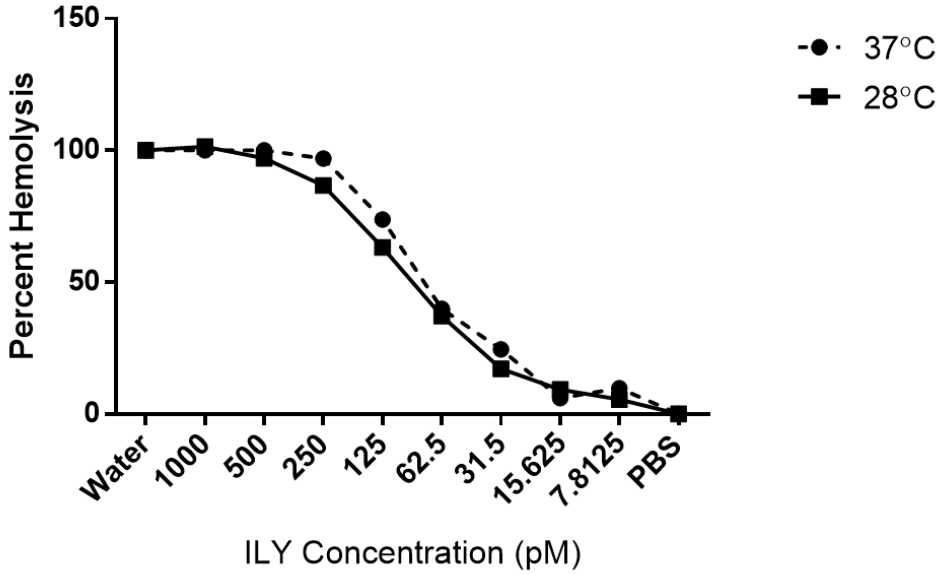

Figure 6.1. Effect of temperature on ILY. Erythrocytes isolated from SD-Tg(HBA1-CD59)Bryd rats (Tg+) were incubated with ILY at a range of concentrations at either 37°C or 28°C for 45 minutes. Percent hemolysis was calculated utilizing water as a positive control (100% lysis) and saline (PBS) as negative control (no lysis).

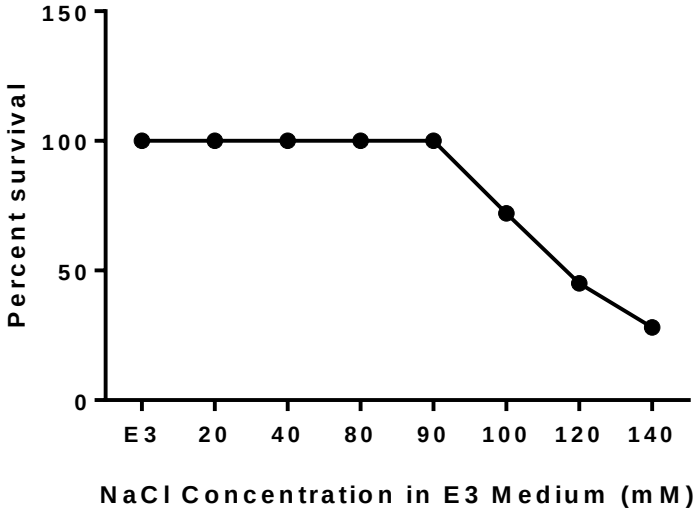

Figure 6.2. Fish tolerance to high salt. Percent survival of wild type zebrafish embryos in a range of salt concentrations. E3 only group, n=47; n=50 for all other groups.

Concentrations greater than 300 mM NaCl resulted in 100% mortality (data not shown). To determine if embryos can tolerate incubation at mammalian body temperature, wild type embryos were incubated for 1 hour at 28°C and 37°C. No gross morphological differences were observed between the two groups and all embryos survived. Wild type embryos were then immersed in varying concentrations of ILY at high salt (95 mM) and high temperature (37°C). Percent survival was at or near 100% for lower concentrations of ILY with mortality increasing drastically above 50 pM ILY (Figure 6.3).

ILY immersion of hCD59-expressing embryos

Following injection of mRNA with WT hCD59 (Figure 6.4) and mut hCD59 (Figure 6.5), zebrafish embryos were positive for ZsGreen as assessed by fluorescent microscopy (Figure 6.6, top right). Uninjected embryos lacked fluorescence and only exhibited auto-fluorescence of the yolk (Figure 6.6, top left). Embryos injected with WT or mut hCD59 has positive ZsGreen expression through 36 hpf. Embryos were then incubated with ILY for 1 hour at 10, 24 and 36 hpf. All 10 hpf embryos, both ZsGreen positive and controls (n=20 per group) died when immersed in 50 pM ILY. Conversely, all 36 hpf embryos, both ZsGreen positive and controls (n=20 per group) survived after ILY immersion. In the 24 hpf group, 13/20 ZsGreen-expressing embryos died following ILY immersion. Unfortunately, some mortality was also observed in the uninjected controls (4/20) at 50 pM ILY (Figure 6.6). No mortality was observed in embryos incubated in saline (no ILY).

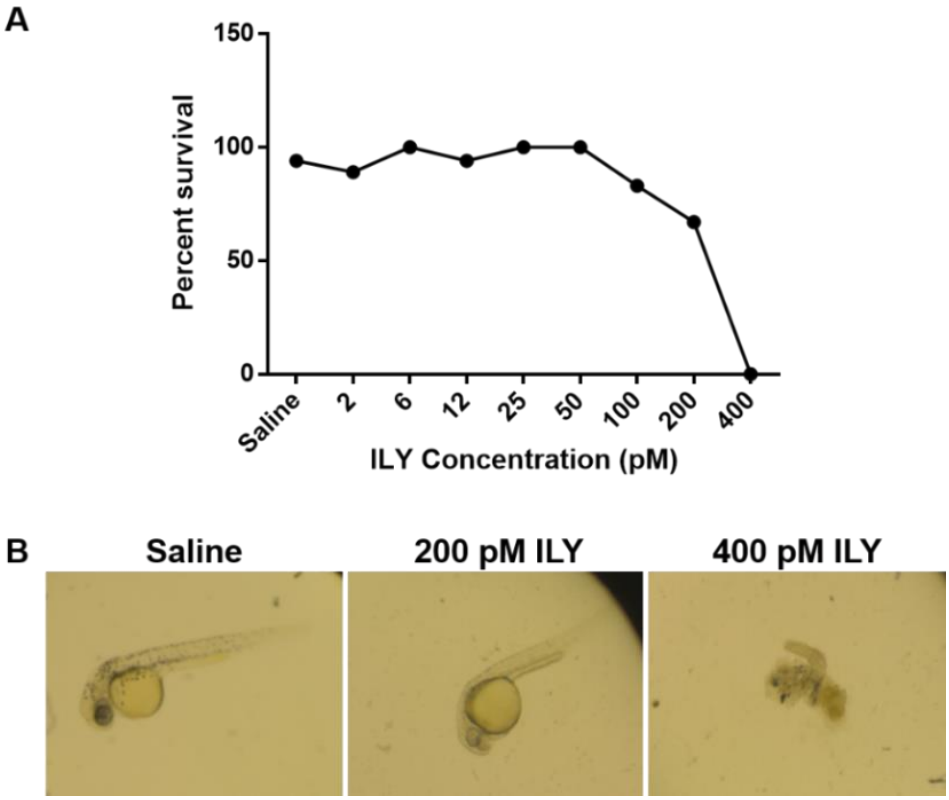

Figure 6.3. Effect of ILY immersion on embryos. Wild type zebrafish at 24 hpf were immersed in a range (2-400 pM) of ILY (n=18 per group) for 1 hour at 37°C. **A.** Percent survival of zebrafish after 1 hour immersion in ILY. **B.** Representative images of zebrafish 1 hour post ILY immersion for saline, 200 pM and 400 pM groups.

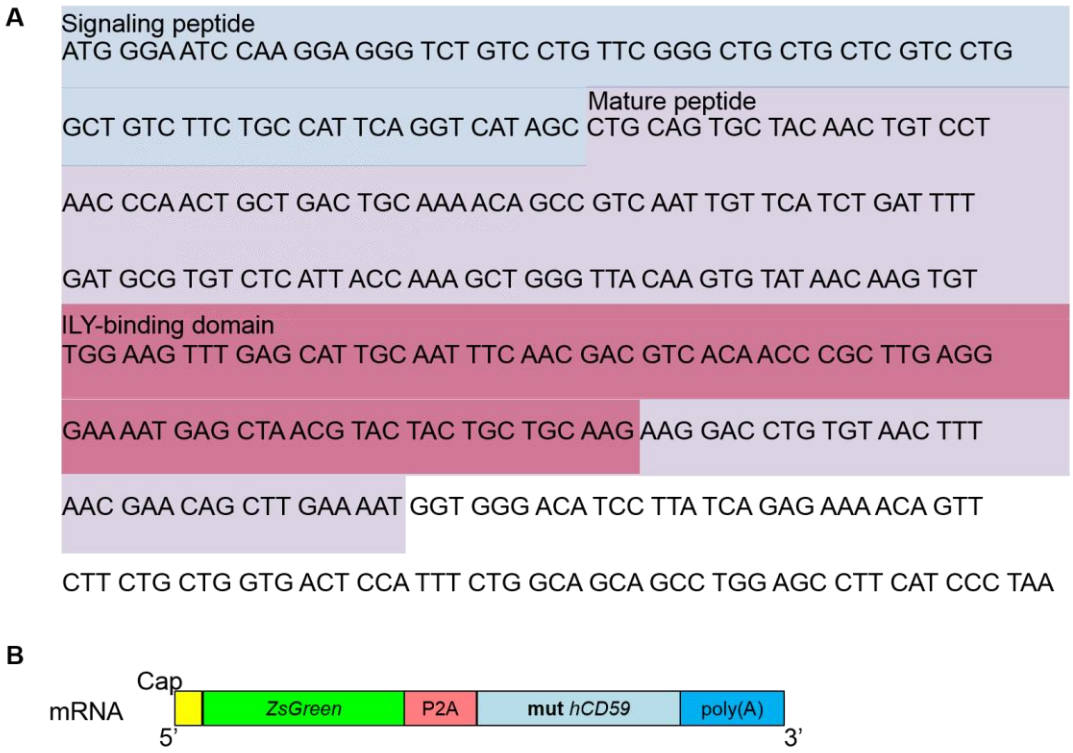

Figure 6.4. Map of pCS2-hCD59. **A.** pCS2+ plasmid following In-Fusion cloning to insert the ZsGreen1-P2A-hCD59 fragment. **B.** SP6 promoter was used to generate WT hCD59 mRNA for microinjection into one-cell zebrafish embryos.

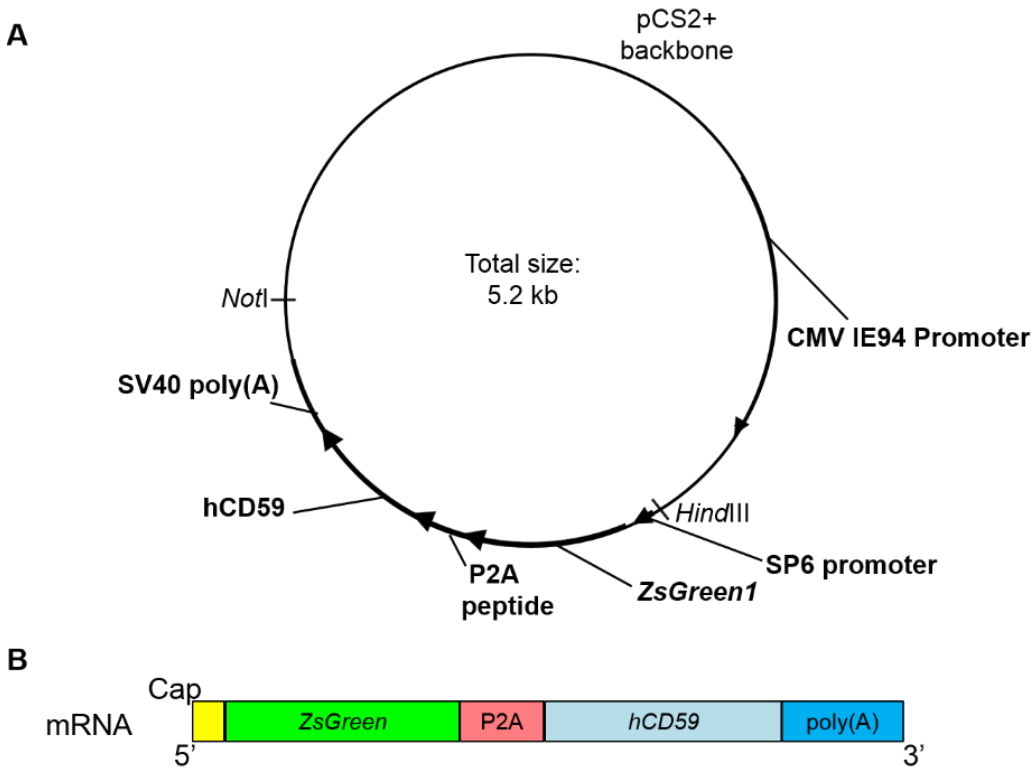

Figure 6.5. Sequence of mut hCD59. A. Human CD59 cDNA sequence highlighting the ILY-binding domain (red) which has been deleted in the mutant (mut) hCD59. **B.** The SP6 promoter was used to generate the mut hCD59 mRNA which will not bind ILY.

When 24 hpf embryos were immersed in a lower concentration of ILY at 33 pM following RNA injections, mortality was only seen in the WT hCD59 injected group at both 1 hour and 1 day post ILY immersion (Figure 6.7A,B). Embryos expressing mut hCD59 or GFP were unaffected, similar to the uninjected group. One hour post ILY immersion, WT hCD59 embryos became fragmented and lacked motility compared to mut hCD59 embryos, which maintained viability (Figure 6.7 C).

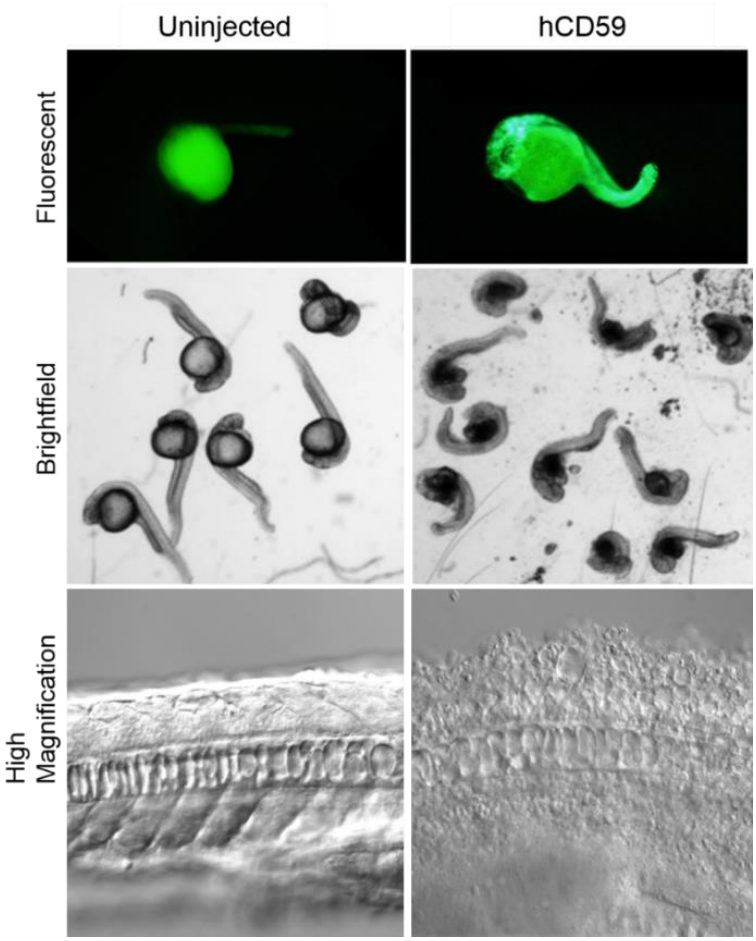

Figure 6.6. Treatment of hCD59-expressing embryos with ILY. Transient expression of ZsGreen1-hCD59 in zebrafish at 24 hpf. WT hCD59 RNA was injected into embryos. Injected embryos were positive for ZsGreen expression (top right). Embryos were immersed in 50 pM ILY and incubated at 37°C. Death was observed in the hCD59 RNA group (13/20) as well as some uninjected embryos (4/20) following ILY immersion (middle panels). At high magnification, vacuolation was observed (bottom right) compared to uninjected control (bottom left). Imaged using an Olympus BX60, 20X objective.

Treatment of adult zebrafish with ILY

No mortality was observed in any of the groups and no clinical signs were observed following intraperitoneal injection of ILY. All fish remained healthy throughout the 5-day observation period. Percent survival was 100% for all groups (Figure 6.8).

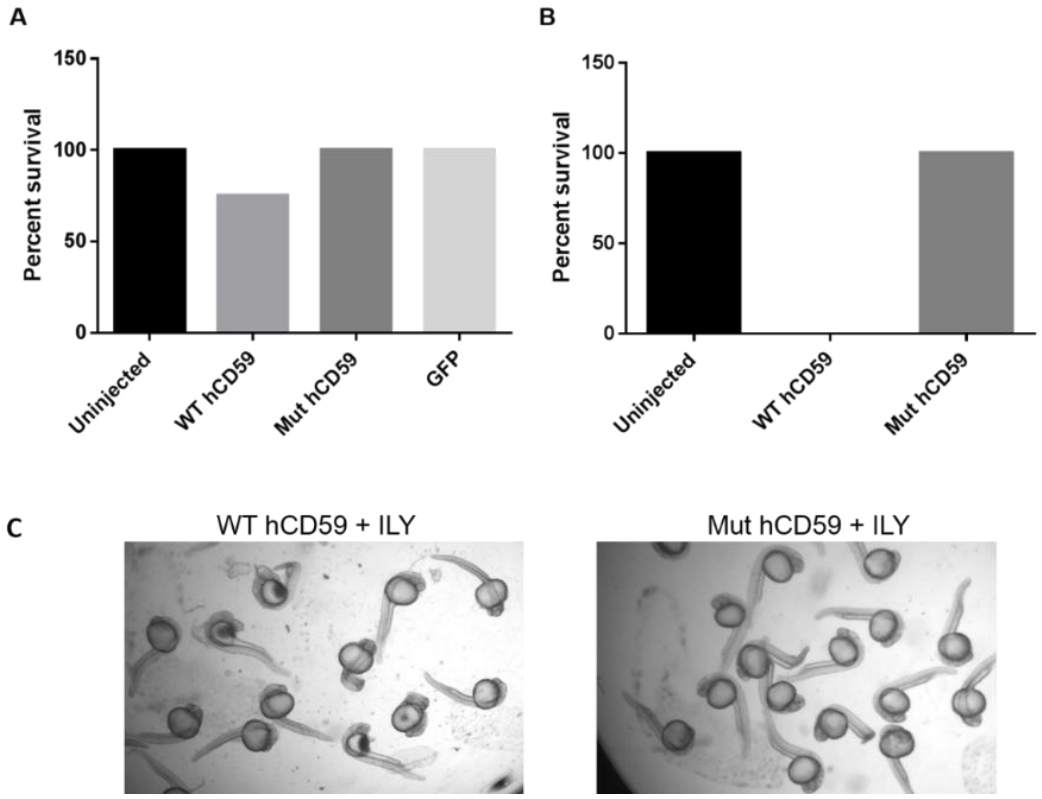

Figure 6.7. Effect of ILY on mRNA-injected embryos. Percent survival of 24 hpf zebrafish 1 hour (A) and 1 day (B) post ILY immersion at 33 pM in E3+90 mM NaCl. Embryos were injected at the one-cell stage with wild type (WT) hCD59 mRNA, mutant hCD59 mRNA lacking the ILY-binding domain or control GFP mRNA. Uninjected embryos received no mRNA. Mortality was observed in WT hCD59 embryos 1 hour post ILY immersion (C, left) while mut hCD59 embryos were healthy (C, right).

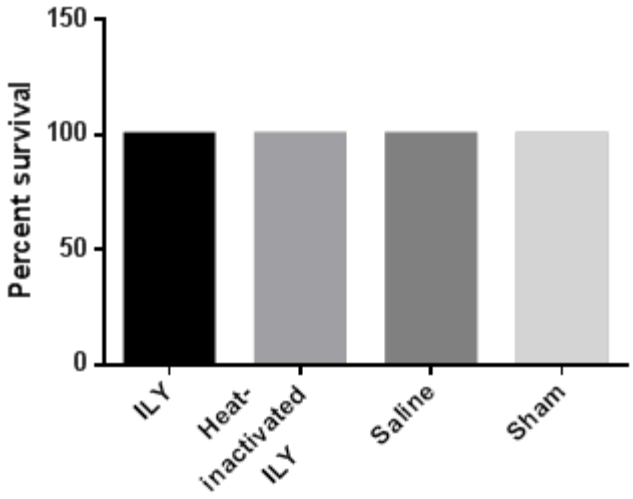

Figure 6.8. Survival of adult zebrafish 5 days post ILY intraperitoneal injection. Fish were anesthetized and injected with active ILY (n=4), heat-inactivated ILY (n=4), saline (n=4) or sham (needle poke with no injection given; n=3).

Discussion

To demonstrate wide application and utility of the hCD59-ILY ablation, we aimed to extend our experiments to an aquatic species, *Danio rerio*. Highlighting this multi-species advantage first required experiments to demonstrate the feasibility of moving from a mammalian system to the zebrafish. Overall, our preliminary data support that ILY-mediated ablation in fish is possible when proper conditions are used. At sodium chloride (NaCl) salt concentrations of 95 mM combined with a brief incubation at 37°C, ILY immersion concentrations less than 50 pM can effectively and specifically induce mortality in ZsGreen-hCD59-expressing embryos.

Earlier work with ILY *in vitro* by Nagamune et al. (1996) has suggested that ILY's lytic activity is affected by temperature and anion salt concentrations. This can present a dilemma for immersion experiments in zebrafish in which embryos are kept in E3 medium

(5 mM NaCl) at approximately 28°C. ILY was observed to have optimal cytolytic activity at near mammalian physiological conditions of 20-45°C [113]. We confirmed that ILY had similar cytolytic activity at both 28°C and 37°C when incubated in PBS containing erythrocytes isolated from transgene-positive *hCD59*^{RBC} rats (Figure 6.1). While ILY activity is similar for a range of temperatures at a consistent salt concentration, it remains unknown if lowered temperature has a compounding effect at less than optimal salt concentrations. According to Nagamune et al. (1996), concentrations of NaCl below 50 mM completely abolished cytolytic activity of ILY (at 37°C). The *in vitro* hemolysis assay must be performed at isotonic salt concentrations (150 mM) as lower concentrations lead to erythrocyte swelling and lysis characteristic of hypotonic solutions. Therefore, we elected to perform all embryo immersion experiments at 37°C after demonstrating that a brief 1 hour incubation at 37°C was not harmful to embryos and did not result in clinical signs (data not shown). Zebrafish are poikilothderms and therefore have a wide range of acceptable environmental temperatures [272]. This is consistent with the literature finding heat shock treatment nonlethal and benign when limited to less than 40°C for less than 1 hour, though such a change could increase rate of development [273] and lead to developmental abnormalities if prolonged [272]. With this in mind, we elected to keep incubations brief as ILY pore formation and lysis occurs rapidly following hCD59 binding. To address the concern of decreased ILY activity with decreasing salt concentrations, we performed salt tolerance testing in zebrafish embryos. Zebrafish embryos can tolerate up to 95 mM NaCl without mortality (Figure 6.2). As this exceeds the 50 mM concentration required for ILY activity, we elected to perform all immersion experiments with E3 medium supplemented with 90 mM NaCl for a final concentration of 95 mM NaCl. While

these conditions appeared to provide sufficient lytic activity to achieve mortality in ZsGreen/hCD59 expressing embryos compared to controls, the degree of ablation is unknown. Further experiments testing the activity of ILY under such conditions combined with the ability to quantify cell lysis over time would help establish time- and dose-dependent cytolytic data to better characterize the hCD59-ILY ablation system in zebrafish.

Once parameters for optimal ILY activity were established, it was important to determine if off-target effects of ILY in wild type zebrafish would be observed. Incubation of ILY with erythrocytes from the mouse, rat, chicken, rabbit, dog, cat, horse, cow and sheep were unaffected, even at 5 times the dose required for human erythrolysis [113]. Phylogenetically, the human CD59 receptor is more closely related to the rodent orthologue than the zebrafish, making it highly unlikely that ILY would bind to zebrafish CD59 and form its deadly pore [274]. To support this data, administration of ILY up to 100 ng/g body w eight IV and 500 ng/g body weight IP in transgene-negative *hCD59*^{RBC} rats had no adverse effects (Chapter 3, Figure 3.4B). Therefore, we hypothesized that, similar to other non-human species, ILY would not induce death in wild type zebrafish embryos. Surprisingly immersion of wild type zebrafish in ILY did cause mortality at concentrations at and above 50 pM (Figure 6.3A). At high ILY concentrations, embryos had decreased or no motility, dark, condensed yolk sac and began to fragment diffusely within 1 hour of ILY exposure (Figure 6.3B). It is possible that other components present in the ILY preparations used for these experiments, perhaps by-products of the ILY purification process, could be contributing to a non-specific, yet dose-dependent, toxicosis. Therefore,

it may be useful to perform mass spectrometry to rule out other noxious chemicals as the cause of mortality in wild type embryos.

To determine if the toxic effects of ILY were restricted to embryos, we performed ILY administration in adult wild type zebrafish. While immersion experiments at the same concentrations tested in embryos was ideal, supply of ILY (generously gifted by the Qin lab) is limited. Therefore, an alternative route of administration was needed and intraperitoneal (IP) injection was the most straightforward. Doses used were comparable to the lethal doses identified in the *hCD59*^{RBC} rat. None of the fish died following IP injection indicating that while more time intensive than immersion, IP injection may be a viable route of administration for ILY-mediated ablation.

When a lower dose of ILY was used (33 pM), death of wild type embryos was abolished (Figure 6.7). Embryos transiently expressing WT ZsGreen/hCD59 began to die 1 hour after ILY immersion leading up to 100 percent mortality after one day. Embryos which transiently expressed the mutant form of hCD59, however, survived. Similarly, uninjected and GFP expressing control groups had no mortality after immersion in 33 pM ILY. It is likely that ILY is indeed specifically binding to hCD59 at these lower concentrations where potential toxicants would be diluted. As immersion dosing is the methodology employed in other zebrafish ablation systems, such as NTR-MTZ, it is vital that this route of administration is optimized for the hCD59-ILY system as well [60]. This dosing method is the simplest and most convenient for researchers, saving time and resources.

When ZsGreen/hCD59-positive embryos were incubated with ILY, their cells became vacuolated and embryos became fragmented. However, a reduction in the number

of fluorescent cells as detected by gross observation was not observed. This could be explained by the ZsGreen protein still being present in high amounts even though the cells containing the protein were dead. Ubiquitous expression of ZsGreen/hCD59 prevents adequate analysis of percent lysis. Utilizing a transgenic fish which has tissue specific expression ZsGreen/hCD59 could provide helpful data through dose-dependent lysis experiments.

Transient expression using mRNA-injected embryos has limitations when attempting to determine the success of dose-dependent ILY-mediated ablation. While microinjection using a microinjector is more accurate than manual syringe injection methods, it is difficult to consistently deliver the same amount of mRNA to each embryo. Therefore individual variation in hCD59 expression following injection can occur, although attempts were made to select embryos with maximal expression of ZsGreen prior to ILY immersion. Generation of stable transgenic zebrafish which express hCD59 would assist in further clarifying the optimal dose of ILY to induce cell ablation while minimizing off-target effects. Additionally, cell ablation of later developmental stages and adults expressing hCD59 could be tested. Such experiments are planned in collaboration with the Chandrasekhar lab, which has generated founder zebrafish containing the ZsGreen-hCD59 transgene under transcriptional control of the zCREST1 promoter [275] for motor neuron expression (Figure 6.9).

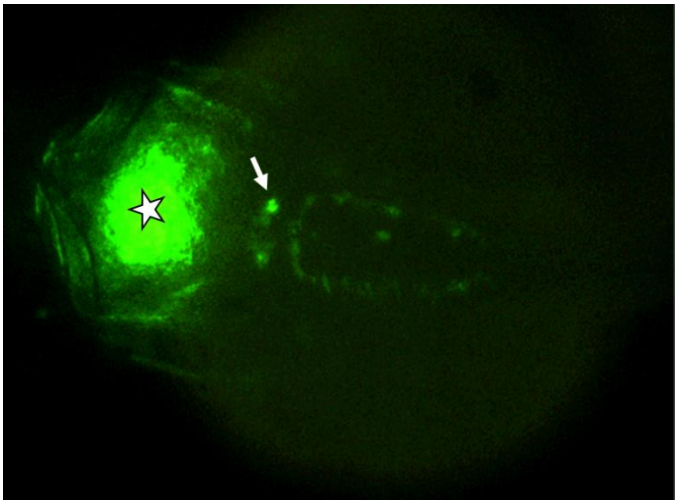

Figure 6.9. zCREST-hCD59 founder. One-cell embryos were injected with Tol2-zCREST-hCD59 DNA and transposase RNA. Dorsal view of larva at 48 hpf positive for ZsGreen in motor neurons (white arrow). Construct also contains *cmlc2*:eGFP (Tol2kit #395) for GFP heart expression (white star) [255].

Chapter 7: Conclusions and Future Directions

The goal of our work was to provide proof of concept that intermedilysin (ILY) administration to ablate cells expressing human CD59 (hCD59) provides a sensitive, specific, and versatile tool for cell ablation in rats and zebrafish. While effective cell ablation using this system has been demonstrated previously in mice, it has not been tested in other model organisms. The *hCD59*^{RBC} and *hCD59*^{END} transgenic mice generated by our collaborator, Dr. Xuebin Qin, established clear advantages of exploiting ILY pore formation as a novel method of cell ablation. These mouse models demonstrated that lysis occurs specifically, rapidly, and without off-target effects in wild type animals. While this data was intriguing for mouse users, we wanted to demonstrate the ability for this new system to work as effectively in other species and in a broader range of cell types.

Chapter 3 of this dissertation further supports the use of ILY-mediated ablation of circulating cells by extending this system to the rat. As rats have a greater blood volume and have been used extensively for cardiovascular and hemodynamic studies, a red cell ablation model has great usefulness. We demonstrated that similar to the mouse model, rats expressing hCD59 on erythrocytes develop anemia and related sequelae following ILY administration. Additionally, wild type rats were unaffected by high doses of ILY, supporting previous work that ILY binds specifically to human CD59 and does not interact with rat CD59. This rat model is available for distribution through the RRRC and should provide researchers with a pertinent model of intravascular hemolysis and anemia.

While we were able to demonstrate that ILY-mediated ablation is attainable in rat circulating cells, Chapters 4 and 5 aimed to extend this work to ablation in solid organs.

This proved challenging as data is limited regarding ILY's ability to perfuse through tissue and as well as the dose of ILY needed to achieve detectable ablation. Therefore, transgene constructs were efficiently generated which included hCD59 cDNA. Testing of the ihCD59 transgene *in vitro* confirmed that hCD59 can be co-expression with a fluorescent protein and maintain functionality, leading to rapid ablation. *In vivo*, the ihCD59 transgene was induced as expected and neurons were decreased in rats dosed with ILY. Unfortunately, both *in vitro* and *in vivo* administration of ILY failed to induce ablation in our RIP-hCD59 transgene.

To extend this work and highlight the multispecies advantage of ILY-mediated ablation, we conducted preliminary feasibility experiments in a common vertebrate model, the zebrafish. As *S. intermedius* has optimized ILY to be a strong virulence factor in its human host, it was unknown if ILY-mediated ablation could be accomplished in a poikilotherm like the zebrafish. The commonly used immersion dosing seen with other ablation methods in zebrafish required optimization for use with ILY as temperature and salt ion differences exist between mammalian and fish models. We found that ILY activity is not affected by a slight decrease in temperature, however salt concentration has been reported to impact lytic activity. By finding an optimal salt concentration for ILY and embryos, we could begin to optimize a protocol for ILY-mediated ablation in zebrafish. Applying these conditions to embryos with and without hCD59 expression demonstrated that ILY could induce cell death and ultimately embryo death, however non-specific death was observed. This is the first species in which off target effects have been observed following ILY administration. Further experiments should be conducted to determine the cause of mortality in wild type zebrafish embryos. Ongoing studies with the Chandrasekhar

lab aim to validate the hCD59-ILY system in transgenic zebrafish expressing *hCD59* in motor neurons.

While this work underscores the potential of the hCD59-ILY system as an approachable method of ablation, there are future experiments that could further this goal and define ILY-mediated ablation as a superior technology over those already in practice. By generating a 'Cre zoo' of tissue specific Cre-driver rat strains, we could quickly develop many ablation models using the ihCD59 rat. Additionally, because the presence of hCD59 appears to have no overt negative effects, the ihCD59 rat could also been a useful reporter rat in the development of future Cre-diver lines.

In addition to validating the hCD59-ILY system in mouse, rat, and zebrafish, extending this technology to another model species would also be of interest to the scientific community. It would be interesting to demonstrate that ILY-mediated ablation can have similar success in the chick embryo (*Gallus gallus*), a popular model of developmental biology [276-278]. Feasibility experiments could first be performed using the iCD59 construct transfected into avian cell lines, chicken DF1 and quail QM7, prior to producing transgenic chicks [279]. Ablation of the same cell type, by the same rapid and specific method, in multiple species could answer simple experimental questions in comparative embryology and genetics not previously attainable.

The single largest limitation of the hCD59-ILY ablation system is the availability of ILY. Currently the Qin lab is the only supplier. ILY production is time-consuming and yields small lots with variable activity between lots, as measured by the *in vitro* hemolysis assay, with some lots showing activity *in vitro* but failing to produce lysis *in vivo.* This is likely due to the labile nature of the toxin and its degradation when not handled

appropriately. With such limitations, careful planning and coordination with the Qin lab are necessary to ensure that experiments can be completed in a timely manner. Researchers requesting ILY from the Qin lab should allow 2 months from placing the order until delivery, depending on the quantity of ILY requested. A longer processing time could be expected as more researchers begin using this novel method. To employ this ablation system as a desirable alternative to other methods, such as NTR or DTR, ILY needs to be mass-produced with stringent quality control measures to assure consistent cell lysis for the end user requiring reproducible results under time constraints.

In summary, we generated several rat models which have validated the use of the hCD59-ILY ablation system in a novel species. We have also presented strong preliminary data for application of this system in zebrafish. The use of hCD59-ILY will have wide application for any studies in any species that can benefit from selective cell ablation *in vivo*.

Appendix

List of Primers Used

Name	Sequence (5'-3')	Use
hCD59 F	AGAGCCCATGGGAATCCAAGGAG	G
hCD59 R	AGAGCCCATCACTATTAGACTTAGGGATGAAGGCTCCA	G
hCD59-EcoRI F	AGAGCCCATGGGAATCCA	C
hCD59-XbaI R	ATCAGCGAGCTCTAGATTAGGGATGAAGGCTCCAG	C
RIP-HindIII F	CGGTATCGATAAGCTTGCTGAGCTAAGAATCCAGC	C
RIP-EcoRI R	ATTCCCATGGGCTCTGAATTCGACCTGGAAGATAG	C
RIP-hCD59 F	GTCCCCAACAACTGCAACTTT	G
RIP-hCD59 R	ACAACCCGCTTGAGGGAAAA	G
iCD59 F	TGCAGCCCAAGCTAGATCGAA	G
iCD59 R	TTGCAGTCAGCAGTTGGGTT	G
pCS2-iCD59 F	CCATCGATTCGAATTATGGCCCAGTCCAAGCAC	C
PCS2-iCD59 R	GAGAGGCCTTGAATTTTAGGGATGAAGGCTCCA	C
T7	TAATACGACTCACTATAGGG	S
M13	GTAAAACGACGGCCAGT	S
ZsGreen F	GTGTACAAGGCCAAGTCCGT	D
ZsGreen R	CCACTTCTGGTTCTTGGCGT	D
ZsGreen Probe	56-FAM/TTCATCCAG/ZEN/CACAAGCTGAC/3IABk	D
Ggt1 F	CCACCCCTTCCCTACTCCTAC	D
Ggt1 R	GGCCACAGAGCTGGTTGTC	D
Ggt1 Probe	5HEX/CCGAGAAGC/ZEN/AGCCACAGCCATACCT/3IABk	D

Primers used for cloning (C), genotyping (G), sequencing (S) and ddPCR (D). F, forward; R, reverse; FAM, FAM flurophore; HEX, HEX™ flurophore; ZEN, ZEN™ internal quencher; IABk, Iowa Black quencher.

Egg water:
1.5 mL stock salts added to 1L distilled water

Stock salts:
40 g “instant ocean” sea salts added to 1L distilled water

E3 medium:
5mM NaCl
0.17 mM KCl
0.33 mM $CaCl_2$
0.33 mM $MgSO_4$
Adjust pH to 6.8-6.9 with NaOH.

Clove Oil:
Stock solution- 9 parts ethanol and 1 part clove oil
Use 2 mL stock solution in 5 L fish water

Bibliography

1. Shin, S., et al., *Ablation of Foxl1-Cre-labeled hepatic progenitor cells and their descendants impairs recovery of mice from liver injury.* Gastroenterology, 2015. **148**(1): p. 192-202.e3.

2. Criscimanna, A., et al., *Activated macrophages create lineage-specific microenvironments for pancreatic acinar- and β-cell regeneration in mice.* Gastroenterology, 2014. **147**(5): p. 1106-1118.e11.

3. Kim, S.K., et al., *A model of liver carcinogenesis originating from hepatic progenitor cells with accumulation of genetic alterations.* International Journal of Cancer, 2014. **134**(5): p. 1067-1076.

4. Willenborg, S., et al., *Genetic ablation of mast cells redefines the role of mast cells in skin wound healing and bleomycin-induced fibrosis.* Journal of Investigative Dermatology, 2014. **134**(7): p. 2005-2015.

5. Yokota, K., et al., *Engrafted Neural Stem/Progenitor Cells Promote Functional Recovery through Synapse Reorganization with Spared Host Neurons after Spinal Cord Injury.* Stem Cell Reports, 2015.

6. Kaestner, K.H., *β Cell transplantation and immunosuppression: Can't live with it, can't live without it.* Journal of Clinical Investigation, 2007. **117**(9): p. 2380-2382.

7. Yang, C.T., R.D. Sengelmann, and S.L. Johnson, *Larval melanocyte regeneration following laser ablation in zebrafish.* J Invest Dermatol, 2004. **123**(5): p. 924-9.

8. Vogel, A. and V. Venugopalan, *Mechanisms of pulsed laser ablation of biological tissues.* Chem Rev, 2003. **103**(2): p. 577-644.

9. Zeigler, M.B. and D.T. Chiu, *Laser selection significantly affects cell viability following single-cell nanosurgery.* Photochem Photobiol, 2009. **85**(5): p. 1218-24.

10. Dijkink, R., et al., *Controlled cavitation-cell interaction: trans-membrane transport and viability studies.* Phys Med Biol, 2008. **53**(2): p. 375-90.

11. Mulholland, G.E., et al., *Near-infrared laser cellular ablation and development in Xenopus laevis embryos.* Journal of Laser Applications, 2016. **28**(1): p. 5.

12. Galbraith, J.A. and M. Terasaki, *Controlled damage in thick specimens by multiphoton excitation.* Mol Biol Cell, 2003. **14**(5): p. 1808-17.

13. Matrone, G., et al., *Laser-targeted ablation of the zebrafish embryonic ventricle: a novel model of cardiac injury and repair.* Int J Cardiol, 2013. **168**(4): p. 3913-9.

14. Angelo, J.R. and K.D. Tremblay, *Laser-Mediated Cell Ablation During Post-Implantation Mouse Development.* Developmental Dynamics, 2013. **242**(10): p. 1202-1209.

15. Matrone, G., et al., *Targeted laser ablation of the zebrafish larval heart induces models of heart block, valvular regurgitation, and outflow tract obstruction.* Zebrafish, 2014. **11**(6): p. 536-41.

16. Dunn, T.W., et al., *Neural Circuits Underlying Visually Evoked Escapes in Larval Zebrafish.* Neuron, 2016. **89**(3): p. 613-28.

17. Severi, K.E., et al., *Neural control and modulation of swimming speed in the larval zebrafish.* Neuron, 2014. **83**(3): p. 692-707.

18. Otten, C. and S. Abdelilah-Seyfried, *Laser-inflicted Injury of Zebrafish Embryonic Skeletal Muscle.* Jove-Journal of Visualized Experiments, 2013(71): p. 5.

19. Powell, C., et al., *Zebrafish Muller glia-derived progenitors are multipotent, exhibit proliferative biases and regenerate excess neurons.* Scientific Reports, 2016. **6**: p. 10.

20. Koshkaryev, A., et al., *2-Butoxyethanol enhances the adherence of red blood cells.* Archives of Toxicology, 2003. **77**(8): p. 465-469.

21. Bauer, A., et al., *The glucocorticoid receptor is required for stress erythropoiesis.* Genes Dev, 1999. **13**(22): p. 2996-3002.

22. Diwan, A., et al., *Targeting erythroblast-specific apoptosis in experimental anemia.* Apoptosis, 2008. **13**(8): p. 1022-30.

23. Udden, M.M., *Rat erythrocyte morphological changes after gavage dosing with 2-butoxyethanol: a comparison with the in vitro effects of butoxyacetic acid on rat and human erythrocytes.* J Appl Toxicol, 2000. **20**(5): p. 381-7.

24. Dornfest, B.S., et al., *Phenylhydrazine is a mitogen and activator of lymphoid cells.* Ann Clin Lab Sci, 1990. **20**(5): p. 353-70.

25. Klinken, S.P., et al., *Phenylhydrazine stimulates lymphopoiesis and accelerates Abelson murine leukemia virus-induced pre-B cell lymphomas.* J Immunol, 1987. **139**(9): p. 3091-8.

26. Ramot, Y., et al., *Age and dose sensitivities in the 2-butoxyethanol F344 rat model of hemolytic anemia and disseminated thrombosis.* Exp Toxicol Pathol, 2007. **58**(5): p. 311-22.

27. Organization, W.H., *Formaldehyde, 2-butoxyethanol and 1-tert-butoxypropan-2-ol.* IARC Monogr Eval Carcinog Risks Hum, 2006. **88**: p. 1-478.

28. Zeljezic, D., et al., *Evaluation of genome damage in subjects occupationally exposed to possible carcinogens.* Toxicol Ind Health, 2015.

29. Eleazu, C.O., et al., *Review of the mechanism of cell death resulting from streptozotocin challenge in experimental animals, its practical use and potential risk to humans.* Journal of Diabetes and Metabolic Disorders, 2013. **12**: p. 60-60.

30. Evan, A.P., et al., *The effect of streptozotocin and streptozotocin-induced diabetes on the kidney.* Ren Physiol, 1984. **7**(2): p. 78-89.

31. Deeds, M.C., et al., *Single dose streptozotocin-induced diabetes: considerations for study design in islet transplantation models.* Lab Anim, 2011. **45**(3): p. 131-40.

32. Kume, E., et al., *Hepatic changes in the acute phase of streptozotocin (SZ)-induced diabetes in mice.* Exp Toxicol Pathol, 2004. **55**(6): p. 467-80.

33. Honjo, K., et al., *Histopathology of streptozotocin-induced diabetic DBA/2N and CD-1 mice.* Lab Anim, 1986. **20**(4): p. 298-303.

34. Whitney, J.L., et al., *Growth hormone exacerbates diabetic renal damage in male but not female rats.* Biol Sex Differ, 2013. **4**: p. 12.

35. Choi, J.W., et al., *Gender dimorphism in regulation of plasma proteins in streptozotocin-induced diabetic rats.* Proteomics, 2013. **13**(16): p. 2482-94.

36. Kaku, K., et al., *A single major gene controls most of the difference in susceptibility to streptozotocin-induced diabetes between C57BL/6J and C3H/HeJ mice.* Diabetologia, 1989. **32**(10): p. 716-23.

37. Murphy, M.P., *How mitochondria produce reactive oxygen species.* Biochem J, 2009. **417**(1): p. 1-13.

38. Perier, C. and M. Vila, *Mitochondrial Biology and Parkinson's Disease.* Cold Spring Harbor Perspectives in Medicine, 2012. **2**(2): p. a009332.

39. Terzioglu, M. and D. Galter, *Parkinson's disease: genetic versus toxin-induced rodent models.* Febs j, 2008. **275**(7): p. 1384-91.

40. Sherer, T.B., et al., *Mechanism of toxicity of pesticides acting at complex I: relevance to environmental etiologies of Parkinson's disease.* J Neurochem, 2007. **100**(6): p. 1469-79.

41. Minnema, D.J., et al., *Dietary administration of paraquat for 13 weeks does not result in a loss of dopaminergic neurons in the substantia nigra of C57BL/6J mice.* Regul Toxicol Pharmacol, 2014. **68**(2): p. 250-8.

42. Chiu, C.C., et al., *Neuroprotective effects of aldehyde dehydrogenase 2 activation in rotenone-induced cellular and animal models of parkinsonism.* Exp Neurol, 2015. **263**: p. 244-53.

43. Cai, Z., et al., *Neonatal systemic exposure to lipopolysaccharide enhances susceptibility of nigrostriatal dopaminergic neurons to rotenone neurotoxicity in later life.* Dev Neurosci, 2013. **35**(2-3): p. 155-71.

44. Sai, Y., et al., *Phosphorylated-ERK 1/2 and neuronal degeneration induced by rotenone in the hippocampus neurons.* Environ Toxicol Pharmacol, 2009. **27**(3): p. 366-72.

45. Naujok, O., et al., *Selective Removal of Undifferentiated Embryonic Stem Cells from Differentiation Cultures Through HSV1 Thymidine Kinase and Ganciclovir Treatment.* Stem Cell Reviews and Reports, 2010. **6**(3): p. 450-461.

46. Cai, L.Y., et al., *Expression of porcine FSHβ subunit promoter-driven herpes simplex virus thymidine kinase gene in transgenic rats.* Journal of Reproduction and Development, 2007. **53**(2): p. 201-209.

47. Mikola, M.K., et al., *Gonadal tumors of mice double transgenic for inhibin-α promoter-driven simian virus 40 T-antigen and herpes simplex virus thymidine kinase are sensitive to ganciclovir treatment.* Journal of Endocrinology, 2001. **170**(1): p. 79-90.

48. Ahtiainen, M., et al., *Indirect Sertoli Cell-Mediated Ablation of Germ Cells in Mice Expressing the Inhibin-α Promoter/Herpes Simplex Virus Thymidine Kinase Transgene.* Biology of Reproduction, 2004. **71**(5): p. 1545-1550.

49. Dancer, A., et al., *Expression of thymidine kinase driven by an endothelial-specific promoter inhibits tumor growth of Lewis lung carcinoma cells in transgenic mice.* Gene Therapy, 2003. **10**(14): p. 1170-1178.

50. Wu, J.X., et al., *Liposomal insulin promoter-thymidine kinase gene therapy followed by ganciclovir effectively ablates human pancreatic cancer in mice.* Cancer Letters, 2015. **359**(2): p. 206-210.

51. Mathis, J.M., et al., *Cancer-specific targeting of an adenovirus-delivered herpes simplex virus thymidine kinase suicide gene using translational control.* Journal of Gene Medicine, 2006. **8**(9): p. 1105-1120.

52. Freund, C.T.F., et al., *Combination of adenovirus-mediated thymidine kinase gene therapy with cytotoxic chemotherapy in bladder cancer in vitro.* Seminars in Urologic Oncology, 2003. **21**(3): p. 197-205.

53. Mercer, K.E., et al., *Mutation of herpesvirus thymidine kinase to generate ganciclovir-specific kinases for use in cancer gene therapies.* Protein Engineering, 2002. **15**(11): p. 903-911.

54. Beck, C., et al., *The thymidine kinase/ganciclovir-mediated "suicide" effect is variable in different tumor cells.* Hum Gene Ther, 1995. **6**(12): p. 1525-30.

55. Mesnil, M. and H. Yamasaki, *Bystander effect in Herpes simplex virus-thymidine kinase/ganciclovir cancer gene therapy: Role of gap-junctional intercellular communication.* Cancer Research, 2000. **60**(15): p. 3989-3999.

56. Bridgewater, J.A., et al., *Expression of the bacterial nitroreductase enzyme in mammalian cells renders them selectively sensitive to killing by the prodrug CB1954.* Eur J Cancer, 1995. **31a**(13-14): p. 2362-70.

57. Huang, Y. and L. Li, *DNA crosslinking damage and cancer - a tale of friend and foe.* Translational cancer research, 2013. **2**(3): p. 144-154.

58. Han, D.D., D. Stein, and L.M. Stevens, *Investigating the function of follicular subpopulations during Drosophila oogenesis through hormone-dependent enhancer-targeted cell ablation.* Development, 2000. **127**(3): p. 573-83.

59. Curado, S., et al., *Conditional targeted cell ablation in zebrafish: a new tool for regeneration studies.* Dev Dyn, 2007. **236**(4): p. 1025-35.

60. Pisharath, H. and M.J. Parsons, *Nitroreductase-mediated cell ablation in transgenic zebrafish embryos.* Methods in molecular biology (Clifton, N.J.), 2009. **546**: p. 133-143.

61. Pisharath, H., et al., *Targeted ablation of beta cells in the embryonic zebrafish pancreas using E. coli nitroreductase.* Mech Dev, 2007. **124**(3): p. 218-29.

62. Cui, W., et al., *Inducible ablation of astrocytes shows that these cells are required for neuronal survival in the adult brain.* Glia, 2001. **34**(4): p. 272-82.

63. Felmer, R.N. and J.A. Clark, *The gene suicide system NTR/CB 1954 causes ablation of differentiated 3T3L1 adipocytes by apoptosis.* Biological Research, 2004. **37**(3): p. 449-460.

64. Bridgewater, J.A., et al., *The bystander effect of the nitroreductase/CB1954 enzyme/prodrug system is due to a cell-permeable metabolite.* Hum Gene Ther, 1997. **8**(6): p. 709-17.

65. MacAry, G., et al., *Transgenic mice expressing nitroreductase gene under the control of the podocin promoter: A new murine model of inductible glomerular injury.* Virchows Archiv, 2010. **456**(3): p. 325-337.

66. Drabek, D., et al., *The expression of bacterial nitroreductase in transgenic mice results in specific cell killing by the prodrug CB1954.* Gene Ther, 1997. **4**(2): p. 93-100.

67. Kwak, S.P., et al., *Ablation of central nervous system progenitor cells in transgenic rats using bacterial nitroreductase system.* J Neurosci Res, 2007. **85**(6): p. 1183-93.

68. Chen, S., et al., *Molecular characterization of binding of substrates and inhibitors to DT-diaphorase: combined approach involving site-directed mutagenesis, inhibitor-binding analysis, and computer modeling.* Mol Pharmacol, 1999. **56**(2): p. 272-8.

69. Palmiter, R., *Interrogation by toxin.* Nat Biotech, 2001. **19**(8): p. 731-732.

70. Naglich, J.G., et al., *Expression cloning of a diphtheria toxin receptor: Identity with a heparin-binding EGF-like growth factor precursor.* Cell, 1992. **69**(6): p. 1051-1061.

71. Wood, W.M., et al., *MyoD-expressing progenitors are essential for skeletal myogenesis and satellite cell development.* Dev Biol, 2013. **384**(1): p. 114-27.

72. Gensch, N., et al., *Different autonomous myogenic cell populations revealed by ablation of Myf5-expressing cells during mouse embryogenesis.* Development, 2008. **135**(9): p. 1597-1604.

73. Lluri, G., et al., *Hematopoietic progenitors are required for proper development of coronary vasculature.* J Mol Cell Cardiol, 2015. **86**: p. 199-207.

74. Hu, W., et al., *Human CD59 inhibitor sensitizes rituximab-resistant lymphoma cells to complement-mediated cytolysis.* Cancer Res, 2011. **71**(6): p. 2298-307.

75. Lee, B., et al., *Conditional cell ablation via diphtheria toxin reveals distinct requirements for the basal plate in the regional identity of diencephalic subpopulations.* Genesis, 2015. **53**(6): p. 356-65.

76. Yun, S., et al., *Stress-Induced Anxiety- and Depressive-Like Phenotype Associated with Transient Reduction in Neurogenesis in Adult Nestin-CreERT2/Diphtheria Toxin Fragment A Transgenic Mice.* PLoS One, 2016. **11**(1): p. e0147256.

77. Kurita, R., et al., *Suppression of lens growth by αA-crystallin promoter-driven expression of diphtheria toxin results in disruption of retinal cell organization in zebrafish.* Developmental Biology, 2003. **255**(1): p. 113-127.

78. Wan, H., et al., *Analyses of pancreas development by generation of gfp transgenic zebrafish using an exocrine pancreas-specific elastaseA gene promoter.* Experimental Cell Research, 2006. **312**(9): p. 1526-1539.

79. Li, Z., V. Korzh, and Z. Gong, *DTA-mediated targeted ablation revealed differential interdependence of endocrine cell lineages in early development of zebrafish pancreas.* Differentiation, 2009. **78**(4): p. 241-252.

80. Brockschnieder, D., et al., *An improved mouse line for Cre-induced cell ablation due to diphtheria toxin A, expressed from the Rosa26 locus.* Genesis, 2006. **44**(7): p. 322-7.

81. Erlandsson, L., et al., *Joining chain-expressing and -nonexpressing B cell populations in the mouse.* J Exp Med, 2001. **194**(5): p. 557-70.

82. Higashiyama, S., et al., *Membrane-anchored growth factors, the epidermal growth factor family: Beyond receptor ligands.* Cancer Science, 2008. **99**(2): p. 214-220.

83. Beaumelle, B., L. Bensammar, and A. Bienvenue, *Selective translocation of the A chain of diphtheria toxin across the membrane of purified endosomes.* J Biol Chem, 1992. **267**(16): p. 11525-31.

84. Iwamoto, R., et al., *Heparin-binding EGF-like growth factor, which acts as the diphtheria toxin receptor, forms a complex with membrane protein DRAP27/CD9, which up-regulates functional receptors and diphtheria toxin sensitivity.* Embo j, 1994. **13**(10): p. 2322-30.

85. Chang, T. and D.M. Neville, Jr., *Demonstration of diphtheria toxin receptors on surface membranes from both toxin-sensitive and toxin-resistant species.* J Biol Chem, 1978. **253**(19): p. 6866-71.

86. Bi, R., et al., *Diphtheria Toxin- and GFP-Based Mouse Models of Acquired Hypoparathyroidism and Treatment With a Long-Acting Parathyroid Hormone Analog.* J Bone Miner Res, 2016. **31**(5): p. 975-84.

87. Raso, V. and J. McGrath, *Cure of experimental human malignant mesothelioma in athymic mice by diphtheria toxin.* J Natl Cancer Inst, 1989. **81**(8): p. 622-7.

88. Petrenko, V., et al., *Apoptotic neurons induce proliferative responses of progenitor cells in the postnatal neocortex.* Experimental Neurology, 2015. **273**: p. 126-137.

89. Buch, T., et al., *A Cre-inducible diphtheria toxin receptor mediates cell lineage ablation after toxin administration.* Nat Methods, 2005. **2**(6): p. 419-26.

90. Rebourcet, D., et al., *Sertoli Cells Modulate Testicular Vascular Network Development, Structure, and Function to Influence Circulating Testosterone Concentrations in Adult Male Mice.* Endocrinology, 2016. **157**(6): p. 2479-2488.

91. Steenberg, V.R., et al., *Acute disruption of glucagon secretion or action does not improve glucose tolerance in an insulin-deficient mouse model of diabetes.* Diabetologia, 2016. **59**(2): p. 363-370.

92. Matsuoka, K., et al., *Generation of mouse models for type 1 diabetes by selective depletion of pancreatic beta cells using toxin receptor-mediated cell knockout.* Biochem Biophys Res Commun, 2013. **436**(3): p. 400-5.

93. Willems, C., et al., *Regeneration in the Pituitary After Cell-Ablation Injury: Time-Related Aspects and Molecular Analysis.* Endocrinology, 2016. **157**(2): p. 705-721.

94. van Blijswijk, J., et al., *Altered lymph node composition in diphtheria toxin receptor-based mouse models to ablate dendritic cells.* J Immunol, 2015. **194**(1): p. 307-15.

95. Chandras, C., et al., *CreZOO—the European virtual repository of Cre and other targeted conditional driver strains.* Database, 2012. **2012**.

96. Wang, W.-L., et al., *Lens Fiber Cell Differentiation and Denucleation Are Disrupted through Expression of the N-Terminal Nuclear Receptor Box of Ncoa6 and Result in p53-dependent and p53-independent Apoptosis.* Molecular Biology of the Cell, 2010. **21**(14): p. 2453-2468.

97. Davies, A., et al., *CD59, an LY-6-like protein expressed in human lymphoid cells, regulates the action of the complement membrane attack complex on homologous cells.* J Exp Med, 1989. **170**(3): p. 637-54.

98. Tegla, C.A., et al., *Membrane attack by complement: The assembly and biology of terminal complement complexes.* Immunologic Research, 2011. **51**(1): p. 45-60.

99. Morgan, B.P., *Regulation of the complement membrane attack pathway*. Critical Reviews in Immunology, 1999. **19**(3): p. 173-198.

100. Meri, S., et al., *Human protectin (CD59), an 18,000-20,000 MW complement lysis restricting factor, inhibits C5b-8 catalysed insertion of C9 into lipid bilayers.* Immunology, 1990. **71**(1): p. 1-9.

101. Farkas, I., et al., *CD59 blocks not only the insertion of C9 into MAC but inhibits ion channel formation by homologous C5b-8 as well as C5b-9.* Journal of Physiology, 2002. **539**(2): p. 537-545.

102. Taylor, D.R. and N.M. Hooper, *GPI-Anchored Proteins in Health and Disease*, in *Post-Translational Modifications in Health and Disease*, J.C. Vidal, Editor. 2011, Springer New York: New York, NY. p. 39-55.

103. Dworacki, G., et al., *Flow cytometric analysis of CD55 and CD59 expression on blood cells in paroxysmal nocturnal haemoglobinuria.* Folia Histochemica et Cytobiologica, 2005. **43**(2): p. 117-120.

104. Brodsky, R.A., *Paroxysmal nocturnal hemoglobinuria.* Blood, 2014. **124**(18): p. 2804-2811.

105. Kimberley, F.C., B. Sivasankar, and B. Paul Morgan, *Alternative roles for CD59.* Molecular Immunology, 2007. **44**(1-3): p. 73-81.

106. Wheeler, S.F., et al., *Comparison of the N-linked glycans from soluble and GPI-anchord CD59 expressed in CHO cells.* Glycobiology, 2002. **12**(4): p. 261-271.

107. Rudd, P.M., et al., *Oligosaccharide analysis and molecular modeling of soluble forms of glycoproteins belonging to the Ly-6, scavenger receptor, and immunoglobulin superfamilies expressed in Chinese hamster ovary cells.* Glycobiology, 1999. **9**(5): p. 443-458.

108. Rudd, P.M., et al., *The glycosylation of the complement regulatory protein, human erythrocyte CD59.* J Biol Chem, 1997. **272**(11): p. 7229-44.

109. Tabata, A., et al., *The diversity of receptor recognition in cholesterol-dependent cytolysins.* Microbiology and Immunology, 2014. **58**(3): p. 155-171.

110. Baran, K., et al., *The Molecular Basis for Perforin Oligomerization and Transmembrane Pore Assembly.* Immunity, 2009. **30**(5): p. 684-695.

111. Whiley, R.A., et al., *Phenotypic differentiation of Streptococcus intermedius, Streptococcus constellatus, and Streptococcus anginosus strains within the "Streptococcus milleri group".* J Clin Microbiol, 1990. **28**(7): p. 1497-501.

112. Sukeno, A., et al., *Intermedilysin is essential for the invasion of hepatoma HepG2 cells by Streptococcus intermedius.* Microbiology and Immunology, 2005. **49**(7): p. 681-694.

113. Nagamune, H., et al., *Intermedilysin, a novel cytotoxin specific for human cells secreted by Streptococcus intermedius UNS46 isolated from a human liver abscess.* Infect Immun, 1996. **64**(8): p. 3093-100.

114. Giddings, K.S., et al., *Human CD59 is a receptor for the cholesterol-dependent cytolysin intermedilysin.* Nat Struct Mol Biol, 2004. **11**(12): p. 1173-8.

115. Giddings, K.S., A.E. Johnson, and R.K. Tweten, *Redefining cholesterol's role in the mechanism of the cholesterol-dependent cytolysins.* Proc Natl Acad Sci U S A, 2003. **100**(20): p. 11315-20.

116. Kawaguchi, Y., et al., *Profiles of ILY, VLY and Sm-hPAF Interaction with Human CD59.* Anticancer Research, 2013. **33**(7): p. 2901-2904.

117. Wickham, S.E., et al., *Mapping the intermedilysin-human CD59 receptor interface reveals a deep correspondence with the binding site on CD59 for complement binding proteins C8alpha and C9.* J Biol Chem, 2011. **286**(23): p. 20952-62.

118. Zhang, H.F., et al., *Identification of the individual residues that determine human CD59 species selective activity.* Journal of Biological Chemistry, 1999. **274**(16): p. 10969-10974.

119. Zhao, X.J., et al., *Identity of the residues responsible for the species-restricted complement inhibitory function of human CD59.* Journal of Biological Chemistry, 1998. **273**(17): p. 10665-10671.

120. LaChapelle, S., R.K. Tweten, and E.M. Hotze, *Intermedilysin-receptor interactions during assembly of the pore complex: assembly intermediates increase host cell susceptibility to complement-mediated lysis.* J Biol Chem, 2009. **284**(19): p. 12719-26.

121. Ohkura, K., et al., *Molecular Profiles of Cholesterol-dependent Cytolysin Family-derived 11mer Regions.* Anticancer Research, 2012. **32**(6): p. 2343-2346.

122. Johnson, S., et al., *Structural basis for recognition of the pore-forming toxin intermedilysin by human complement receptor CD59.* Cell Rep, 2013. **3**(5): p. 1369-77.

123. Soltani, C.E., et al., *Structural elements of the cholesterol-dependent cytolysins that are responsible for their cholesterol-sensitive membrane interactions.* Proc Natl Acad Sci U S A, 2007. **104**(51): p. 20226-31.

124. Farrand, A.J., et al., *The Cholesterol-dependent Cytolysin Membrane-binding Interface Discriminates Lipid Environments of Cholesterol to Support beta-Barrel Pore Insertion.* J Biol Chem, 2015. **290**(29): p. 17733-44.

125. Tilley, S.J., et al., *Structural Basis of Pore Formation by the Bacterial Toxin Pneumolysin.* Cell, 2005. **121**(2): p. 247-256.

126. Ohkura, K., H. Nagamune, and H. Kourai, *Structural analysis of human specific cytolysin intermedilysin aiming application to cancer immunotherapy.* Anticancer Research, 2004. **24**(5C): p. 3343-3353.

127. Masin, J., et al., *Differences in purinergic amplification of osmotic cell lysis by the pore-forming RTX toxins bordetella pertussis CyaA and actinobacillus pleuropneumoniae ApxIA: The role of pore size.* Infection and Immunity, 2013. **81**(12): p. 4571-4582.

128. LaRocca, T.J., et al., *Human-specific bacterial pore-forming toxins induce programmed necrosis in erythrocytes.* MBio, 2014. **5**(5): p. e01251-14.

129. LaRocca, T.J., et al., *CD59 signaling and membrane pores drive Syk-dependent erythrocyte necroptosis.* Cell Death & Disease, 2015. **6**.

130. Chandrasekaran, S. and M.G. Caparon, *The NADase-Negative Variant of the Streptococcus pyogenes Toxin NAD(+) Glycohydrolase Induces JNK1-Mediated Programmed Cellular Necrosis.* Mbio, 2016. **7**(1).

131. Flaherty, R.A., et al., *Streptolysin S Promotes Programmed Cell Death and Enhances Inflammatory Signaling in Epithelial Keratinocytes during Group A Streptococcus Infection.* Infection and Immunity, 2015. **83**(10): p. 4118-4133.

132. Barcena-Uribarri, I., et al., *Pore forming activity of the potent RTX-toxin produced by pediatric pathogen Kingella kingae: Characterization and comparison to other RTX-family members.* Biochimica Et Biophysica Acta-Biomembranes, 2015. **1848**(7): p. 1536-1544.

133. Hu, W., et al., *Rapid conditional targeted ablation of cells expressing human CD59 in transgenic mice by intermedilysin.* Nat Med, 2008. **14**(1): p. 98-103.

134. Hu, W., et al., *The critical roles of platelet activation and reduced NO bioavailability in fatal pulmonary arterial hypertension in a murine hemolysis model.* Blood, 2010. **116**(9): p. 1613-22.

135. Kooyman, D.L., et al., *In vivo transfer of GPI-linked complement restriction factors from erythrocytes to the endothelium.* Science, 1995. **269**(5220): p. 89-92.

136. Chai, R., et al., *Efficient, glucose responsive and islet-specific transgene expression by a modified rat insulin promoter.* Gene Ther, 2009. **16**(10): p. 1202-9.

137. Ehrt, S. and D. Schnappinger, *Isolation of plasmids from E. coli by boiling lysis.* Methods Mol Biol, 2003. **235**: p. 79-82.

138. Pérez-Pinera, P., M. Menéndez-González, and J.A. Vega, *Deletion of DNA sequences of using a polymerase chain reaction based approach*. 2006. 2006.

139. Sheehan DC, H.B., *Theory and practice of histotechnology*. 2nd ed. 1987, Columbus, Ohio: Battelle Press.

140. Witten, I.B., et al., *Recombinase-driver rat lines: tools, techniques, and optogenetic application to dopamine-mediated reinforcement.* Neuron, 2011. **72**(5): p. 721-33.

141. Gregoire, D. and M. Kmita, *Genetic cell ablation.* Methods Mol Biol, 2014. **1092**: p. 421-36.

142. Feng, D., et al., *Cre-inducible human CD59 mediates rapid cell ablation after intermedilysin administration.* J Clin Invest, 2016. **126**(6): p. 2321-33.

143. Gill, T.J., et al., *The rat as an experimental animal.* Science, 1989. **245**(4915): p. 269-276.

144. Stoll, M. and H.J. Jacob, *Genetic rat models of hypertension: Relationship to human hypertension.* Current Hypertension Reports, 2001. **3**(2): p. 157-164.

145. Abbott, A., *The Renaissance rat.* Nature, 2004. **428**(6982): p. 464-466.

146. Ramot, Y., et al., *Phenylhydrazine as a partial model for β-thalassaemia red blood cell hemodynamic properties.* British Journal of Haematology, 2008. **140**(6): p. 692-700.

147. Sato, H., et al., *Gene expression profiling in the lungs of phenylhydrazine-treated rats: the contribution of pro-inflammatory response and endothelial dysfunction to acute thrombosis.* Exp Toxicol Pathol, 2015. **67**(2): p. 205-10.

148. Ramot, Y., et al., *Age and dose sensitivities in the 2-butoxyethanol F344 rat model of hemolytic anemia and disseminated thrombosis.* Experimental and Toxicologic Pathology, 2007. **58**(5): p. 311-322.

149. Amir, G., et al., *2-Butoxyethanol model of haemolysis and disseminated thrombosis in female rats: a preliminary study of the vascular mechanism of osteoarthritis in the temporomandibular joint.* Br J Oral Maxillofac Surg, 2011. **49**(1): p. 21-5.

150. Lewis, D.A., et al., *Hemostatic activation in a chemically induced rat model of severe hemolysis and thrombosis.* Thromb Res, 2006. **118**(6): p. 747-53.

151. Koshkaryev, A., et al., *2-Butoxyethanol enhances the adherence of red blood cells.* Arch Toxicol, 2003. **77**(8): p. 465-9.

152. Iacovache, I., F.G. van der Goot, and L. Pernot, *Pore formation: an ancient yet complex form of attack.* Biochim Biophys Acta, 2008. **1778**(7-8): p. 1611-23.

153. Tilley, S.J. and H.R. Saibil, *The mechanism of pore formation by bacterial toxins.* Curr Opin Struct Biol, 2006. **16**(2): p. 230-6.

154. Ghanayem, B.I., et al., *Hemolytic anemia, thrombosis, and infarction in male and female F344 rats following gavage exposure to 2-butoxyethanol.* Exp Toxicol Pathol, 2001. **53**(2-3): p. 97-105.

155. Ghanayem, B.I., et al., *Comparison of the acute hematotoxicity of 2-butoxyethanol in male and female F344 rats.* Hum Exp Toxicol, 2000. **19**(3): p. 185-92.

156. Holt, D.S., et al., *Targeted deletion of the CD59 gene causes spontaneous intravascular hemolysis and hemoglobinuria.* Blood, 2001. **98**(2): p. 442-9.

157. Frei, A.C., et al., *Vascular dysfunction in a murine model of severe hemolysis.* Blood, 2008. **112**(2): p. 398-405.

158. Corrigan, J.J., Jr. and F.G. Boineau, *Hemolytic-uremic syndrome.* Pediatr Rev, 2001. **22**(11): p. 365-9.

159. Noris, M., et al., *Relative role of genetic complement abnormalities in sporadic and familial aHUS and their impact on clinical phenotype.* Clin J Am Soc Nephrol, 2010. **5**(10): p. 1844-59.

160. Sallee, M., et al., *Myocardial infarction is a complication of factor H-associated atypical HUS.* Nephrol Dial Transplant, 2010. **25**(6): p. 2028-32.

161. Azukaitis, K., et al., *Macrovascular involvement in a child with atypical hemolytic uremic syndrome.* Pediatr Nephrol, 2014. **29**(7): p. 1273-7.

162. Zhang, D., et al., *Preclinical experimental models of drug metabolism and disposition in drug discovery and development.* Acta Pharmaceutica Sinica B, 2012. **2**(6): p. 549-561.

163. Mordes, J.P., et al., *Rat models of type 1 diabetes: genetics, environment, and autoimmunity.* Ilar j, 2004. **45**(3): p. 278-91.

164. Menke, A., et al., *The Prevalence of Type 1 Diabetes in the United States.* Epidemiology, 2013. **24**(5): p. 773-4.

165. Lado, J.J. and T.H. Lipman, *Racial and Ethnic Disparities in the Incidence, Treatment, and Outcomes of Youth with Type 1 Diabetes.* Endocrinol Metab Clin North Am, 2016. **45**(2): p. 453-61.

166. Virtanen, S.M., *Dietary factors in the development of type 1 diabetes.* Pediatr Diabetes, 2016. **17 Suppl 22**: p. 49-55.

167. Pociot, F. and A. Lernmark, *Genetic risk factors for type 1 diabetes.* Lancet, 2016. **387**(10035): p. 2331-9.

168. Weir, G.C., *Islet-cell biology in 2015: Understanding secretion, ageing and death in beta cells.* Nat Rev Endocrinol, 2016. **12**(2): p. 72-4.

169. Cnop, M., et al., *Mechanisms of pancreatic beta-cell death in type 1 and type 2 diabetes: many differences, few similarities.* Diabetes, 2005. **54 Suppl 2**: p. S97-107.

170. Fujino-Kurihara, H., et al., *Morphological aspects on pancreatic islets of non-obese diabetic (NOD) mice.* Virchows Arch B Cell Pathol Incl Mol Pathol, 1985. **49**(2): p. 107-20.

171. Chao, N.J., et al., *Molecular characterization of MHC class II antigens (beta 1 domain) in the BB diabetes-prone and -resistant rat.* Immunogenetics, 1989. **29**(4): p. 231-4.

172. Dotta, F. and G.S. Eisenbarth, *Type I diabetes mellitus: a predictable autoimmune disease with interindividual variation in the rate of beta cell destruction.* Clin Immunol Immunopathol, 1989. **50**(1 Pt 2): p. S85-95.

173. Baxter, A.G., M. Koulmanda, and T.E. Mandel, *High and low diabetes incidence nonobese diabetic (NOD) mice: origins and characterisation.* Autoimmunity, 1991. **9**(1): p. 61-7.

174. Makino, S., et al., *Breeding of a non-obese, diabetic strain of mice.* Jikken Dobutsu, 1980. **29**(1): p. 1-13.

175. Mordes, J., et al., *Rat models of type 1 diabetes: genetics, environment, and autoimmunity.* ILAR, 2004. **45**(3): p. 278-91.

176. Grant, C.W., et al., *Testing agents for prevention or reversal of type 1 diabetes in rodents.* PLoS One, 2013. **8**(8): p. e72989.

177. Damond, N., et al., *Blockade of glucagon signaling prevents or reverses diabetes onset only if residual beta-cells persist.* Elife, 2016. **5**.

178. Popova, E., et al., *Efficiency of transgenic rat production is independent of transgene-construct and overnight embryo culture.* Theriogenology, 2004. **61**(7-8): p. 1441-53.

179. Charreau, B., et al., *Transgenesis in rats: technical aspects and models.* Transgenic Res, 1996. **5**(4): p. 223-34.

180. Martin, D.I. and E. Whitelaw, *The vagaries of variegating transgenes.* Bioessays, 1996. **18**(11): p. 919-23.

181. Kobayashi, T., et al., *Identification of rat Rosa26 locus enables generation of knock-in rat lines ubiquitously expressing tdTomato.* Stem Cells Dev, 2012. **21**(16): p. 2981-6.

182. Hanson, M.M., et al., *A rapid conditional targeted ablation model for hemolytic anemia in the rat.* Physiol Genomics, 2016: p. physiolgenomics.00026.2016.

183. Wilson, R.D. and M.S. Islam, *Fructose-fed streptozotocin-injected rat: an alternative model for type 2 diabetes.* Pharmacol Rep, 2012. **64**(1): p. 129-39.

184. Qinna, N.A. and A.A. Badwan, *Impact of streptozotocin on altering normal glucose homeostasis during insulin testing in diabetic rats compared to normoglycemic rats.* Drug Design, Development and Therapy, 2015. **9**: p. 2515-2525.

185. Canas, X., et al., *Rat insulin turnover in vivo.* Endocrinology, 1995. **136**(9): p. 3871-6.

186. Togashi, Y., et al., *Evaluation of the appropriateness of using glucometers for measuring the blood glucose levels in mice.* Scientific Reports, 2016. **6**: p. 25465.

187. Weitgasser, R., A.M. Davalli, and G.C. Weir, *Measurement of glucose concentrations in rats: differences between glucose meter and plasma laboratory results.* Diabetologia, 1999. **42**(2): p. 256.

188. Vanavanan, S., et al., *Performance of a new interference-resistant glucose meter.* Clin Biochem, 2010. **43**(1-2): p. 186-92.

189. Ramljak, S., et al., *Hematocrit interference of blood glucose meters for patient self-measurement.* J Diabetes Sci Technol, 2013. **7**(1): p. 179-89.

190. Kurrer, M.O., et al., *Beta cell apoptosis in T cell-mediated autoimmune diabetes.* Proc Natl Acad Sci U S A, 1997. **94**(1): p. 213-8.

191. Shiao, M.S., et al., *Adaptive evolution of the insulin two-gene system in mouse.* Genetics, 2008. **178**(3): p. 1683-91.

192. Vasavada, R.C., et al., *Overexpression of parathyroid hormone-related protein in the pancreatic islets of transgenic mice causes islet hyperplasia, hyperinsulinemia, and hypoglycemia.* Journal of Biological Chemistry, 1996. **271**(2): p. 1200-1208.

193. Dahl, U., A. Sjödin, and H. Semb, *Cadherins regulate aggregation of pancreatic β-cells in vivo.* Development, 1996. **122**(9): p. 2895-2902.

194. Song, J., et al., *Brain expression of Cre recombinase driven by pancreas-specific promoters.* Genesis, 2010. **48**(11): p. 628-34.

195. Dor, Y., et al., *Adult pancreatic beta-cells are formed by self-duplication rather than stem-cell differentiation.* Nature, 2004. **429**(6987): p. 41-6.

196. Lee, J.Y., et al., *RIP-Cre revisited, evidence for impairments of pancreatic beta-cell function.* J Biol Chem, 2006. **281**(5): p. 2649-53.

197. Hara, M., et al., *Transgenic mice with green fluorescent protein-labeled pancreatic β-cells.* American Journal of Physiology - Endocrinology and Metabolism, 2003. **284**(1 47-1): p. E177-E183.

198. Fukazawa, T., et al., *Development of a novel beta-cell specific promoter system for the identification of insulin-producing cells in in vitro cell cultures.* Exp Cell Res, 2006. **312**(17): p. 3404-12.

199. Dumonteil, E. and J. Philippe, *Insulin gene: organisation, expression and regulation.* Diabetes Metab, 1996. **22**(3): p. 164-73.

200. Nir, U., M.D. Walker, and W.J. Rutter, *Regulation of rat insulin 1 gene expression: evidence for negative regulation in nonpancreatic cells.* Proc Natl Acad Sci U S A, 1986. **83**(10): p. 3180-4.

201. Andrali, S.S., et al., *Glucose regulation of insulin gene expression in pancreatic beta-cells.* Biochem J, 2008. **415**(1): p. 1-10.

202. Han, X.G. and B.E. Tuch, *Cloning and characterization of porcine insulin gene.* Comparative Biochemistry and Physiology - B Biochemistry and Molecular Biology, 2001. **129**(1): p. 87-95.

203. Kennedy, G.C. and W.J. Rutter, *Pur-1, a zinc-finger protein that binds to purine-rich sequences, transactivates an insulin promoter in heterologous cells.* Proceedings of the National Academy of Sciences of the United States of America, 1992. **89**(23): p. 11498-11502.

204. Grzech, M., et al., *Specific transgene expression in mouse pancreatic beta-cells under the control of the porcine insulin promoter.* Mol Cell Endocrinol, 2010. **315**(1-2): p. 219-24.

205. Richards, B., et al., *Stable expression of Anthozoa fluorescent proteins in mammalian cells.* Cytometry, 2002. **48**(2): p. 106-12.

206. Mizuno, M., et al., *A Novel Model of Intravital Platelet Imaging Using CD41-ZsGreen1 Transgenic Rats.* PLoS One, 2016. **11**(4): p. e0154661.

207. Fumoto, S., et al., *Three-Dimensional Imaging of the Intracellular Fate of Plasmid DNA and Transgene Expression: ZsGreen1 and Tissue Clearing Method CUBIC Are an Optimal Combination for Multicolor Deep Imaging in Murine Tissues.* PLoS One, 2016. **11**(1): p. e0148233.

208. Yan, J., et al., *Signal sequence is still required in genes downstream of "autocleaving" 2A peptide for secretary or membrane-anchored expression.* Anal Biochem, 2010. **399**(1): p. 144-6.

209. Donnelly, M.L., et al., *Analysis of the aphthovirus 2A/2B polyprotein 'cleavage' mechanism indicates not a proteolytic reaction, but a novel translational effect: a putative ribosomal 'skip'.* J Gen Virol, 2001. **82**(Pt 5): p. 1013-25.

210. Alexopoulou, A.N., J.R. Couchman, and J.R. Whiteford, *The CMV early enhancer/chicken beta actin (CAG) promoter can be used to drive transgene expression during the differentiation of murine embryonic stem cells into vascular progenitors.* BMC Cell Biol, 2008. **9**: p. 2.

211. Utomo, A.R., A.Y. Nikitin, and W.H. Lee, *Temporal, spatial, and cell type-specific control of Cre-mediated DNA recombination in transgenic mice.* Nat Biotechnol, 1999. **17**(11): p. 1091-6.

212. Liu, Z., et al., *Tissue Specific Expression of Cre in Rat Tyrosine Hydroxylase and Dopamine Active Transporter-Positive Neurons.* PLoS One, 2016. **11**(2): p. e0149379.

213. Ma, Y., et al., *Generation of eGFP and Cre knockin rats by CRISPR/Cas9.* Febs j, 2014. **281**(17): p. 3779-90.

214. Gopalakrishna, A. and S.A. Alexander, *Understanding Parkinson Disease: A Complex and Multifaceted Illness.* J Neurosci Nurs, 2015. **47**(6): p. 320-6.

215. Clark, L.F. and T. Kodadek, *The Immune System and Neuroinflammation as Potential Sources of Blood-Based Biomarkers for Alzheimers Disease, Parkinsons Disease, and Huntingtons Disease.* ACS Chemical Neuroscience, 2016. **7**(5): p. 520-527.

216. Wu, Y.H., et al., *Premotor symptoms as predictors of outcome in parkinsons disease: A case-control study.* PLoS ONE, 2016. **11**(8).

217. Garrett Morgan, R., et al., *Relative contributions of severe dopaminergic neuron ablation and dopamine depletion to cognitive impairment.* Exp Neurol, 2015. **271**: p. 205-14.

218. Müller, T. and P. Foley, *Clinical drug research in chronic central neurodegenerative disorders.* Expert Review of Neurotherapeutics, 2016. **16**(5): p. 497-504.

219. Gumulka, W., et al., *Lesion of substantia nigra: biochemical and behavioral effects in rats.* Eur J Pharmacol, 1970. **10**(1): p. 79-82.

220. Fink, J.S. and G.P. Smith, *Mesolimbic and mesocortical dopaminergic neurons are necessary for normal exploratory behavior in rats.* Neurosci Lett, 1980. **17**(1-2): p. 61-5.

221. Hebb, M.O., et al., *Neonatal ablation of the nigrostriatal dopamine pathway does not influence limb development in rats.* Exp Neurol, 2002. **177**(2): p. 547-56.

222. Tristao, F.S., et al., *Evaluation of nigrostriatal neurodegeneration and neuroinflammation following repeated intranasal 1-methyl-4-phenyl-1,2,3,6-tetrahydropyridine (MPTP) administration in mice, an experimental model of Parkinson's disease.* Neurotox Res, 2014. **25**(1): p. 24-32.

223. Castro, A.A., et al., *Atorvastatin improves cognitive, emotional and motor impairments induced by intranasal 1-methyl-4-phenyl-1,2,3,6-tetrahydropyridine (MPTP) administration in rats, an experimental model of Parkinson's disease.* Brain Res, 2013. **1513**: p. 103-16.

224. Jiang, W., et al., *Ginsenoside Rg1 Ameliorates Motor Function in an Animal Model of Parkinson's Disease.* Pharmacology, 2015. **96**(1-2): p. 25-31.

225. Brown, Z.J., D.A. Kupferschmidt, and S. Erb, *Reinstatement of cocaine seeking in rats by the pharmacological stressors, corticotropin-releasing factor and yohimbine: role for D1/5 dopamine receptors.* Psychopharmacology (Berl), 2012. **224**(3): p. 431-40.

226. Gradinaru, V., et al., *Optical deconstruction of parkinsonian neural circuitry.* Science, 2009. **324**(5925): p. 354-9.

227. Teh, C., et al., *Optogenetic in vivocell manipulation in KillerRed-expressing zebrafish transgenics.* BMC Developmental Biology, 2010. **10**(1): p. 110.

228. Xu, S. and A.D. Chisholm, *Highly efficient optogenetic cell ablation in C. elegans using membrane-targeted miniSOG.* Sci Rep, 2016. **6**: p. 21271.

229. Zhang, F., et al., *Optogenetics in Freely Moving Mammals: Dopamine and Reward.* Cold Spring Harb Protoc, 2015. **2015**(8): p. 715-24.

230. Karnan, S., et al., *Improved methods of AAV-mediated gene targeting for human cell lines using ribosome-skipping 2A peptide.* Nucleic Acids Res, 2016. **44**(6): p. e54.

231. Lewis, J.E., et al., *The use of a viral 2A sequence for the simultaneous over-expression of both the vgf gene and enhanced green fluorescent protein (eGFP) in vitro and in vivo.* J Neurosci Methods, 2015. **256**: p. 22-9.

232. Kim, J.H., et al., *High cleavage efficiency of a 2A peptide derived from porcine teschovirus-1 in human cell lines, zebrafish and mice.* PLoS One, 2011. **6**(4): p. e18556.

233. Vuagnat, B.B., J. Mach, and J.M. Le Doussal, *Activation of the alternative pathway of human complement by autologous cells expressing transmembrane recombinant properdin.* Mol Immunol, 2000. **37**(8): p. 467-78.

234. Murakami, H., et al., *Comparison of blood-brain barrier permeability in mice and rats using in situ brain perfusion technique.* Am J Physiol Heart Circ Physiol, 2000. **279**(3): p. H1022-8.

235. Alam, M. and W.J. Schmidt, *Rotenone destroys dopaminergic neurons and induces parkinsonian symptoms in rats.* Behav Brain Res, 2002. **136**(1): p. 317-24.

236. Cannon, J.R., et al., *A highly reproducible rotenone model of Parkinson's disease.* Neurobiol Dis, 2009. **34**(2): p. 279-90.

237. Campos, F.L., et al., *Rodent models of Parkinson's disease: beyond the motor symptomatology.* Frontiers in Behavioral Neuroscience, 2013. **7**: p. 175.

238. Strome, E.M., et al., *Evaluation of the integrity of the dopamine system in a rodent model of Parkinson's disease: small animal positron emission tomography compared to behavioral assessment and autoradiography.* Mol Imaging Biol, 2006. **8**(5): p. 292-9.

239. Metz, G.A. and I.Q. Whishaw, *The Ladder Rung Walking Task: A Scoring System and its Practical Application.* 2009(28): p. e1204.

240. Farr, T.D., et al., *Bilateral alteration in stepping pattern after unilateral motor cortex injury: a new test strategy for analysis of skilled limb movements in neurological mouse models.* J Neurosci Methods, 2006. **153**(1): p. 104-13.

241. Faraji, J. and G.A. Metz, *Sequential bilateral striatal lesions have additive effects on single skilled limb use in rats.* Behavioural Brain Research, 2007. **177**(2): p. 195-204.

242. Klein, A. and S.B. Dunnett, *Analysis of skilled forelimb movement in rats: the single pellet reaching test and staircase test.* Curr Protoc Neurosci, 2012. **Chapter 8**: p. Unit8.28.

243. Saint-Cyr, J.A., A.E. Taylor, and A.E. Lang, *Procedural learning and neostriatal dysfunction in man.* Brain, 1988. **111 (Pt 4)**: p. 941-59.

244. Haik, K.L., et al., *7-Nitroindazole Attenuates 6-Hydroxydopamine-Induced Spatial Learning Deficits and Dopamine Neuron Loss in a Presymptomatic Animal Model of Parkinson's Disease.* Experimental and Clinical Psychopharmacology, 2008. **16**(2): p. 178-189.

245. Luchtman, D.W., Q. Meng, and C. Song, *Ethyl-eicosapentaenoate (E-EPA) attenuates motor impairments and inflammation in the MPTP-probenecid mouse model of Parkinson's disease.* Behavioural Brain Research, 2012. **226**(2): p. 386-396.

246. Nakagawa, M., et al., *Dopaminergic agonists and muscarinic antagonists improve lateralization in hemiparkinsonian rats in a novel exploratory Y-maze*. J Pharmacol Exp Ther, 2004. **309**(2): p. 737-44.

247. Costa, R., et al., *Handling of Adolescent Rats Improves Learning and Memory and Decreases Anxiety.* Journal of the American Association for Laboratory Animal Science : JAALAS, 2012. **51**(5): p. 548-553.

248. Kirov, J.V., et al., *Reporter Gene Silencing in Targeted Mouse Mutants Is Associated with Promoter CpG Island Methylation.* PLoS ONE, 2015. **10**(8): p. e0134155.

249. Rosser, J.M. and W. An, *Repeat-induced gene silencing of L1 transgenes is correlated with differential promoter methylation.* Gene, 2010. **456**(1-2): p. 15-23.

250. Chevalier-Mariette, C., et al., *CpG content affects gene silencing in mice: evidence from novel transgenes.* Genome Biol, 2003. **4**(9): p. R53.

251. Ciavatta, D., et al., *A DNA insulator prevents repression of a targeted X-linked transgene but not its random or imprinted X inactivation.* Proc Natl Acad Sci U S A, 2006. **103**(26): p. 9958-63.

252. Srinivas, S., et al., *Cre reporter strains produced by targeted insertion of EYFP and ECFP into the ROSA26 locus.* BMC Dev Biol, 2001. **1**: p. 4.

253. Chung, S.H. and E. Mazur, *Surgical applications of femtosecond lasers.* Journal of Biophotonics, 2009. **2**(10): p. 557-572.

254. Essner, J.J., et al., *Kupffer's vesicle is a ciliated organ of asymmetry in the zebrafish embryo that initiates left-right development of the brain, heart and gut.* Development, 2005. **132**(6): p. 1247-1260.

255. White, D.T. and J.S. Mumm, *The nitroreductase system of inducible targeted ablation facilitates cell-specific regenerative studies in zebrafish.* Methods, 2013. **62**(3): p. 232-240.

256. Chen, E. and S.C. Ekker, *Zebrafish as a Genomics Research Model.* Current Pharmaceutical Biotechnology, 2004. **5**(5): p. 409-413.

257. Lieschke, G.J. and P.D. Currie, *Animal models of human disease: zebrafish swim into view.* Nat Rev Genet, 2007. **8**(5): p. 353-367.

258. Detrich, H.W., et al., *The Zebrafish: Biology*. 1999: Academic Press.

259. Clark, K.J., et al., *Transgenic Zebrafish Using Transposable Elements.* Methods in cell biology, 2011. **104**: p. 137-149.

260. Harrold, I., et al., *Efficient transgenesis mediated by pigmentation rescue in zebrafish.* Biotechniques, 2016. **60**(1): p. 13-20.

261. Wang, J., et al., *The regenerative capacity of zebrafish reverses cardiac failure caused by genetic cardiomyocyte depletion.* Development, 2011. **138**(16): p. 3421-30.

262. Wang, Y., et al., *Genetic inducible fate mapping in larval zebrafish reveals origins of adult insulin-producing beta-cells.* Development, 2011. **138**(4): p. 609-17.

263. Nakamasu, A., et al., *Interactions between zebrafish pigment cells responsible for the generation of Turing patterns.* Proc Natl Acad Sci U S A, 2009. **106**(21): p. 8429-34.

264. Reber, L.L., et al., *Selective ablation of mast cells or basophils reduces peanut-induced anaphylaxis in mice.* J Allergy Clin Immunol, 2013. **132**(4): p. 881-888 e11.

265. Whiddon, B.B. and R.D. Palmiter, *Ablation of neurons expressing melanin-concentrating hormone (MCH) in adult mice improves glucose tolerance independent of MCH signaling.* J Neurosci, 2013. **33**(5): p. 2009-16.

266. van Blijswijk, J., B.U. Schraml, and C.R.e. Sousa, *Advantages and limitations of mouse models to deplete dendritic cells.* European Journal of Immunology, 2013. **43**(1): p. 22-26.

267. Montgomery, J.E., M.J. Parsons, and D.R. Hyde, *A novel model of retinal ablation demonstrates that the extent of rod cell death regulates the origin of the regenerated zebrafish rod photoreceptors.* J Comp Neurol, 2010. **518**(6): p. 800-14.

268. Ariga, J., S.L. Walker, and J.S. Mumm, *Multicolor time-lapse imaging of transgenic zebrafish: visualizing retinal stem cells activated by targeted neuronal cell ablation.* J Vis Exp, 2010(43).

269. Grohmann, M., et al., *A mammalianized synthetic nitroreductase gene for high-level expression.* BMC Cancer, 2009. **9**: p. 301.

270. Mathias Jonathan R., Z.Z., Saxena Meera T., and Mumm Jeff S.. , *Enhanced Cell-Specific Ablation in Zebrafish Using a Triple Mutant of Escherichia Coli Nitroreductase.* Zebrafish, 2014. **11**(2): p. 85-97.

271. Waymouth, C., *Osmolality of mammalian blood and of media for culture of mammalian cells.* In Vitro, 1970. **6**(2): p. 109-27.

272. Pype, C., et al., *Incubation at 32.5 °C and above causes malformations in the zebrafish embryo.* Reproductive Toxicology, 2015. **56**: p. 56-63.

273. Schirone, R.C. and L. Gross, *Effect of temperature on early embryological development of the zebra fish, Brachydanio rerio.* Journal of Experimental Zoology, 1968. **169**(1): p. 43-52.

274. Sun, C., et al., *Zebrafish CD59 has both bacterial-binding and inhibiting activities.* Dev Comp Immunol, 2013. **41**(2): p. 178-88.

275. Uemura, O., et al., *Comparative functional genomics revealed conservation and diversification of three enhancers of the isl1 gene for motor and sensory neuron-specific expression.* Dev Biol, 2005. **278**(2): p. 587-606.

276. Palmquist-Gomes, P., J.A. Guadix, and J.M. Perez-Pomares, *A chick embryo cryoinjury model for the study of embryonic organ development and repair.* Differentiation, 2016. **91**(4-5): p. 72-7.

277. Wang, J., et al., *Rapid transient isoform-specific neuregulin1 transcription in motor neurons is regulated by neurotrophic factors and axon-target interactions.* Mol Cell Neurosci, 2015. **68**: p. 73-81.

278. Bressan, M. and T. Mikawa, *Avians as a model system of vascular development.* Methods Mol Biol, 2015. **1214**: p. 225-42.

279. Park, T.S., S.W. Kim, and J.H. Lee, *Efficient transgene expression system using a cumate-inducible promoter and Cre-loxP recombination in avian cells.* Asian-Australas J Anim Sci, 2016.

Vita

Marina Hanson (formerly known as Marina Rose McCoy) was born in Camden, New Jersey on June 22, 1984. She has loved animals since birth, growing up with a menagerie which included many hamsters, mice, rats, rabbits, fish, chickens, and horses (most to her parents' dismay). Quickly, she decided she wanted to be a rat veterinarian, as they have long been her favorite animal. It was her passion for exotic pets that led to her active involvement in 4H where she assumed many leadership roles and competed with her pocket pets, livestock and horses. She graduated from Bishop Eustace Preparatory School in 2002 and began undergraduate studies at Rutgers University-- Cook College in New Brunswick, New Jersey, receiving her Bachelors of Science degree in laboratory animal science in 2006. Upon graduating from Rutgers, Marina entered in the pharmaceutical industry as a study coordinator and animal caretaker at Sanofi-Aventis in Bridgewater, New Jersey. After one year of employment, she was admitted to the Iowa State University College of Veterinary Medicine in Ames, IA. Here, she continued to pursue her interest in laboratory animal medicine, interning with the office of lab animal resources. She graduated with her DVM in 2011 and was accepted into the comparative medicine residency program at the University of Missouri in Columbia, MO under the direction of Dr. Craig Franklin. She completed her residency in 2014 and enjoyed her research experience so much that she continued her training, completing a PhD in Dr. Elizabeth Bryda's lab in December 2016. After completing her comprehensive exam, she married her supportive husband, Aaron, in September 2014. She and Aaron welcomed their first child, Chase Donald Hanson, on April 6, 2016. Marina's future plans involve a career in comparative and translational medicine, specializing in novel model development.